AD_____

Award Number: W81XWH-12-1-0555

TITLE: Imaging Prostate Cancer Microenvironment by Collagen Hybridization

PRINCIPAL INVESTIGATOR: Dr. Michael S. Yu

CONTRACTING ORGANIZATION: Johns Hopkins University
Baltimore, MD 21218-2680

REPORT DATE: October 2013

TYPE OF REPORT: Annual

PREPARED FOR: U.S. Army Medical Research and Materiel Command
Fort Detrick, Maryland 21702-5012

REPORT DOCUMENTATION PAGE

Form Approved
OMB No. 0704-0188

1. REPORT DATE	**2. REPORT TYPE**	**3. DATES COVERED**
October 2013	Annual	30 September 2012-29 September 2013

4. TITLE AND SUBTITLE
Imaging Prostate Cancer Microenvironment by Collagen Hybridization

5a. CONTRACT NUMBER

5b. GRANT NUMBER
W81XWH-12-1-0555

5c. PROGRAM ELEMENT NUMBER

6. AUTHOR(S)
Dr. Michael S. Yu

E-Mail: michael.yu@utah.edu

5d. PROJECT NUMBER

5e. TASK NUMBER

5f. WORK UNIT NUMBER

7. PERFORMING ORGANIZATION NAME(S) AND ADDRESS(ES)

Johns Hopkins University
3400 N. Charles St, W400 Wyman Park Bldg
Baltimore, MD 21218-2680

8. PERFORMING ORGANIZATION REPORT NUMBER

9. SPONSORING / MONITORING AGENCY NAME(S) AND ADDRESS(ES)
U.S. Army Medical Research and Materiel Command
Fort Detrick, Maryland 21702-5012

10. SPONSOR/MONITOR'S ACRONYM(S)

11. SPONSOR/MONITOR'S REPORT NUMBER(S)

12. DISTRIBUTION / AVAILABILITY STATEMENT
Approved for Public Release; Distribution Unlimited

13. SUPPLEMENTARY NOTES

14. ABSTRACT

The major goal of the proposed work is to develop new PCa imaging methods based on the collagen mimetic peptide (CMP)-mediated structural interrogation of the collagens associated with invasive tumor. In this proposal, we propose to use collagen mimetic peptide (CMP) as a collagen targeting agents that will allow imaging of invasive PCa. Since CMP binds to unstructured collagens more readily, it is expected to exhibit selective affinity to metastatic PCa tumors known to contain processed and denatured collagens. The motivating hypothesis is that the CMP's ability to bind to collagen/denatured collagen can be used to image PCa *in vivo* as well as to determine the level of PCa malignancy.

15. SUBJECT TERMS
Collagen Hybridization

16. SECURITY CLASSIFICATION OF:			**17. LIMITATION OF ABSTRACT**	**18. NUMBER OF PAGES**	**19a. NAME OF RESPONSIBLE PERSON**
a. REPORT	**b. ABSTRACT**	**c. THIS PAGE**			USAMRMC
U	U	U	UU	45	**19b. TELEPHONE NUMBER** *(include area code)*

Table of Contents

INTRODUCTION

Prostate cancer (PCa) is the leading cancer in the U.S. population and the second leading cause of cancer death in men[1]. One of the most pressing issues in PCa management is the need to predict, at the time of diagnosis, which tumors will remain indolent and which will progress rapidly. The ability to fulfill that goal would eliminate the prostate-specific antigen (PSA)-mediated over-detection and over-treatment of clinically insignificant disease. PCa tends to undergo definitive treatment despite the side effects of bowel, bladder and/or sexual dysfunction. The ability to predict the "bad actors" among diagnosed tumors would provide rationale for expectant management, which may be appropriate and obviate serious morbidity. There is an emerging concept of using non-cellular solid state compartment as a source for therapeutic targets and for selective imaging of micro-metastasis[2-5]. In particular, collagens in metastatic tumors have been one of the major targets for this purpose since hallmark of malignant tumor progression involves proteolytic remodeling of the ECM which results in unique structural and biochemical state of stromal collagens[6,7]. Traditionally, these collagens were targeted by antibodies (monoclonal antibody raised against denatured collagen); however antibodies have poor pharmacokinetics for *in vivo* imaging[2]. Recently, small collagen mimetic peptide (CMP) that mimics the amino acid sequence and three dimensional structure of collagen was shown to have specific binding affinity to type I collagen fibers[8-10]. Although exact mechanism of binding is not known fully, evidences are accumulating that support the idea that the CMP is binding to partially denatured domains of natural collagen by triple helical hybridization[11]. We propose to use CMP as a collagen targeting agents that will allow imaging of PCa. Since CMP binds to unstructured collagen domains more readily, it is expected to exhibit selective affinity to metastatic PCa tumors known to contain processed and denatured collagens. *This is the first time that the remodeled ECM of tumor microenvironment is targeted for cancer imaging which is an entirely new way to image PCa with a potential to revolutionize the cancer community.*

BODY

1. Demonstration of CMP mediated in vivo targeting of tissues undergoing normal (e.g. skeleton) and pathological (arthritis) remodeling.

In the preliminary data of the proposed work, we demonstrated that CMP can target denatured collagens in the PC tumor in xenograph mouse model. In the prostate tumor targeting studies, we were surprised to see consistent and high level accumulation of CMPs at the knee joints, which also colocalized with MMP activity. Normal joints are known for continual tissue remolding by MMP; however, targeting this area by systemic delivery is difficult due to the avascular nature of the cartilage and fast synovial fluid clearance [12]. To study the CMP accumulation at the joints and other tissues specifically, we conducted further *in vivo* CMP targeting experiments using BLAB/c mice. Figure 1*A* shows the whole-body fluorescence image of the normal mouse four days after intravenous injection of the photo-decaged peptide. The images show clear accumulation of the CMPs within the skeleton, especially in the spine and ribs, as well as within the knees, ankles, wrists, and lower mandibles. A mouse injected with sequence-scrambled peptide (IR′-Ahx-$^{S}G_9P_9O_9$) showed signal only from the digestive system (fluorescent chlorophylls from food). Furthermore, under similar experimental condition, neither the caged-CMP lacking the folding capacity nor the pre-folded triple helical CMP showed signs of skeletal uptake after four days (Fig. 1*B*). These results strongly suggest that the targeting of the skeletal tissue was mainly driven by the triple helical propensity of the monomeric CMPs.

To identify the location of CMP binding more clearly, mice were co-injected with the calcium chelating fluorescent probe (IRDye800CW BoneTag^{TM}) which targets calcifying tissues [13]. Although the overall distributions of the two probes [IR′-Ahx-$(GPO)_9$: red; BonTag^{TM}: green] seemed similar (Fig. 1*C* top panel), close observation (Fig. 1*C* bottom panels) revealed that CMP targets both calcified and non-calcified bones

(cartilages of the wrists, ribs, and knee) while the BoneTag™ targets only the calcified bones. *Ex vivo* histologic analysis of the knee joint cartilage (unfixed frozen tissue section) showed CMP localizing at the superficial zone which was also co-stained by antibodies for MMP-1 cleaved, type II collagen fragments (Fig. 1*D*). The superficial zone is densely populated by type II collagen fibers part of which are reported to be in denatured state due to steady remodeling activity [14]. Because of continual bone remodeling, collagens within bone are metabolized throughout the lifespan, and products of collagen degradation (e.g. protein fragments, hydroxyproline) are markers for bone resorption activity [15]. These results suggest that the CMP could be used as cartilage imaging agent, and appropriate derivatives may likewise become bone- and cartilage-seeking therapeutics. More work is underway to determine the effects of CMP hybridization on the process of collagen remodeling in the skeletal tissue and in tumor growth.

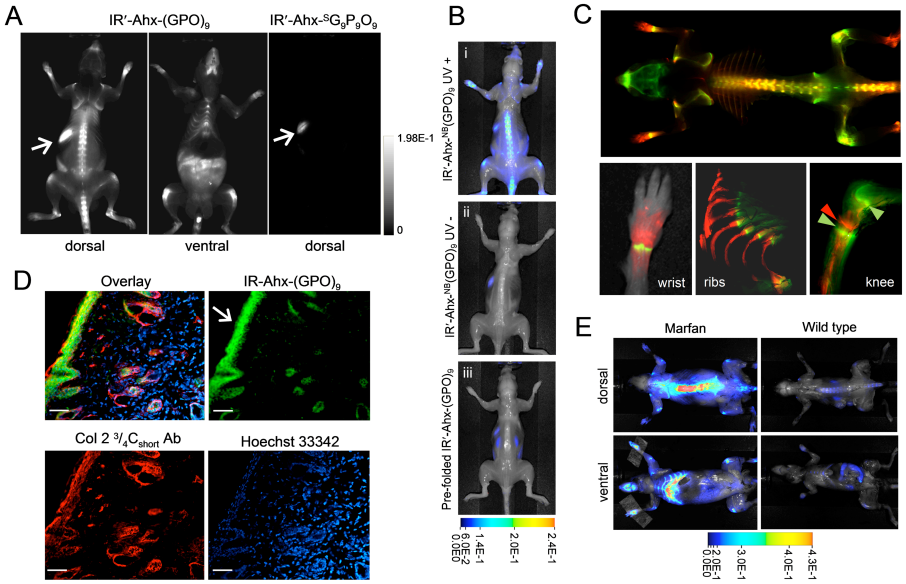

Figure 1. *In vivo* targeting of collagen remodeling in bones and cartilages by CMP hybridization. (*A*) Whole body NIRF images of BLAB/c mice injected intravenously with photo-decaged IR′-Ahx-$(GPO)_9$ or IR′-Ahx-$^{S}G_9P_9O_9$ showing skeletal uptake of only the IR′-Ahx-$(GPO)_9$ probes. Arrows show fluorescence from the chlorophyll in the digestive system. (*B*) Dorsal NIRF images of mice injected intravenously with photo-decaged IR′-Ahx-$(GPO)_9$ (i), caged IR′-Ahx-$^{NB}(GPO)_9$ (ii), or pre-folded triple helical IR′-Ahx-$(GPO)_9$ (iii). The absence of signal from mice ii and iii strongly suggests that the skeletal CMP uptake is due to its triple helical folding propensity. (*C*) Dual-NIRF image of the whole skeleton showing the overall uptake of IR′-Ahx-$(GPO)_9$ (red) and BoneTag™ (stains calcifying tissues in green) and corresponding high resolution images (colocalization shown in yellow). In the wrist, specific CMP uptake (red) is seen in carpal-metacarpal structures and BoneTag uptake is seen in epiphyseal line of radius and ulna; costochondral junctions within the ribs are visualized where mineralized bone ends (green-yellow) and cartilaginous ribs begin (red); CMPs co-localize with BoneTag™ at endochondral junctions (green arrowheads) in the knee while CMP-specific uptake can be seen within the articular cartilage and meniscus (red arrowhead) as well as focal regions within the tibia and the femur head. (*D*) Immunofluorescence micrographs of *ex vivo* knee cartilage sections subsequently stained with anti-Col 2 $^{3}/_{4}C_{short}$ antibody and Hoechst 33342 showing high CMP accumulation at the superficial zone of the cartilage (arrow, scale bars: 100 μm). (*E*) Whole body NIRF images of mouse model with Marfan syndrome 96 hr after IR′-Ahx-$(GPO)_9$ administration showing high CMP uptake in the skeleton of the diseased mouse. Whole body images were taken after skin removal.

We tested CMP's potential to detect bone abnormality in a mouse models of arthritis and Marfan syndrome [16]. CMP's ability to target bone disease was first tested on a mouse with rheumatoid arthritis (RA). RA mice were produced by immunization (*via* tail injection) with type II collagen (and complete Freund's adjuvant). When the IR-Ahx-$(GPO)_9$ was injected to these mice *via* tail vein, a strong IR signal was detected at the ankles of RA mice compared to the normal mice (Fig. 1*D*). The results suggest that the CMP could be used as bone and cartilage imaging agent, and appropriate derivatives may likewise become bone- and cartilage-seeking therapeutics. Photo-triggered IR′-Ahx-$(GPO)_9$ was injected into Marfan mice with a heterozygous missense mutation in fibrillin-1, which was previously shown to exhibit marked skeletal pathology, including severe kyphosis) and rib overgrowth [16]. Whole-body fluorescence images of the mutant and normal mice 96 hr after the CMP injection showed a striking difference in CMP uptake: strong CMP signal was detected at the spine and ribs of the mutant mice with at least four times the intensity of the wild-type mice (Fig. 1*E*). The mechanism of bone overgrowth in Marfan syndrome is complex and still not

fully understood; however the strong correlation between collagen remodeling and bone growth in both physiological and pathological contexts [15], as well as high TGF-β signaling in multiple tissues of this mouse model support the conclusion that prominent CMP uptake in the Marfan mice, at least in part, derives from increased collagen remodeling in skeletal tissues that display pathological overgrowth.

To our knowledge, this is the first time that the structural remodeling of ECM has been directly interrogated by peptide hybridization. CMP is a simple peptide that can be readily conjugated to imaging and therapeutic moieties. Therefore, CMP mediated collagen strand targeting opens new avenues, beyond tumor, bone and joint imaging, for applications in detection and treatment of a wide range of pathologic conditions associated with high MMP activity such as wound healing, ECM degeneration, and fibrous tissue formation.

2. Demonstration of the use of CMP as collagen staining agent in SDS-PAGE gel and tissue sections.

Although fibrous collagens are major structural components of extracellular matrix in mammals, collagen overproduction is associated with many human diseases including cancers and fibrosis. Collagen is typically identified in biomedical research by western blot and immunohistochemistry; however anti-collagen antibodies employed in these analyses are difficult to prepare and their affinities to collagen can diminish if collagen becomes denatured during analyses. Previously, we discovered that single-stranded collagen mimetic peptides [CMPs, sequence: $(GlyProHyp)_9$] can bind to denatured collagen chains by triple helix hybridization. In this work, we demonstrated collagen-specific staining methods using simple CMPs conjugated to common fluorophores (e.g. carboxyfluorescein), which allowed direct detection of collagens and collagen-like proteins in SDS-PAGE and in various mammalian tissue sections.

By directly staining SDS-PAGE gels with fluorescently labeled CMPs, both intact (type I, II, and IV) and MMP-1 cleaved collagen (type I) chains as well as complement factor C1q were detected (Figure 2-1). Collagen bands containing as little as 5 ng were optically visualized while no staining was observed for fibronectin, laminin, and a collection of proteins from mammalian cell lysate. The CMP was unable to stain collagen-like bacterial protein which contains numerous charged amino acids that are believed to stabilize triple helix

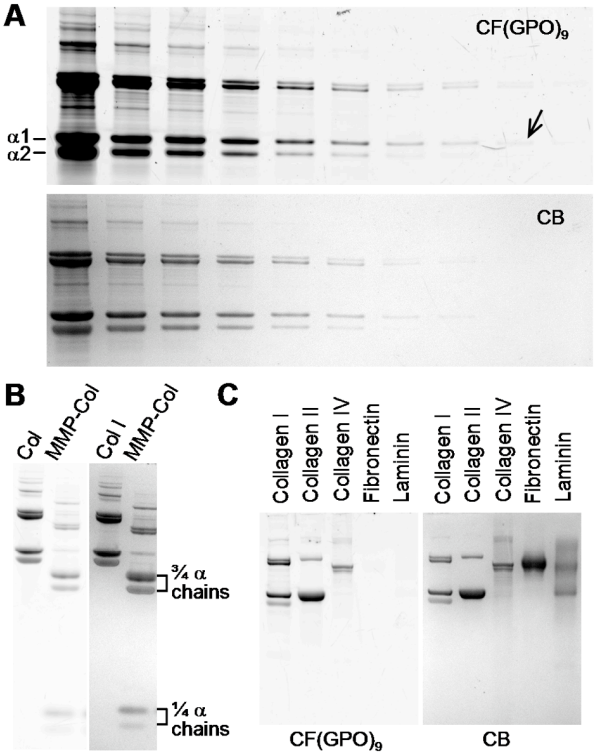

Figure 2-1. Detection of collagen in SDS-PAGE by heat activated fluorescent CMPs. (A) SDS-PAGE loaded with a dilution series of type I collagen, stained and imaged first with $CF(GPO)_9$ (top panel) followed by coomassie blue (CB) staining (bottom panel). From left to right, each lane was loaded with 4 μg, 2 μg, 1 μg, 500 ng, 250 ng, 125 ng, 62.5 ng, 31.2 ng, 15.6 ng and 7.8 ng of denatured collagen, respectively. The arrow points to the least recognizable band in the image which contains approximately 5 ng of collagen α1 chains. (B) SDS-PAGE of intact and MMP-1 cleaved type I collagens (3 μg in each lane) similarly stained with $CF(GPO)_9$ and CB. (C) SDS-PAGE loaded with collagen type I, II, IV, fibronectin and laminin (2 μg of each protein), and stained with $CF(GPO)_9$ and CB. (D) Comparative fluorescence levels of the ECM protein bands in SDS-PAGE stained by $CF(GPO)_9$ (C) or $CF^SG_9P_9O_9$ (Supporting Information Figure S3). The measured fluorescence intensities were normalized by collagen I, and the experiment was performed in triplicate (±s.d.). (E) SDS-PAGE of collagen I (0.7 μg) and a lysate of HUVECs stained by $CF(GPO)_9$ and CB showing remarkable specificity of CMP for collagen detection. Images of the $CF(GPO)_9$ stained gels were recorded using a Typhoon fluorescent imager (λ_{ex} = 488 nm), and CB stained gels were photographed using a Gel Doc EQ system.

in place of Hyp. We also demonstrated that fluorescently labeled CMPs can specifically visualize collagens in fixed tissue sections (e.g., skin, cornea, and bone) more effectively than anti-collagen I antibody (Figure 2-2), and allow facile identification of pathologic conditions in fibrotic liver tissues (data not shown).

In summary, this study has validated the use of fluorescently labeled collagen mimetic peptides for direct and efficient detection of Hyp rich collagenous proteins in SDS-PAGE and immunohistostaining. Our results indicate that CMPs are highly effective at staining collagens in extensively processed tissue sections which are not easily probed by conventional antibodies. We believe that the fluorescent CMP is an excellent alternative to co llagen antibodies for detecting fibrous collagens in various assays and tissue imaging. Although CMP probes cannot distinguish different types of collagens, they offer higher specificity to collagens when compared to conventional staining agents. [17] Conventional collagen staining agents such as Sirus Red rely on electrostatic interactions for binding to collagens; negatively charged probes bind to positively charged collagens. Therefore the staining is not specific to collagen and can stain other proteins with high content of basic amino acids. [18] Since CMP recognizes the triple helical amino acid sequence of collagen, it is a true broad-spectrum collagen-specific staining agent with almost no binding affinity for non-collagenous proteins as demonstrated in this paper. As a potent collagen targeting molecule, CMP is a structurally simple peptide that is easy to prepare and conjugate to other bioactive moieties. The two orthogonal activation mechanisms (Figure 1: heat activation of CMP and light activation of caged CMP) provide great flexibility for the incorporation of additional functionalities to this peptide: the heat activation system is suitable for conjugation of chemically reactive compounds that may be sensitive to UV light or photo-cleaved by-products, while the light activation system is suitable for conjugation of delicate biomolecules (e.g. proteins) that might be incompatible with heat. The ability to synthesize more complex CMP derivatives that can target collagen strands may lead to new applications in tissue scaffold engineering, collagen-targeted drug delivery and *in vivo* collagen imaging.

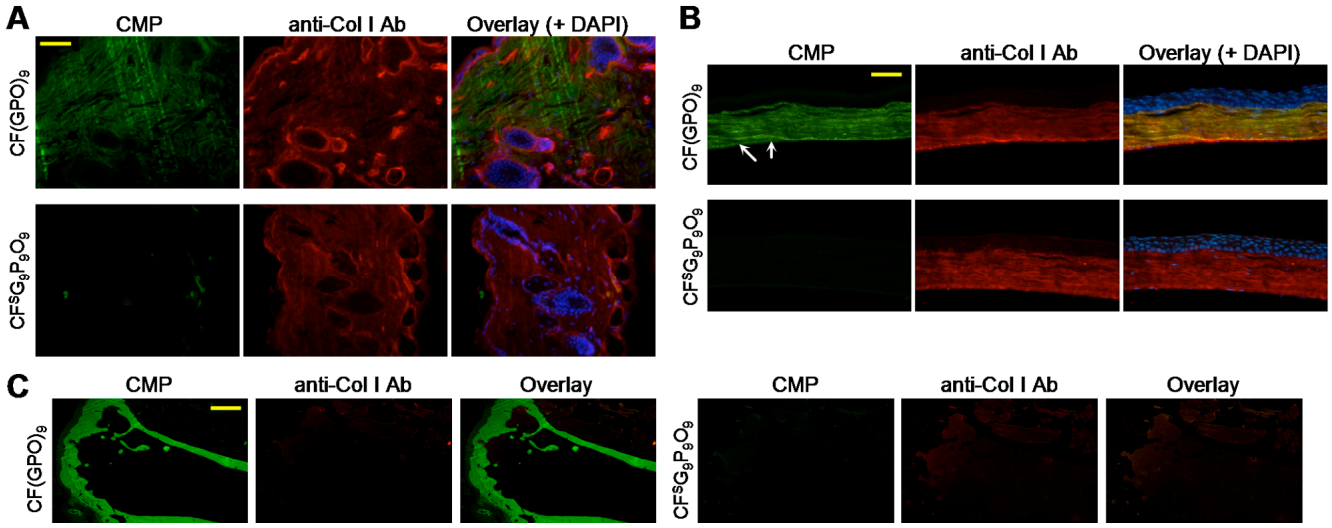

Figure 2-2. Histological tissue staining using photo-activated caged CMPs. Fluorescent micrographs of fixed mouse skin (A) and cornea (B) sections probed by photo-triggered $CF^{NB}(GPO)_9$ (in green, top panels) or scrambled peptide $CF^{S}G_9P_9O_9$ (in green, bottom panels) and co-stained with anti-collagen I antibody (red), and DAPI (blue). The $CF^{NB}(GPO)_9$ staining revealed fine irregular collagen fibers of the dermis (A) and parallel collagen fibrils in the corneal stroma as well as the collagens in Descemet's membrane (arrows) (B). (C) Fluorescent images of paraffin embedded, demineralized mouse tibia sections stained with photo-triggered $CF^{NB}(GPO)_9$ (green, left panels) or scrambled peptide $CF^{S}G_9P_9O_9$ (green, right panels), and co-stained with anti-collagen I antibody (red), showing prominent CMP signals and only weak non-specific antibody signals from the collagenous bone. Concentrations of $CF^{NB}(GPO)_9$ and $CF^{S}G_9P_9O_9$ used in this study are: (A), 25 μM; (B), 2.5 μM; (C), 8 μM. (scale bars: A, 50 μm; B, 100 μm; C, 0.5 mm).

3. Synthesis and *in vivo* targeting of dual modality CMPs which has both fluorescent and radioactive.

As mentioned in the Specific Aim 2.1 of the original proposal, we synthesized and tested 6 different types of CMP derivatives that either contain radioactive moiety or dual, optical and radiological detection modalities. Our first target compound was iodinated CMP, [Y-Ahx-^{NB}(GPO)$_9$] which was synthesized by iodination of tyrosine residue which is attached to the N-terminus of the CMP with aminohexanoic acid (Ahx) linker (Figure 3-1). In vivo experiment in mouse (pancreatic tumor bearing) indicated that the radioactive iodine is detached from the peptide and is collected in the thyroid and stomach as evidenced by the SPECT-CT (Figure 3-1). We then synthesized a peptide with its N-terminus capped with acetyl group in the hopes that the capping will inhibit any exo-proteolytic activity and protect the iodinated Tyr (Figure 3-2). However, the in vivo results similarly showed radioactivity concentrating on the thyroid suggesting de-iodination. Although inconclusive, we did see some indications of bone accumulation when the SPECT-CT was performed 53 hr after injection, particularly in the tail bone area. However, the signal from thyroid was much more stronger indicating significant de-iodination.

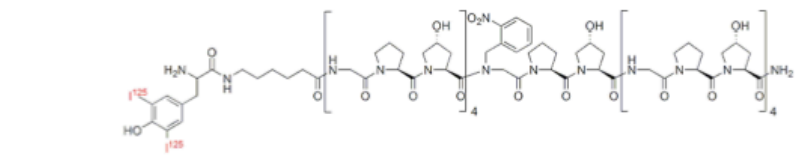

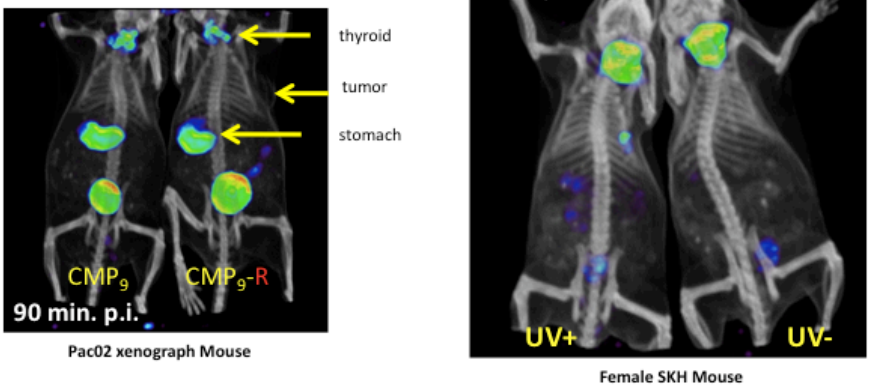

Figure 3-1. Structure of radiolabeled CMP (top), and SPECT-CT of tumor bearing (lower left) and normal (lower right) mouse injected with this compound after decaging. The image indicate presence of abundant amount of free iodines which are cleaved from the peptides.

In an attempt to inhibit de-iodination, we synthesized a synthetic derivative of above peptide which contained iodobenzylcarbonly moiety at the N-terminus. Since this is not an amino acid, it is often used as an enzymatically stable substitute for iodinated Tyr. Unfortunately, in vivo experiment indicated no improvement in terms of preventing de-iodination (data not shown).

Since we were faced with difficulty with the use of iodinated CMP, we decided to produce dual modality CMPs that contain near IR fluorescent dye and a metal chelator which can be loaded with radioactive compounds (In^{111}). We synthesized three different analogues which all have a general sequence of acetyl-Cys(IRDye680)-Lys(Chelator)-Ahx-CMP$_9$. Figure 3-3 shows the structure of the three compound, compound ***[In^{111}+DTPA]-[IR680]-Ahx-^{NB}(GPO)$_9$*** contains DTPA as a chelator, compound ***[In^{111}+CHX-A''-DTPA]-[IR680]-Ahx-^{NB}(GPO)$_9$*** contains A″-DTPA which are known to have higher metal chelating affinity compared to DTPA, and compound ***[In^{111}+ DOTA]-[IR680]-Ahx-^{NB}(GPO)$_9$*** contains DOTA which has the highest metal binding affinity among all three chelators. None of the dual modality CMP showed marked accumulation of

radioactivity in the skeletal tissues (SPECT-CT) even though they were clearly targeted by CMP as evidenced by the near IR fluorescence signals (Figure 3-4). We are currently working on identifying the cause of metal dissociation from the CMP.

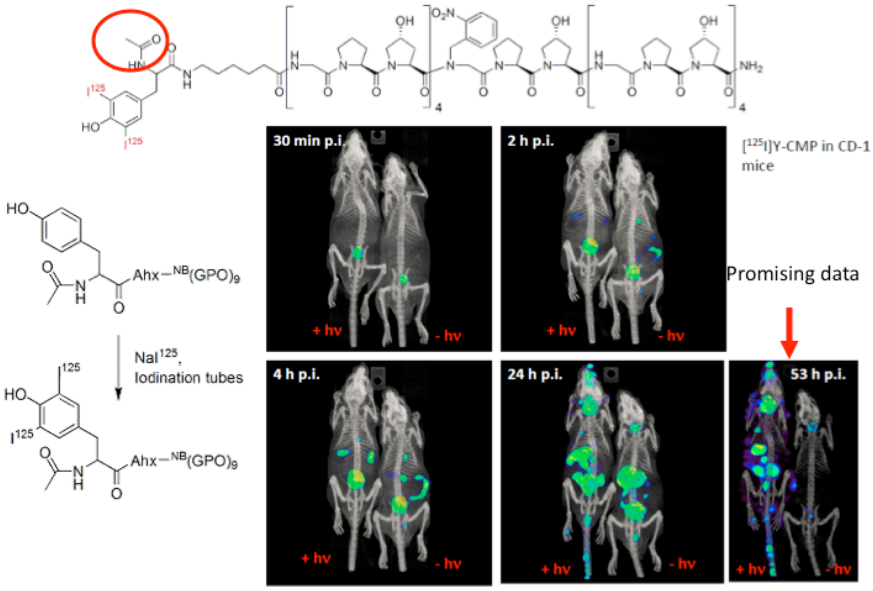

Figure 3-2. Structure of acetylated radiolabeled peptide and SPECT-CT of normal (lower right) mouse injected with this compound after decaging. The image again indicates presence of abundant amount of free iodines which are cleaved from the peptides.

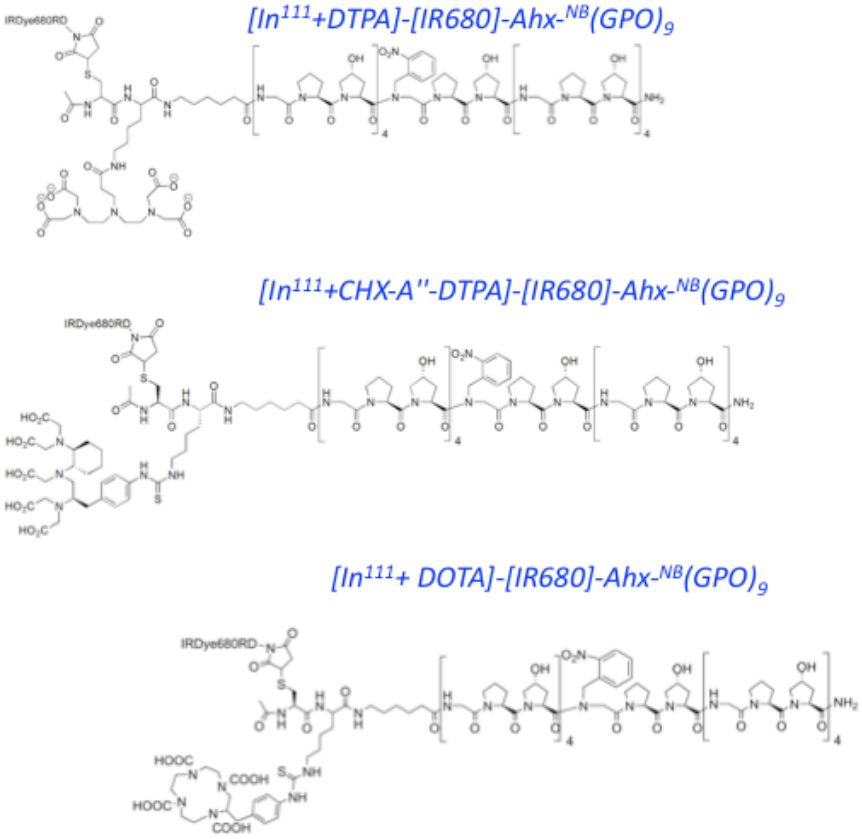

Figure 3-3. Structure of dual modality CMP. These CMPs have near IR fluorophores at the N-termini as well as metal binding chelators that can bind to In^{111}.

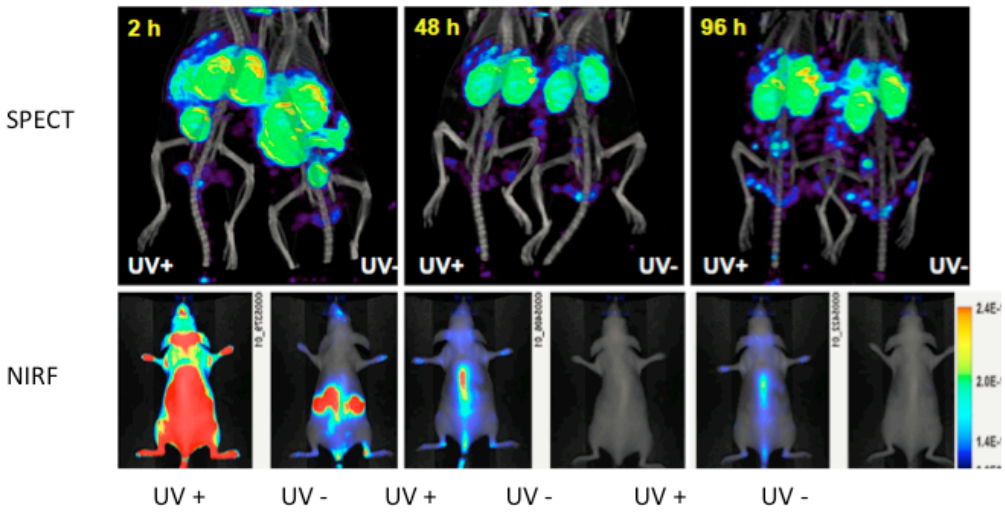

Figure 3-4. SPECT-CT and NIRF imaging of ***[In^{111}+ DOTA]-[IR680]-Ahx-^{NB}(GPO)$_9$*** in SKL mice. Although the NIRF images clearly indicates peptide uptake in the skeleton, the radioactivity do not colocalize with fluorescence suggesting that the In^{111} is detached from the peptide.

KEY RESEARCH ACCOMPLISHMENTS

During the past funding period (year 1), we have made major progress in the following areas.

1. Demonstration of CMP mediated in vivo targeting of tissues undergoing normal (e.g. skeleton) and pathological (arthritis) remodeling.
2. Demonstration of the use of CMP as collagen staining agent in SDS-PAGE gel and tissue sections.
3. Synthesis and *in vivo* targeting of dual modality CMPs which has both fluorescent and radioactive.

These research activities resulted in publication of 5 high impact research papers (in *Proc. Nat. Acad. Sci. USA*, *Bioconj. Chem., J. Vis. Exp. (JoVE), Curr. Opin. Chem. Biol*. and *Soft Matter*), 5 invited presentations in major institutions, and the PNAS publication was covered by over 20 major media outlets.

REPORTABLE OUTCOMES

Journal publications

1. Y. Li, and S. M. Yu, (2013) Targeting and mimicking collagens *via* triple helical peptide assembly. *Curr. Opin. Chem. Biol*., in press.

2. Y. Li, C. A. Foss, M. G. Pomper, and S. M. Yu (2013) Imaging denatured collagen strands *in vivo* and *ex vivo via* photo-triggered hybridization of caged collagen mimetic peptides. *J. Vis. Exp. (JoVE)*, in press.

3. Y. Li, D. Ho, H. Meng, T. R. Chan, B. An, H. Yu, B. Brodsky, A. S. Jun, and S. M. Yu (2013) Direct detection of collagenous proteins by fluorescently labeled collagen mimetic peptides. *Bioconj. Chem.* 24, 9.

4. Y. Li, C. A. Foss, D. D. Summerfield, J. J. Doyle, C. M. Torok, H.C. Dietz, M. G. Pomper and S. M. Yu (2012) Targeting Collagen Strands by Photo-Triggered Triple Helix Hybridization. *Proc. Nat. Acad. Sci. USA* 109, 14767.

5. P. J. Stahl, and S. M. Yu (2012) Encoding Cell-Instructive Cues to PEG-Based Hydrogels via Triple Helical Peptide Assembly, *Soft Matter* 8, 10408.

Degrees obtained that are supported by this award

- Ph.D. Yang Li : *Photo-triggered CMP-collagen hybridization*
- Ph.D. Patrick Stahl: *PEG hydrogel with CMP-mediated and tunable crosslinks*
- Ph.D. Tania Chan: *Mimetic approach for microvasculature engineering in collagen scaffolds*

Media Coverage

Publication, *PNAS* 109, 14767 (2012) on collagen targeting has been covered in over 20 major media outlets, including Science Daily, Medical News Today, American Association for Cancer Research, and Science360 (NSF sponsored radio program). Full list with direct link to the articles can be found below.

	media	link
	jhu news	http://releases.jhu.edu/2012/08/29/collagen-seeking-synthetic-protein-could-lead-doctors-to-tumor-locations/
	sciencedaily	http://www.sciencedaily.com/releases/2012/08/120829151147.htm
3	futurity	http://www.futurity.org/protein-sticks-to-damaged-collagen-near-cancer/
4	**medicalnewstoday**	http://www.medicalnewstoday.com/articles/249648.php
5	**medicine digest**	http://medicine.top10-digest.com/collagen-seeking-synthetic-protein-could-lead-doctors-to-tumor-locations/
6	**medicalnewstoday**	http://www.medicalnewstoday.com/releases/249691.php
7	**NCI**	http://www.cancer.gov/newscenter/cancerresearchnews/2012/SyntheticProteinTumorLocations
8	mideast clinics directory	http://www.mideastclinics.com/healthNews/5313/UU1/New-Ultraviolet-Light-Can-Pinpoint-Location-Of-Diseases.html#.UkRPF4bOWpV
9	plextek consulting	http://www.plextek.com/about-us/industry-news/29-medical-news/688-new-ultraviolet-light-could-pinpoint-tumour-locations.html
10	medicalquack	http://ducknetweb.blogspot.com/2012/09/collagen-seeking-synthetic-protein.html
11	alltop	http://holykaw.alltop.com/protein-sticks-to-cancer-damage-sites-video
12	ALN	http://www.alnmag.com/news/2012/08/synthetic-protein-leads-doctors-tumors-mice
13	ebiotrade	http://www.ebiotrade.com/newsf/2012-8/2012830155605327.htm
14	jhu HUB	http://hub.jhu.edu/2012/08/30/uv-tumor-detection
15	news-medical	http://www.news-medical.net/news/20120830/Johns-Hopkins-team-creates-synthetic-protein-that-can-help-locate-tumors.aspx
16	redorbit	http://www.redorbit.com/news/science/1112684089/doctors-medical-disorders-collagen-seeking-synthetic-protein-082912/
17	sciencecodex	http://www.sciencecodex.com/collagenseeking_synthetic_protein_could_lead_doctors_to_tumor_locations-97530
18	laboratoryequipment	http://www.laboratoryequipment.com/news/2012/08/synthetic-protein-can-lead-doctors-tumor-locations
19	ecancer.org	http://ecancer.org/news/3338.php
20	**AACR**	http://cancerdiscovery.aacrjournals.org/content/early/2012/09/11/2159-8290.CD-NB2012-107.full
21	**science360.gov**	http://www.science360.gov/radio
22	**nano.cancer.gov**	http://nano.cancer.gov/action/news/2012/oct/nanotech_news_2012-10-16c.asp
23	nanowerk	http://www.nanowerk.com/news2/newsid=27038.php

CONCLUSION

We made a significant progress in terms of understanding the in vivo targeting capacity of CMP both in normal and diseased tissues. The results were published in 5 peer-reviewed journals and were highly accepted by the biomedical field as evidenced by numerous coverage by major media outlets. Our progress in terms of developing radioactive CMP has been met with challenges; despite our attempts of developing 6 different types of radiolabeled and dual labeled peptide, we have yet to see in vivo targeting by radiological imaging techniques. This is mainly due to the instability of radioactive ions and metals as they are conjugated to the peptide. We are currently working on identifying the cause of the instability as well as the means to increase the stability.

References.

1. Jemal, A.*, et al.* Cancer statistics, 2003. *Ca-a Cancer Journal for Clinicians* **53**, 5-26 (2003).
2. Cretu, A. & Brooks, P.C. Impact of the non-cellular tumor microenvironment on metastasis: potential therapeutic and imaging opportunities. *Journal of Cellular Physiology* **213**, 391-402 (2007).
3. Tlsty, T.D. & Coussens, L.M. Tumor stroma and regulation of cancer development. *Annual Review of Pathology: Mechanisms of Disease* **1**, 119-150 (2006).
4. Friedl, P. & Wolf, K. Tumour-cell invasion and migration: Diversity and escape mechanisms. *Nature Reviews Cancer* **3**, 362-374 (2003).
5. Seftor, E.A.*, et al.* Epigenetic transdifferentiation of normal melanocytes by a metastatic melanoma microenvironment. *Cancer Research* **65**, 10164-10169 (2005).
6. Conklin, M.W.*, et al.* Aligned collagen is a prognostic signature for survival in human breast carcinoma. *The American Journal of Pathology* **178**, 1221-1232 (2011).
7. Burns-Cox, N., Avery, N.C., Gingell, J.C. & Bailey, A.J. Changes in collagen metabolism in prostate cancer: a host response that may alter progression. *Journal of Urology* **166**, 1698-1701 (2001).
8. Wang, A.Y., Mo, X., Chen, C.S. & Yu, S.M. Facile modification of collagen directed by collagen mimetic peptides. *Journal of the American Chemical Society* **127**, 4130-4131 (2005).
9. Mo, X., An, Y.J., Yun, C.S. & Yu, S.M. Nanoparticle-assisted visualization of binding interactions between collagen mimetic peptide and collagen fibers. *Angewandte Chemie International Edition* **45**, 2267-2270 (2006).
10. Yu, S.M., Li, Y. & Kim, D. Collagen mimetic peptides: progress towards functional applications. *Soft Matter* **7**, 7927-7938 (2011).
11. Li, Y., Mo, X., Kim, D. & Yu, S.M. Template-tethered collagen mimetic peptides for studying heterotrimeric triple-helical interactions. *Biopolymers* **95**, 94-104 (2011).
12. Rothenfluh, D.A., Bermudez, H., O'Neil, C.P. & Hubbell, J.A. Biofunctional polymer nanoparticles for intra-articular targeting and retention in cartilage. *Nature Materials* **7**, 248-254 (2008).
13. Zaheer, A.*, et al.* In vivo near-infrared fluorescence imaging of osteoblastic activity. *Nature Biotechnology* **19**, 1148-1154 (2001).
14. Hollander, A.P.*, et al.* Damage to type II collagen in aging and osteoarthritis starts at the articular surface, originates around chondrocytes, and extends into the cartilage with progressive degeneration. *The Journal of Clinical Investigation* **96**, 2859-2869 (1995).
15. Risteli, J. & Risteli, L. Products of bone collagen metabolism. in *Dynamics of Bone And Cartilage Metabolism* (eds. Seibel, M.J., Robins, S.P. & Bilezikian, J.P.) 391 (Academic Press, New York, 2006).
16. Judge, D.P.*, et al.* Evidence for a critical contribution of haploinsufficiency in the complex pathogenesis of Marfan syndrome. *The Journal of Clinical Investigation* **114**, 172-181 (2004).
17. Armendáriz-Borunda, J., and Rojkind, M. (1984) A simple quantitative method for collagen typing in tissue samples: its application to human liver with schistosomiasis. *Coll. Relat. Res. 4*, 35-47.
18. Nielsen, L. F., Moe, D., Kirkeby, S., and Garbarsch, C. (1998) Sirius red and acid fuchsin staining mechanisms. *Biotech. Histochem. 73*, 71-77.

Bioconjugate Chemistry

Communication

pubs.acs.org/bc

Direct Detection of Collagenous Proteins by Fluorescently Labeled Collagen Mimetic Peptides

Yang Li,[†] Daniel Ho,[‡] Huan Meng,[§] Tania R. Chan,[‡,∥] Bo An,[#] Hanry Yu,[⊥] Barbara Brodsky,[#] Albert S. Jun,[§] and S. Michael Yu*[,†,‡,∥]

[†]Department of Chemistry, [‡]Department of Materials Science and Engineering, and [∥]Institute for NanoBiotechnology, Johns Hopkins University, Baltimore, Maryland 21218, United States

[§]Wilmer Eye Institute, Johns Hopkins Medical Institutions, Baltimore, Maryland 21287, United States

[#]Department of Biomedical Engineering, Tufts University, Medford, Massachusetts 02155, United States

[⊥]Department of Physiology & MBI, National University of Singapore, IBN & SMART, Singapore

Supporting Information

ABSTRACT: Although fibrous collagens are major structural components of extracellular matrix in mammals, collagen overproduction is associated with many human diseases including cancers and fibrosis. Collagen is typically identified in biomedical research by Western blot and immunohistochemistry; however, anticollagen antibodies employed in these analyses are difficult to prepare and their affinities to collagen can diminish if collagen becomes denatured during analyses. Previously, we discovered that single-stranded collagen mimetic peptides [CMPs, sequence: $(GlyProHyp)_9$] can bind to denatured collagen chains by triple helix hybridization. Here, we present collagen-specific staining methods using simple CMPs conjugated to common fluorophores (e.g., carboxyfluorescein), which allow direct detection of collagens and collagen-like proteins in SDS-PAGE and in various mammalian tissue sections. By directly staining SDS-PAGE gels with fluorescently labeled CMPs, both intact (type I, II, and IV) and MMP-1 cleaved collagen (type I) chains as well as complement factor C1q were detected. Collagen bands containing as little as 5 ng were optically visualized, while no staining was observed for fibronectin, laminin, and a collection of proteins from mammalian cell lysate. The CMP was unable to stain collagen-like bacterial protein, which contains numerous charged amino acids that are believed to stabilize triple helix in place of Hyp. We also show that fluorescently labeled CMPs can specifically visualize collagens in fixed tissue sections (e.g., skin, cornea, and bone) more effectively than anticollagen I antibody, and allow facile identification of pathologic conditions in fibrotic liver tissues.

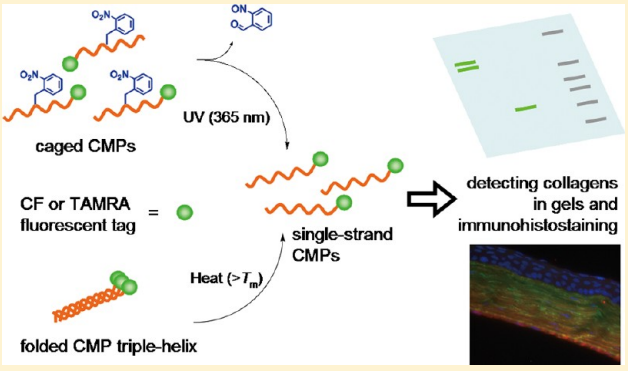

Fibrous collagens, a major structural component of the extracellular matrix (ECM), are largely found in connective tissues. Biosynthesis and degradation of collagens, which are mediated by growth factors and proteases secreted by cells, are widely studied in developmental biology,[1−3] wound healing, and aging.[4] Numerous human diseases including osteogenesis imperfecta,[5] atherosclerosis,[6] fibrosis,[7−10] arthritis,[11−14] and tumors[15] are associated with abnormalities in either the structure or metabolism of collagens.

Western blot and immunohistochemistry are the two most common techniques for detecting collagens,[5,7−15] where a particular type of collagen is identified by antibody binding. However, because the triple helical domains which constitute the major part of the fibrous collagen (type I and II) have a highly repetitive triplet amino acid sequence (Gly-X-Y) and a tight rod-like structure, it is difficult to generate antibodies with high specificities against fibrous collagens.[16,17] Therefore, extensive purification and selection steps, which involve multiple immunoaffinity purification against serum proteins and other noncollagenous ECM proteins, are needed to create collagen antibodies with low levels of cross-affinity. For antibodies that recognize the intact triple helical collagen epitopes, their affinity decreases dramatically when they are used in Western blot and in formalin-fixed and/or paraffin-embedded tissue samples, because collagens in those samples are partially denatured. Moreover, antibody detection usually requires overnight reactions and additional detection steps involving secondary antibodies labeled with either a reporter enzyme or a fluorescent dye, which are often tedious and time-consuming. Considering these limitations, we sought to develop a broad-spectrum collagen staining agent that is easy

Received: October 31, 2012
Revised: December 18, 2012
Published: December 19, 2012

   dx.doi.org/10.1021/bc3005842 | *Bioconjugate Chem.* 2013, 24, 9−16

to use and can bind not only to native collagens, but also to denatured fibrous collagens.

Here, we report a convenient collagen-specific staining method that is based on triple helix forming peptide probe, which can directly detect collagenous proteins in SDS-PAGE as well as in immunohistochemical staining (Figure 1). Previously,

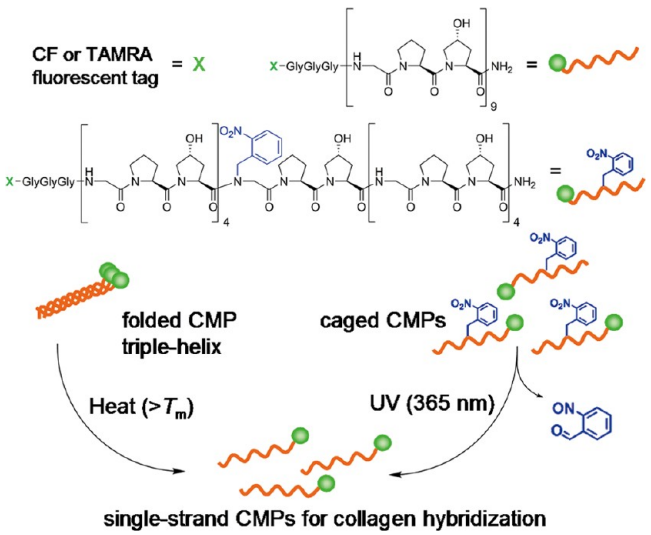

Figure 1. Structures of fluorescently labeled CMP and nitrobenzyl (NB) caged CMP, designated, respectively, as $CF(GPO)_9$ and $CF^{NB}(GPO)_9$ for CF labeled peptides, and schematic illustration of the two approaches (heat or UV activation) of generating single-stranded CMPs that can hybridize with collagen strands.

we discovered that single-strand collagen mimetic peptides [CMP, sequence: $(GPO)_x$, x = 6−10, O: hydroxyproline] can bind to unfolded collagen chains presumably through the formation of collagen−CMP heterotrimeric complexes.[18−25] The binding interaction originates from the unique triple helical structure of the collagens[26] and the inherently strong triple helical folding propensity of the CMPs.[27] Because CMPs self-assemble into homotrimers at room temperature which have little driving force for collagen binding, monomeric CMPs were generated by heating the peptide solution above the melting temperature of CMP just prior to applying to collagen substrates (Figure 1).[20−22,28] Although such thermally activated CMPs were successfully used for collagen tissue scaffold modification, they could not be used for *in vivo* experiments for concerns associated with heat-induced tissue damage. Recently, we developed a new type of CMP, namely, caged CMP [$(GPO)_4{}^{NB}GPO(GPO)_4$, Figure 1], whose triple helical folding can be controlled by UV light.[18] The caged CMP contains a photocleavable nitrobenzyl group attached to the central glycine of the peptide, which sterically prevents the CMP from folding into triple helix; yet, removal of the protective cage group by UV irradiation immediately recovers the folding and collagen binding abilities of CMP. Taking advantage of this efficient nonthermal trigger, we were able to employ CMP with strong triple helical propensity (high T_m) to perform *in vivo* collagen targeting studies in mice. This led to a surprising discovery that systemically delivered CMPs can target denatured collagens of tissues undergoing normal or pathologic remodeling.[18] Realizing the effectiveness of CMPs in targeting denatured collagen from these studies,[18,20,21,23] we set out to explore their full capacity for *in vitro* collagen/gelatin targeting using both the heat and light activation approaches (Figure 1). We were particularly interested in devising a new and easy collagen staining method that can help biomedical researchers and clinicians.

The rate of single-stranded CMPs self-assembling into homotrimers depends strongly on the concentration of CMP solution, because trimer formation follows a third-order folding kinetics.[29,30] Previously, for diagnostic imaging[18] and tissue scaffold engineering[21,22] applications, it was necessary to use high concentrations (50 μM to 0.2 mM) of CMPs in order to achieve binding levels high enough for collagen detection and for activating cellular response in collagen scaffolds. Since homotrimer formation is fast in concentrated CMP solutions, we employed thermal quenching and caging−decaging strategies to minimize the homotrimer formation in those studies. We realized that such strategies are not necessary for *in vitro* collagen staining application, since the concentration of CMP staining solutions can be very dilute (5−10 μM) with the trimerization half time on the order of hours at room temperature.[29,30] Therefore, we decided to test staining of SDS-PAGE and tissue sections using dilute solutions of CMPs.

We synthesized a peptide with $(GPO)_9$ sequence conjugated to a fluorophore through a flexible GGG linker to minimize fluorophore's influence on the peptide's triple helical folding process (Figure 1). We chose 5(6)-carboxyfluorescein (CF) and 5(6)-carboxytetramethylrhodamine (TAMRA) as the fluorophores, since they are compatible with standard fluorescence microscopes and imaging systems. All peptides were prepared by conventional solid-phase peptide synthesis (SPPS) using Fmoc/HBTU chemistry. The caged CMP was synthesized by inserting Fmoc(*N-o*-nitrobenzyl)Gly-OH in the middle of standard SPPS; the coupling reaction following the ^{NB}Gly was run using excess amount of Hyp and PyBroP as previously reported.[18] The fluorophores were conjugated to the amino termini of the peptide on the solid phase in the presence of PyAOP and DIPEA (see Supporting Information, Materials and Methods, and Figure S1).[31] The CD spectra and thermal melting curves of the fluorescent peptides (Supporting Information Figure S2) confirmed that the triple helical folding propensity of the peptides remains largely unchanged even when they are conjugated to the fluorophores. A sequence-scrambled peptide, $CF^SG_9P_9O_9$ (CF-GGG-PGOGPGPOPO-GOGOPPGOOPGGOOPPG) that cannot fold into triple helix was also prepared for comparison.[18]

To test the collagen probing capacity of the CMPs in SDS-PAGE under dilute CMP concentration, denatured type I collagen was resolved by SDS-PAGE. After the electrophoresis, the gel was washed with deionized water three times to remove the remaining SDS, and immersed in a solution of $CF(GPO)_9$ (6 μM) that had been preheated to 85 °C, which is above the peptide's melting temperature (see Supporting Information, Materials and Methods). After 3 h of incubation at room temperature followed by washing with deionized water, the gel was photographed using a fluorescent imaging system. The image of the gels showed distinct fluorescent emission from the bands of type I collagen chains (Figure 2A): not only were the α1 and α2 chains visible, but higher molecular weight bands corresponding to the naturally cross-linked collagen chains were also prominently visualized with high fluorescence intensity. Under dilute conditions, the thermally melted CMPs remain mostly in single strands immediately after the cooling due to their slow triple helix folding rate as described above.[29,30] These monomeric CMPs seem to be able to

dx.doi.org/10.1021/bc3005842 | *Bioconjugate Chem.* 2013, 24, 9−16

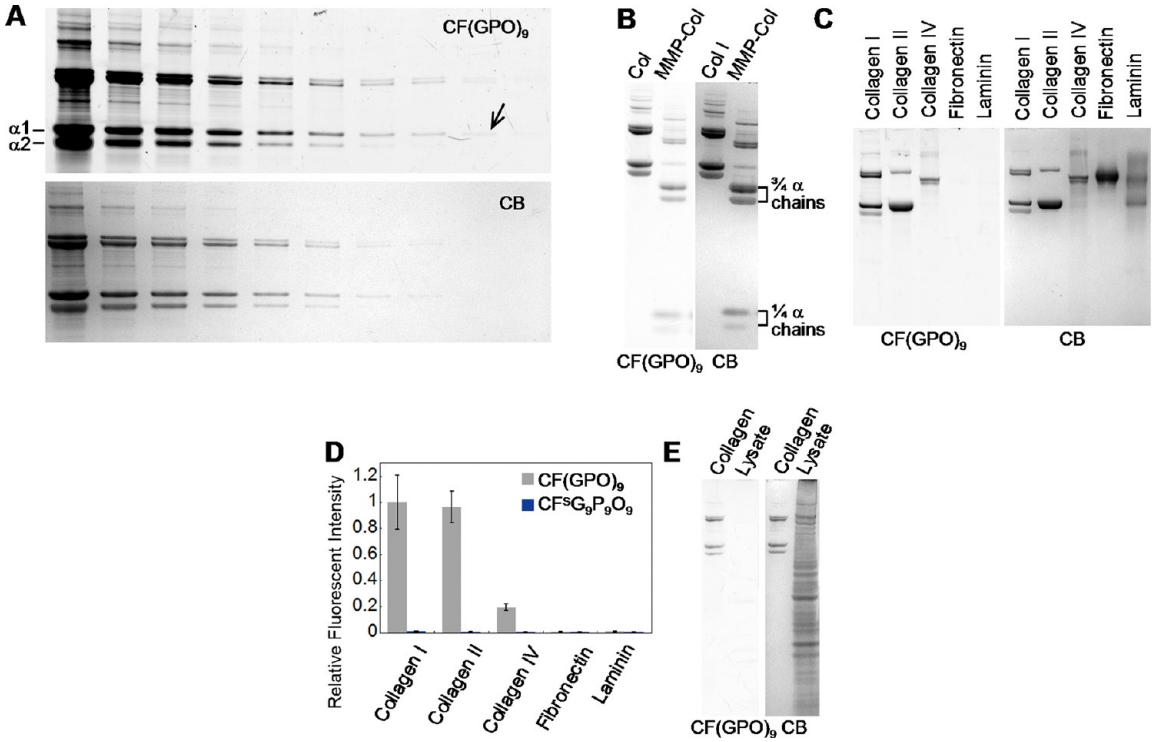

Figure 2. Detection of collagen in SDS-PAGE by heat-activated fluorescent CMPs. (A) SDS-PAGE loaded with a dilution series of type I collagen, stained and imaged first with $CF(GPO)_9$ (top panel) followed by Coomassie blue (CB) staining (bottom panel). From left to right, each lane was loaded with 4 μg, 2 μg, 1 μg, 500 ng, 250 ng, 125 ng, 62.5 ng, 31.2 ng, 15.6 ng, and 7.8 ng of denatured collagen, respectively. The arrow points to the least recognizable band in the image, which contains approximately 5 ng of collagen α1 chains. (B) SDS-PAGE of intact and MMP-1 cleaved type I collagens (3 μg in each lane) similarly stained with $CF(GPO)_9$ and CB. (C) SDS-PAGE loaded with collagen type I, II, IV; fibronectin; and laminin (2 μg of each protein), and stained with $CF(GPO)_9$ and CB. (D) Comparative fluorescence levels of the ECM protein bands in SDS-PAGE stained by $CF(GPO)_9$ (C) or $CF^SG_9P_9O_9$ (Supporting Information Figure S3). The measured fluorescence intensities were normalized by collagen I, and the experiment was performed in triplicate (±s.d.). (E) SDS-PAGE of collagen I (0.7 μg) and a lysate of HUVECs stained by $CF(GPO)_9$ and CB showing remarkable specificity of CMP for collagen detection. Images of the $CF(GPO)_9$ stained gels were recorded using a Typhoon fluorescent imager (λ_{ex} = 488 nm), and CB stained gels were photographed using a Gel Doc EQ system.

hybridize with the unfolded collagen chains in the SDS-PAGE, which are denatured and densely aggregated in the bands. To estimate the sensitivity of the CMP probe, a dilution series of type I collagen was run. The most dilute band that could be visualized by the $CF(GPO)_9$ probe contained as little as 5 ng of collagen chains (Figure 2A, arrow), which is similar to the sensitivity level of the conventional Coomassie brilliant blue (CB) staining (Figure 2A bottom panel). We also found out that enzymatically digested collagen fragments can be readily visualized on SDS-PAGE by the heat-activated $CF(GPO)_9$ just as well as the UV activated caged peptide previously reported from our group (Figure 2B).[18]

We further determined the binding specificity of $CF(GPO)_9$ for different collagen types and other major ECM proteins. Fluorescent images of the gel after SDS-PAGE showed that $CF(GPO)_9$ binds to collagen types I, II, and IV but has no affinity to fibronectin and laminin (Figure 2C). Same gel stained with the sequence-scrambled peptide $CF^SG_9P_9O_9$ revealed no collagen bands (Supporting Information Figure S3). These results clearly show that the CMPs bind by triple helical hybridization and only to proteins with triple helical domains. Intensity of the fluorescence emission in each collagen lane (Figure 2D) indicated that type IV collagen was stained to a lesser degree than the type I and II collagens. This is most likely because the type IV collagen has lower triple-helical content due to the presence of large globular noncollagenous domains, as well as over 20 interruptions in the collagenous domain that break up the triple helix.[32] Finally, when $CF(GPO)_9$ was used to stain the SDS-PAGE of whole cell lysate of human umbilical vein endothelial cells (HUVEC), no protein band was visualized (Figure 2E). This result demonstrates the remarkable specificity of the CMP probe for detecting collagen strands.

Although the Gly-*X*-*Y* triplet repeat is the signature protein sequence of collagen family, a similar sequence is also found in several noncollagenous proteins, typically as a triple helix-triple helix association domain of a larger protein (e.g., mannose binding protein and complement factor C1q).[26] The Gly-*X*-*Y* repeats capable of forming triple helical structure are also found on the surface of bacteria and viruses.[19,33,34] We were curious to see if these collagen-like domains can also be detected in SDS-PAGE by CMP binding. We tested two proteins: the complement protein C1q which is constructed of eighteen globular heads connected to six collagen-like triple helical assemblies,[35,36] and a recombinant protein, Scl2.28CL, derived from the cell-surface protein (Scl2) of *Streptococcus pyogenes* previously reported to form collagen-like triple helices.[37] The Scl2 folds into lollipop-like structure similar to C1q monomers and is speculated to interact with mammalian collagens and proteins with collagenous domains (e.g., macrophage scavenger receptor[38]), facilitating their adhesion to host cells and tissues.[19,37,38] The collagen-like domain of complement factor C1q is rich in Hyp and Pro, which are strong triple helix stabilizers, respectively, in the positions *X* and *Y* of the Gly-*X*-*Y*

dx.doi.org/10.1021/bc3005842 | *Bioconjugate Chem.* 2013, 24, 9−16

repeats;[39] however, in the Scl 2 protein, these positions are populated by charged amino acids[37] which are believed to stabilize collagen triple helix by electrostatic interactions.[40]

We found out that $CF(GPO)_9$ can stain the SDS-PAGE bands of C1q chains almost as effectively as collagens (Figure 3A). This indicates that the CMPs are capable of hybridizing

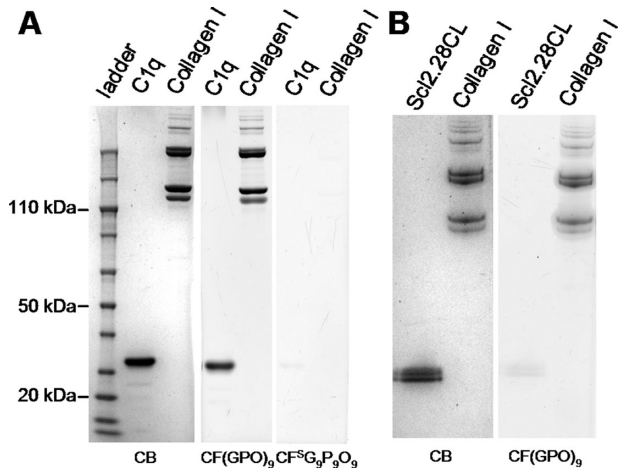

Figure 3. SDS-PAGE of collagen-like proteins stained with CMP. (A) SDS-PAGE loaded with 2 μg of complement factor C1q and type I collagen, stained by CB, $CF(GPO)_9$, or $CF^SG_9P_9O_9$, showing specific visualization of the C1q chains by $CF(GPO)_9$ hybridization. (B) SDS-PAGE loaded with 2.5 μg of type I collagen and streptococcal collagen-like protein Scl2.28CL stained by $CF(GPO)_9$, showing almost no staining of the Scl2.28CL band.

with the collagen-like domain of the C1q chains. In drastic contrast, $CF(GPO)_9$ failed to stain the Scl2.28CL bands (Figure 3B). In mammalian collagens, hydroxyprolines play a critical role in folding and stabilization of the triple helical structure,[27] while collagen-like domains of bacterial proteins that lack Hyp rely, in part, on charge−charge interactions for making stable triple helix.[40] Heat-denatured mammalian collagens partially recover their triple helical structure and turn into gelatin when cooled.[41] The Scl2.28CL chains, however, are unable to refold into triple helix after denaturation.[42,43] The results suggest that CMP can hybridize with the denatured strands of the Hyp-rich collagen and C1q, but it does not make stable heterotrimeric helices with collagen-like sequences of Scl2, presumably because the CMP is a neutral peptide that cannot participate in electrostatic interactions and because of inherently low triple helix folding propensity of the Pro-poor Scl2 sequence.

Compared to conventional antibody-mediated detection, CMP probes are more convenient to use. Antibody binding in Western blot requires transferring the proteins from PAGE gel onto a polyvinylidene difluoride (PVDF) or nitrocellulose membrane, followed by blocking, and long hours of immunoreactions. In contrast, because of the small size and high affinity of CMPs, detection of collagen by CMP probes can be performed directly in gels, without transfer and blocking, and in a relatively short period of time. In addition, the CMP hybridization relies on the overall secondary structure of the proteins instead of a few well-defined epitopes. Therefore, even fragments of collagen chains can be recognized, a feature useful for studying collagen degradation, which is common to many degenerative diseases (e.g., arthritis). The main limitation of the CMP probes is that the probes cannot distinguish different collagen types, since the Pro- and Hyp-rich Gly-*X*-*Y* motif recognized by the CMP is universal in all types of collagens. Therefore, CMP probes should be considered a broad-spectrum collagen targeting molecule.

While Western blot is useful for molecular-level detection and quantification of collagens, direct visualization of collagens can help identify the location of collagens in tissue samples and a pathological state of diseased tissues with abnormal collagen remodeling activity. In immunohistochemistry, harvested

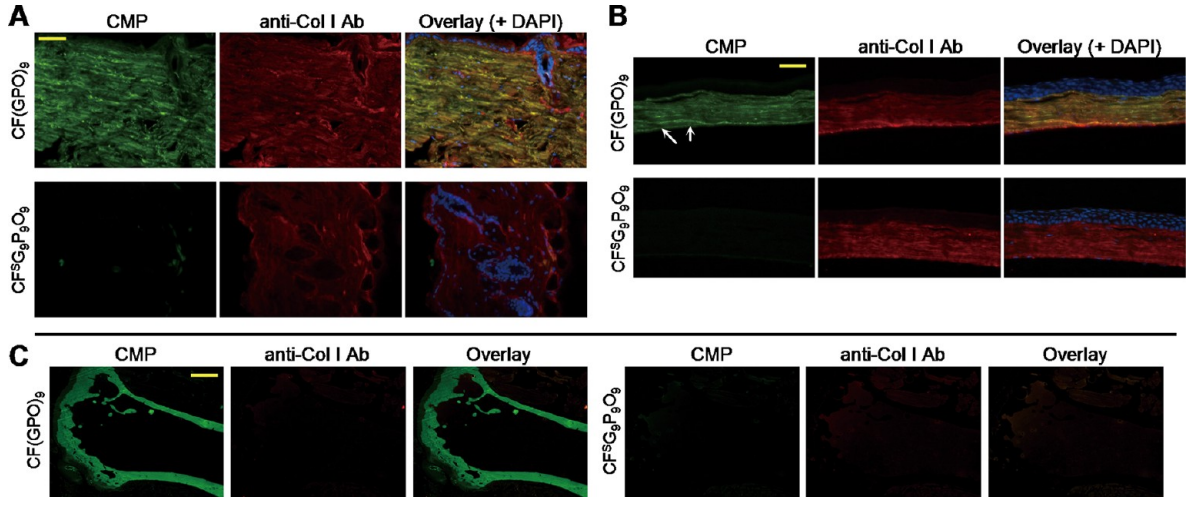

Figure 4. Histological tissue staining using photoactivated caged CMPs. Fluorescent micrographs of fixed mouse skin (A) and cornea (B) sections probed by phototriggered $CF^{NB}(GPO)_9$ (in green, top panels) or scrambled peptide $CF^SG_9P_9O_9$ (in green, bottom panels) and costained with anticollagen I antibody (red) and DAPI (blue). The $CF^{NB}(GPO)_9$ staining revealed fine irregular collagen fibers of the dermis (A) and parallel collagen fibrils in the corneal stroma as well as the collagens in Descemet's membrane (arrows) (B). (C) Fluorescent images of paraffin embedded, demineralized mouse tibia sections stained with phototriggered $CF^{NB}(GPO)_9$ (green, left panels) or scrambled peptide $CF^SG_9P_9O_9$ (green, right panels), and costained with anticollagen I antibody (red), showing prominent CMP signals and only weak nonspecific antibody signals from the collagenous bone. Concentrations of $CF^{NB}(GPO)_9$ and $CF^SG_9P_9O_9$ used in this study are as follows: (A), 25 μM; (B), 2.5 μM; (C), 8 μM. (scale bars: A, 50 μm; B, 100 μm; C, 0.5 mm).

dx.doi.org/10.1021/bc3005842 | *Bioconjugate Chem.* 2013, 24, 9−16

tissues are often preserved by fixation, followed by cryosectioning and probing by different antibodies to determine the location of biomolecules. The fixation step is needed to keep the cellular components and overall tissue morphology from deterioration during histological study and long-term storage; however, the fixing procedures, which often include heat (microwave), and treatment with organic solvents (e.g., acetone and alcohols) and cross-linking reagents (e.g., paraformaldehyde), can denature the collagen molecules.[44] Although such denaturation can reduce the number of epitopes for antibody binding, it could have an opposite effect on CMP probes. The denaturation may increase the number of binding sites for the CMP probes because the CMP preferentially hybridizes with denatured collagen strands over intact collagen fibers. For this reason, we anticipated that the fluorescent CMP probes could be an ideal collagen staining agent for histology. Since addition of heat-activated peptide probes to tissue sections could result in further tissue damage and destruction of other heat-sensitive antibodies (for co-staining), the caged CMP that can be activated by UV light was used for staining tissue sections.

Caged CMP, $CF^{NB}(GPO)_9$, was applied to tissue sections (fixed tissue sections from mouse skin, cornea, and bone), followed by exposure to UV light to activate collagen binding. Anticollagen I antibody (second antibody: anti-rabbit-Alexa-Fluor594) was also applied to the tissue samples for comparison (see Supporting Information, Materials and Methods). As shown in Figure 4A and B, the decaged $CF(GPO)_9$ effectively stained the collagen-rich dermis layer of the fixed mouse skin and the stroma of the cornea sections. The control groups stained by scrambled peptide $CF^{S}G_9P_9O_9$ showed no discernible binding under identical experimental conditions (Figure 4A and B, bottom panels). The fluorescent signals from the $CF(GPO)_9$ overlapped largely with those from the antibody, which confirmed the specificity of the probes for the collagen fibrils. Compared to the anticollagen antibody, the $CF(GPO)_9$ showed more intense signals, which also revealed finer details of the collagen fibril organization in the dermis and the corneal stroma (Figure 4A and B). In addition, a bright green line corresponding to the Descemet's membrane of cornea, which contains type VIII collagen, was clearly visualized by the CMP probe (Figure 4B, arrow). We also noticed that the processing of the tissue seems to enhance the CMP binding. Paraformaldehyde fixed cornea samples were significantly brighter than the fresh unfixed samples when identical CMP staining and imaging protocols were employed (Supporting Information Figure S4). In particular, the mouse tibia bone sections that have undergone an acidic demineralization process as well as fixation and paraffin embedding exhibited strong $CF(GPO)_9$ signals, but almost no collagen antibody signal was detected (Figure 4C). It is highly likely that the tertiary protein structure of the epitopes targeted by the collagen antibody had been compromised by the heat during the paraffin-embedding and the highly acidic demineralization process; yet, the CMP probe can still target such collagens because it recognizes the unfolded secondary protein structure that is prevalent in collagens.

The CMP probe's remarkable ability to target collagen in bone even after acidic demineralization and extensive preservation process demonstrates the robustness and versatility of the CMP mediated collagen staining. Histological preservation and processing often cause alteration or masking of epitopes targeted by immunohistochemical agents. Even for the same target biomolecule, different histological processing (e.g., frozen vs paraffin-embedded) may require different types of primary antibody. Sometimes, a heat- or enzyme-induced antigen retrieval step is necessary to improve the antibody binding.[45] In contrast, CMP probes recognize the secondary protein structure, the metastable polyproline-II-like helix that is waiting for triple helix hybridization partners. For this reason, perturbation of the tertiary and quaternary protein structures of collagen seems to have little effect on the binding affinity of CMP to collagen strands.

To showcase the ability of CMP to identify pathological conditions, a set of healthy and fibrotic rat liver sections were stained utilizing the phototriggered CMP probe. Two common fibrosis models were tested: a fibrosis induced by repetition of a toxic insult, thioacetamide (TAA), to the liver, and the secondary biliary fibrosis model induced by bile duct ligation (BDL).[46] Because the liver tissues emit strong autofluorescence whose spectrum overlaps with the emission spectrum of CF,[47] TAMRA-$^{NB}(GPO)_9$ was used for the liver fibrosis staining. In addition, $CuSO_4$ solution was applied to the tissue sections during optical imaging to selectively reduce the lipofuscin-like background autofluorescence (see Materials and Methods, Supporting Information).[48] As shown in Figure 5, TAMRA-$(GPO)_9$ revealed minimal collagen staining in healthy liver: collagens can only be found surrounding the major vessels in the portal area. In the tissue sections of TAA and BDL fibrotic models, the CMP successfully exposed the abnormal presence

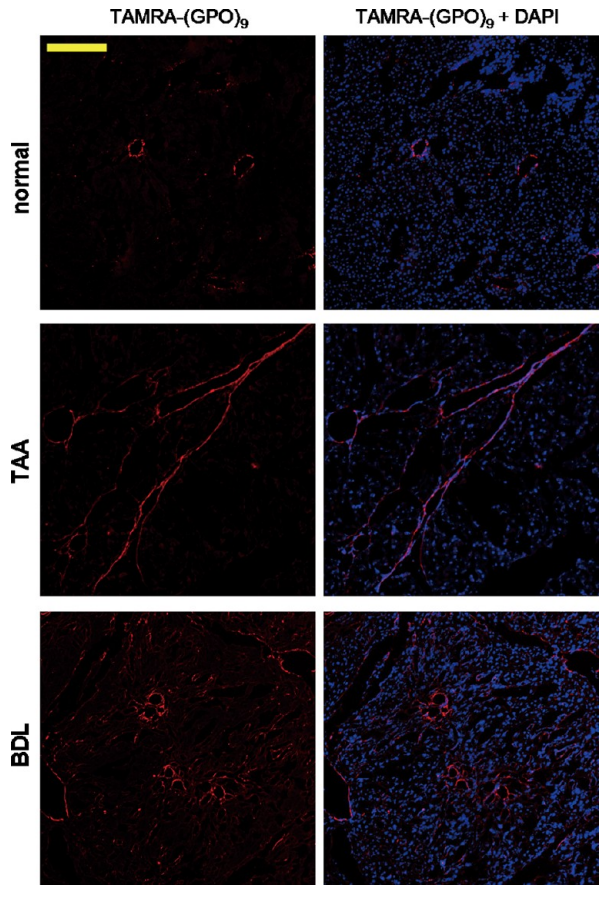

Figure 5. Identification of fibrotic conditions using CMP staining. Fluorescence micrographs of normal and fibrotic rat liver sections (TAA and BDL) stained with phototriggered TAMRA-$^{NB}(GPO)_9$ (10 μM, in red) and DAPI (in blue), showing distinct collagen distributions in fibrotic liver models. (scale bar: 200 μm).

dx.doi.org/10.1021/bc3005842 | *Bioconjugate Chem.* 2013, 24, 9–16

of collagens.[49,50] In the TAA sample, long and thin bridged septa of aggregated collagens were readily seen, and in the BDL model, excess fibrotic collagens were detected around the circular proliferating bile ducts (Figure 5). These results are consistent with the hepatic fibrosis patterns for those classical fibrosis models.[46] Compared to Masson Trichrome staining, a common non-immunochemical staining procedure that chemically stains collagen fibers in blue on top of pink-colored cellular background (Supporting Information, Figure S5), the fluorescent CMP probe offers more clear and collagen-specific imaging as well as simultaneous co-staining with other biomarkers that can be easily distinguished by the multicolor channels of fluorescence microscope. The results demonstrate the potential application of CMP probes not only for histology of clinical biopsies, but also for live imaging and targeting of fibrotic tissues.[51]

In summary, this study has validated the use of fluorescently labeled collagen mimetic peptides for direct and efficient detection of Hyp-rich collagenous proteins in SDS-PAGE and immunohistostaining. Our results indicate that CMPs are highly effective at staining collagens in extensively processed tissue sections which are not easily probed by conventional antibodies. We believe that the fluorescent CMP is an excellent alternative to collagen antibodies for detecting fibrous collagens in various assays and tissue imaging. Although CMP probes cannot distinguish different types of collagens, they offer higher specificity to collagens when compared to conventional staining agents.[52] Conventional collagen staining agents such as Sirus Red rely on electrostatic interactions for binding to collagens; negatively charged probes bind to positively charged collagens. Therefore, the staining is not specific to collagen and can stain other proteins with high content of basic amino acids.[53] Since CMP recognizes the triple helical amino acid sequence of collagen, it is a true broad-spectrum collagen-specific staining agent with almost no binding affinity for noncollagenous proteins as demonstrated in this paper. As a potent collagen targeting molecule, CMP is a structurally simple peptide that is easy to prepare and conjugate to other bioactive moieties. The two orthogonal activation mechanisms (Figure 1: heat activation of CMP and light activation of caged CMP) provide great flexibility for the incorporation of additional functionalities to this peptide: the heat activation system is suitable for conjugation of chemically reactive compounds that may be sensitive to UV light or photocleaved byproducts, while the light activation system is suitable for conjugation of delicate biomolecules (e.g., proteins) that might be incompatible with heat. The ability to synthesize more complex CMP derivatives that can target collagen strands may lead to new applications in tissue scaffold engineering, collagen-targeted drug delivery, and *in vivo* collagen imaging.

■ ASSOCIATED CONTENT

Supporting Information

Materials and Methods, MALDI-TOF and CD analysis of the peptides, control gel images, additional fluorescent immuohistostaining images, and Masson Trichrome stained tissue sections. This material is available free of charge via the Internet at http://pubs.acs.org.

■ AUTHOR INFORMATION

Corresponding Author

*Tel: 1-410-516-8935. E-mail: yu@jhu.edu.

Notes

The authors declare no competing financial interest.

■ ACKNOWLEDGMENTS

We thank Drs. Catherine Foss and Collin Torok for the gift of the mouse tibia bone sections, Jie Yan and Yuzhan Kang for the gift of rat liver samples, and Dr. Lijuan He for technical assistance and informative discussion. We also thank Dr. Michael McCaffery of the Integrated Imaging Center at Johns Hopkins University for the access to the Typhoon 9410 imager. This work was supported by grants from NIAMS/NIH (R01-AR060484) and DOD (W81XWH-12-1-0555) awarded to S.M.Y., and grants from NIH, K08-EY15523, R01-EY019874 awarded to A.S.J. and P30-EY001765 awarded to Wilmer Microscopy Core Facility, as well as NIH EB011620 awarded to B.B.

■ ABBREVIATIONS

SDS-PAGE, sodium dodecyl sulfate polyacrylamide gel electrophoresis; Fmoc, fluorenylmethyloxycarbonyl; HBTU, 2-(1*H*-benzotriazole-1-yl)-1,1,3,3-tetramethyluronium hexafluorophosphate; PyBroP, bromotripyrrolidinophosphonium hexafluorophosphate; PyAOP, (7-azabenzotriazol-1-yloxy)-tripyrrolidinophosphonium hexafluorophosphate; DIPEA, *N*,*N*-diisopropylethylamine; CD, circular dichroism; MMP, matrix metalloproteinase; DAPI, 4′,6-diamidino-2-phenylindole

■ REFERENCES

(1) Nagata, K. (2003) HSP47 as a collagen-specific molecular chaperone: function and expression in normal mouse development. *Semin. Cell Dev. Biol. 14*, 275−282.

(2) Quantock, A. J., and Young, R. D. (2008) Development of the corneal stroma, and the collagen-proteoglycan associations that help define its structure and function. *Dev. Dyn. 237*, 2607−2621.

(3) von der Mark, H., von der Mark, K., and Gay, S. (1976) Study of differential collagen synthesis during development of the chick embryo by immunofluorescence: I. Preparation of collagen type I and type II specific antibodies and their application to early stages of the chick embryo. *Dev. Biol. 48*, 237−249.

(4) Fisher, G. J., Kang, S., Varani, J., Bata-Csorgo, Z., Wan, Y., Datta, S., and Voorhees, J. J. (2002) Mechanisms of photoaging and chronological skin aging. *Arch. Dermatol. 138*, 1462−1470.

(5) Willaert, A., Malfait, F., Symoens, S., Gevaert, K., Kayserili, H., Megarbane, A., Mortier, G., Leroy, J. G., Coucke, P. J., and De Paepe, A. (2009) Recessive osteogenesis imperfecta caused by LEPRE1 mutations: clinical documentation and identification of the splice form responsible for prolyl 3-hydroxylation. *J. Med. Genet. 46*, 233−241.

(6) Rekhter, M. D. (1999) Collagen synthesis in atherosclerosis: too much and not enough. *Cardiovasc. Res. 41*, 376−384.

(7) Haist, V., Ulrich, R., Kalkuhl, A., Deschl, U., and Baumgartner, W. (2012) Distinct spatio-temporal extracellular matrix accumulation within demyelinated spinal cord lesions in theiler's murine encephalomyelitis. *Brain Pathol. 22*, 188−204.

(8) He, W., Zhang, L. N., Ni, A. G., Zhang, Z. P., Mirotsou, M., Mao, L., Pratt, R. E., and Dzau, V. J. (2010) Exogenously administered secreted frizzled related protein 2 (Sfrp2) reduces fibrosis and improves cardiac function in a rat model of myocardial infarction. *Proc. Natl. Acad. Sci. U.S.A. 107*, 21110−21115.

(9) Ulsamer, A., Wei, Y., Kim, K. K., Tan, K., Wheeler, S., Xi, Y., Thies, R. S., and Chapman, H. A. (2012) Axin pathway activity regulates in vivo pY654-beta-catenin accumulation and pulmonary fibrosis. *J. Biol. Chem. 287*, 5164−5172.

(10) Kim, K. K., Wei, Y., Szekeres, C., Kugler, M. C., Wolters, P. J., Hill, M. L., Frank, J. A., Brumwell, A. N., Wheeler, S. E., Kreidberg, J. A., and Chapman, H. A. (2009) Epithelial cell alpha3 beta1 integrin

links beta-catenin and Smad signaling to promote myofibroblast formation and pulmonary fibrosis. *J. Clin. Invest. 119*, 213−224.
(11) Mo, X. T., Guo, S. C., Xie, H. Q., Deng, L., Zhi, W., Xiang, Z., Li, X. Q., and Yang, Z. M. (2009) Variations in the ratios of co-cultured mesenchymal stem cells and chondrocytes regulate the expression of cartilaginous and osseous phenotype in alginate constructs. *Bone 45*, 42−51.
(12) Shen, J. B., Yang, M. Z., Jiang, H., Ju, D. H., Zheng, J. P., Xu, Z. H., Liao, T. D., and Li, L. (2011) Arterial injury promotes medial chondrogenesis in Sm22 knockout mice. *Cardiovasc. Res. 90*, 28−37.
(13) Cairns, D. M., Uchimura, T., Kwon, H., Lee, P. G., Seufert, C. R., Matzkin, E., and Zeng, L. (2010) Muscle cells enhance resistance to pro-inflammatory cytokine-induced cartilage destruction. *Biochem. Biophys. Res. Commun. 392*, 22−28.
(14) Rankin, K. S., Lakey, R. L., Gerrand, C. H., Sprowson, A. P., McCaskie, A. W., and Birch, M. A. (2010) A novel in vitro model to investigate behavior of articular chondrocytes in osteoarthritis. *J. Rheumatol. 37*, 426−431.
(15) Chen, P. S., Su, J. L., Cha, S. T., Tarn, W. Y., Wang, M. Y., Hsu, H. C., Lin, M. T., Chu, C. Y., Hua, K. T., Chen, C. N., Kuo, T. C., Chang, K. J., Hsiao, M., Chang, Y. W., Chen, J. S., Yang, P. C., and Kuo, M. L. (2011) miR-107 promotes tumor progression by targeting the let-7 microRNA in mice and humans. *J. Clin. Invest. 121*, 3442−3455.
(16) Srinivas, G. R., Chichester, C. O., Barrach, H. J., Pillai, V., and Matoney, A. L. (1994) Production of Type II collagen specific monoclonal antibodies. *Immunol. Invest. 23*, 85−98.
(17) Chichester, C., Barrach, H. J., Chichester, A., Matoney, A., and Srinivas, G. R. (1991) Evidence for polyreactivity seen with monoclonal antibodies produced against type II collagen. *J. Immunol. Methods 140*, 259−267.
(18) Li, Y., Foss, C. A., Summerfield, D. D., Doyle, J. J., Torok, C. M., Dietz, H. C., Pomper, M. G., and Yu, S. M. (2012) Targeting collagen strands by photo-triggered triple-helix hybridization. *Proc. Natl. Acad. Sci. U.S.A. 109*, 14767−14772.
(19) Yu, S. M., Li, Y., and Kim, D. (2011) Collagen mimetic peptides: progress towards functional applications. *Soft Matter 7*, 7927−7938.
(20) Wang, A. Y., Mo, X., Chen, C. S., and Yu, S. M. (2005) Facile modification of collagen directed by collagen mimetic peptides. *J. Am. Chem. Soc. 127*, 4130−4131.
(21) Wang, A. Y., Foss, C. A., Leong, S., Mo, X., Pomper, M. G., and Yu, S. M. (2008) Spatio-temporal modification of collagen scaffolds mediated by triple helical propensity. *Biomacromolecules 9*, 1755−1763.
(22) Wang, A. Y., Leong, S., Liang, Y. C., Huang, R. C. C., Chen, C. S., and Yu, S. M. (2008) Immobilization of growth factors on collagen scaffolds mediated by polyanionic collagen mimetic peptides and its effect on endothelial cell morphogenesis. *Biomacromolecules 9*, 2929−2936.
(23) Mo, X., An, Y. J., Yun, C. S., and Yu, S. M. (2006) Nanoparticle-assisted visualization of binding interactions between collagen mimetic peptide and collagen fibers. *Angew. Chem., Int. Ed. 45*, 2267−2270.
(24) Li, Y., Mo, X., Kim, D., and Yu, S. M. (2011) Template-tethered collagen mimetic peptides for studying heterotrimeric triple-helical interactions. *Biopolymers 95*, 94−104.
(25) Lee, H. J., Lee, J.-S., Chansakul, T., Yu, C., Elisseeff, J. H., and Yu, S. M. (2006) Collagen mimetic peptide-conjugated photopolymerizable PEG hydrogel. *Biomaterials 27*, 5268−5276.
(26) Engel, J., and Bächinger, H. P. (2005) Structure, stability and folding of the collagen triple helix. In *Collagen* (Brinckmann, J., Notbohm, H., and Müller, P. K., Eds.) pp 7−33, Springer Verlag, Berlin.
(27) Shoulders, M. D., and Raines, R. T. (2009) Collagen structure and stability. *Annu. Rev. Biochem. 78*, 929−958.
(28) Chan, T. R., Stahl, P. J., and Yu, S. M. (2011) Matrix-bound VEGF mimetic peptides: design and endothelial cell activation in collagen scaffolds. *Adv. Funct. Mater. 21*, 4252−4262.
(29) Boudko, S., Frank, S., Kammerer, R. A., Stetefeld, J., Schulthess, T., Landwehr, R., Lustig, A., Bächinger, H. P., and Engel, J. (2002) Nucleation and propagation of the collagen triple helix in single-chain and trimerized peptides: transition from third to first order kinetics. *J. Mol. Biol. 317*, 459−470.
(30) Ackerman, M. S., Bhate, M., Shenoy, N., Beck, K., Ramshaw, J. A. M., and Brodsky, B. (1999) Sequence dependence of the folding of collagen-like peptides. *J. Biol. Chem. 274*, 7668−7673.
(31) Stahl, P. J., Cruz, J. C., Li, Y., Yu, S. M., and Hristova, K. (2012) On-the-resin N-terminal modification of long synthetic peptides. *Anal. Biochem. 424*, 137−139.
(32) Khoshnoodi, J., Pedchenko, V., and Hudson, B. G. (2008) Mammalian collagen IV. *Microsc. Res. Technol. 71*, 357−370.
(33) Bamford, D. H., and Bamford, J. K. H. (1990) Collagenous proteins multiply. *Nature 344*, 497−497.
(34) Smith, M. C. M., Burns, N., Sayers, J. R., Sorrell, J. A., Casjens, S. R., and Hendrix, R. W. (1998) Bacteriophage collagen. *Science 279*, 1834−1834.
(35) Kishore, U., and Reid, K. B. M. (1999) Modular organization of proteins containing C1q-like globular domain. *Immunopharmacology 42*, 15−21.
(36) Tschopp, J. (1982) Kinetics of activation of the first component of complement (C1) by IgG oligomers. *Mol. Immunol. 19*, 651−657.
(37) Xu, Y., Keene, D. R., Bujnicki, J. M., Höök, M., and Lukomski, S. (2002) Streptococcal Scl1 and Scl2 proteins form collagen-like triple helices. *J. Biol. Chem. 277*, 27312−27318.
(38) Andersson, L., and Freeman, M. W. (1998) Functional changes in scavenger receptor binding conformation are induced by charge mutants spanning the entire collagen domain. *J. Biol. Chem. 273*, 19592−19601.
(39) Rosano, C. L., Braun, C. B., and Hurwitz, C. (1987) A method for serum C1q based on its hydroxyproline content. *Clin. Chem. 33*, 398−400.
(40) Mohs, A., Silva, T., Yoshida, T., Amin, R., Lukomski, S., Inouye, M., and Brodsky, B. (2007) Mechanism of stabilization of a bacterial collagen triple helix in the absence of hydroxyproline. *J. Biol. Chem. 282*, 29757−29765.
(41) Leikina, E., Mertts, M. V., Kuznetsova, N., and Leikin, S. (2002) Type I collagen is thermally unstable at body temperature. *Proc. Natl. Acad. Sci. U.S.A. 99*, 1314−1318.
(42) Cheng, H., Rashid, S., Yu, Z., Yoshizumi, A., Hwang, E., and Brodsky, B. (2010) Location of glycine mutations within a bacterial collagen protein affects degree of disruption of triple-helix folding and conformation. *J. Biol. Chem. 286*, 2041−2046.
(43) Yoshizumi, A., Yu, Z., Silva, T., Thiagarajan, G., Ramshaw, J. A. M., Inouye, M., and Brodsky, B. (2009) Self-association of streptococcus pyogenes collagen-like constructs into higher order structures. *Protein Sci. 18*, 1241−1251.
(44) Bächinger, H. P., and Morris, N. P. (1990) Analysis of the thermal stability of type II collagen in various solvents used for reversed-phase high performance chromatography. *Matrix 10*, 331−338.
(45) Hecke, D. V. (2002) Routine immunohistochemical staining today: choices to make, challenges to take. *Journal of Histotechnology 25*, 45−54.
(46) Starkel, P., and Leclercq, I. A. (2011) Animal models for the study of hepatic fibrosis. *Best Practice & Research Clinical Gastroenterology 25*, 319−333.
(47) Croce, A. C., De Simone, U., Freitas, I., Boncompagni, E., Neri, D., Cillo, U., and Bottiroli, G. (2010) Human liver autofluorescence: An intrinsic tissue parameter discriminating normal and diseased conditions. *Lasers Surg. Med. 42*, 371−378.
(48) Schnell, S. A., Staines, W. A., and Wessendorf, M. W. (1999) Reduction of lipofuscin-like autofluorescence in fluorescently labeled tissue. *J. Histochem. Cytochem. 47*, 719−730.
(49) Tai, D. C. S., Tan, N., Xu, S., Kang, C. H., Chia, S. M., Cheng, C. L., Wee, A., Wei, L. C., Raja, A. M., Xiao, G., Chang, S., Rajapakse, J. C., So, P. T. C., Tang, H.-H., Chen, C. S., and Yu, H. (2009) Fibro-C-Index: comprehensive, morphology-based quantification of liver fibrosis using second harmonic generation and two-photon microscopy. *J. Biomed. Opt. 14*, 044013.

(50) Salguero Palacios, R., Roderfeld, M., Hemmann, S., Rath, T., Atanasova, S., Tschuschner, A., Gressner, O. A., Weiskirchen, R., Graf, J., and Roeb, E. (2008) Activation of hepatic stellate cells is associated with cytokine expression in thioacetamide-induced hepatic fibrosis in mice. *Lab. Invest. 88*, 1192−1203.
(51) Wynn, T. A., and Ramalingam, T. R. Mechanisms of fibrosis: therapeutic translation for fibrotic disease. *Nat. Med. 18*, 1028−1040.
(52) Armendáriz-Borunda, J., and Rojkind, M. (1984) A simple quantitative method for collagen typing in tissue samples: its application to human liver with schistosomiasis. *Coll. Relat. Res. 4*, 35−47.
(53) Nielsen, L. F., Moe, D., Kirkeby, S., and Garbarsch, C. (1998) Sirius red and acid fuchsin staining mechanisms. *Biotechnol. Histochem. 73*, 71−77.

Targeting collagen strands by photo-triggered triple-helix hybridization

Yang Li[a], Catherine A. Foss[b], Daniel D. Summerfield[c], Jefferson J. Doyle[d], Collin M. Torok[b], Harry C. Dietz[d,e], Martin G. Pomper[b,f], and S. Michael Yu[a,c,f,1]

[a]Department of Chemistry, Johns Hopkins University, Baltimore, MD 21218; [b]Department of Radiology and Radiological Science, Johns Hopkins University School of Medicine, Baltimore, MD 21231; [c]Department of Materials Science and Engineering, Johns Hopkins University, Baltimore, MD 21218; [d]Howard Hughes Medical Institute and Institute of Genetic Medicine, Johns Hopkins University School of Medicine, Baltimore, MD 21205; [e]Division of Pediatric Cardiology, Department of Pediatrics, and Department of Medicine, Johns Hopkins University School of Medicine, Baltimore, MD 21205; and [f]Institute for NanoBiotechnology, Johns Hopkins University, Baltimore, MD 21218

Edited by* David A. Tirrell, California Institute of Technology, Pasadena, CA, and approved August 3, 2012 (received for review June 7, 2012)

Collagen remodeling is an integral part of tissue development, maintenance, and regeneration, but excessive remodeling is associated with various pathologic conditions. The ability to target collagens undergoing remodeling could lead to new diagnostics and therapeutics as well as applications in regenerative medicine; however, such collagens are often degraded and denatured, making them difficult to target with conventional approaches. Here, we present caged collagen mimetic peptides (CMPs) that can be photo-triggered to fold into triple helix and bind to collagens denatured by heat or by matrix metalloproteinase (MMP) digestion. Peptide-binding assays indicate that the binding is primarily driven by stereo-selective triple-helical hybridization between monomeric CMPs of high triple-helical propensity and denatured collagen strands. Photo-triggered hybridization allows specific staining of collagen chains in protein gels as well as photo-patterning of collagen and gelatin substrates. In vivo experiments demonstrate that systemically delivered CMPs can bind to collagens in bones, as well as prominently in articular cartilages and tumors characterized by high MMP activity. We further show that CMP-based probes can detect abnormal bone growth activity in a mouse model of Marfan syndrome. This is an entirely new way to target the microenvironment of abnormal tissues and could lead to new opportunities for management of numerous pathologic conditions associated with collagen remodeling and high MMP activity.

cancer | diagnostic imaging | connective tissue | degenerative disease | caged peptide

As the most abundant protein in mammals, collagens play a crucial role in tissue development and regeneration, and their structural or metabolic abnormalities are associated with debilitating genetic diseases and various pathologic conditions. Although collagen remodeling occurs during development and normal tissue maintenance, particularly for renewing tissues (e.g., bones), excess remodeling activity is commonly seen in tumors, arthritis, and many other chronic wounds. During collagen remodeling, large portions of collagens are degraded and denatured by proteolytic enzymes, which can be explored for diagnostic and therapeutic purposes. Since unstructured proteins are not ideal targets for rational drug design, library approaches have been employed to develop monoclonal antibody (1, 2) and peptide probes (3) that specifically bind to cryptic sites in collagen strands that become exposed when denatured. However, these probes suffer from poor pharmacokinetics (4), and/or low specificity, and binding affinity (5).

We envisioned that triple helix, the hallmark structural feature of collagen, could provide a unique targeting mechanism for the denatured collagens. The triple helix is nearly exclusively seen in collagens except as small subdomains in a few noncollagen proteins (6). Considering its striking structural similarity to the DNA double helix in terms of multiplex formation by periodic interchain hydrogen bonds along the polymer backbone (6), we thought that a small peptide sequence with strong triple-helix propensity could specifically recognize collagen sequence and hybridize to collagen strands by forming triple helix in a manner similar to DNA fragments or peptide nucleic acids binding to complementary DNA strands (7).

Previously, we discovered that small collagen mimetic peptides (CMPs, molecular weight: 2–3 kDa) capable of reversibly forming collagen triple helices are able to bind to type I collagen (8–11). Binding was observed only when CMPs [$(ProHypGly)_x$, $x = 6$, 7, and 10] in a thermally melted, single-strand form and not in folded trimeric form were allowed to fold by cooling in the presence of type I collagen fibers (9, 10). Although we observed apparent CMP binding to collagens at temperatures below collagen's T_m, the binding was significantly enhanced when hot CMP solution (typically above 70 °C) was applied to the collagen film. This suggested that the binding is facilitated by collagen denaturation, which could provide more open collagen strands that can hybridize the CMPs. However, we were unable to quantitatively assess the effects of collagen denaturation on CMP binding because it was impossible to decouple CMP melting from collagen denaturation. In addition, application of hot CMP solution was not compatible with in vivo and ex vivo collagen-targeting experiments. Therefore, we explored nonthermal means to control triple-helix folding and identified photo-caging as an ideal alternative.

In this article, we present the design and synthesis of a new caged CMP that can be photo-triggered to fold into triple helix. Using the new caged CMP, we compare the CMP's binding affinity to intact type I collagen and the same collagen denatured by heat or by matrix metalloproteinase (MMP) digestion, as well as study its stereo-selective hybridization mechanism. We further show that fluorescently labeled CMPs can be used in vivo to target and image denatured collagens in tissues undergoing remodeling, either due to normal renewal process (e.g., bones and cartilages) or pathologic conditions, such as tumor progression (e.g., prostate and pancreatic cancers) and musculoskeletal disease (e.g., Marfan syndrome).

Results and Discussion

Design and Photo-triggered Folding of the Caged Collagen Mimetic Peptide. In the collagen triple helix, small Gly residues are periodically located at every third position in each collagen strand to allow close packing of three protein chains in a right-handed twist (Fig. 1*A*) (12, 13). Mutations at even a single Gly position can

Y.L., C.A.F., M.G.P., and S.M.Y. designed research; Y.L., C.A.F., D.D.S., and C.M.T. performed research; J.J.D. and H.C.D. contributed reagent/analytical tools; Y.L., C.A.F., J.J.D., M.G.P., and S.M.Y. analyzed data; and Y.L., C.A.F., J.J.D., H.C.D., M.G.P., and S.M.Y. wrote the paper.

The authors declare no conflict of interest.

*This Direct Submission article had a prearranged editor.

[1]To whom correspondence should be addressed. E-mail: yu@jhu.edu.

This article contains supporting information online at www.pnas.org/lookup/suppl/doi:10.1073/pnas.1209721109/-/DCSupplemental.

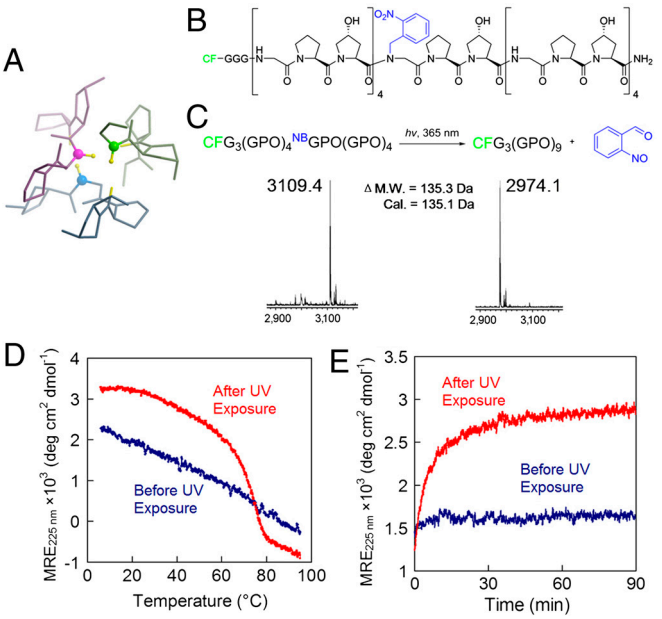

Fig. 1. Photo-triggered triple-helical folding of caged CMPs. (*A*) The backbone NH groups of Gly (represented by the ball-and-stick model) play a key role in stabilizing the collagen triple helix. (*B*) Structure of $CF^{NB}(GPO)_9$ featuring the photo-reactive nitrobenzyl (NB) group (in blue) conjugated to the central Gly. (*C*) Photo-cleavage of the NB cage group is monitored by MALDI-MS. (*D*, *E*) The NB cage group completely abolishes the triple-helical folding capacity of $CF^{NB}(GPO)_9$ and the photo-cleaving of the NB cage leads to CMP folding into stable triple helices, evidenced by CD melting studies (*D*) and refolding kinetics (*E*) of the peptides before and after UV exposure. For the refolding kinetic study (*E*), $CF^{NB}(GPO)_9$ (before and after UV exposure) were thermally quenched from 80 °C to 25 °C and the change in CD ellipticity at 225 nm was monitored at 25 °C.

destabilize the collagen structure and cause debilitating genetic disease (14). Therefore, we reasoned that a bulky, photo-cleavable cage group conjugated to the central Gly nitrogen of the CMP would fully negate its ability to fold (*SI Appendix*, Fig. S1), while exposure to light could liberate the cage group and trigger triple-helix folding and collagen binding. This approach was also appealing from a synthetic perspective as caged Gly, among all amino acids, is the easiest to synthesize and has the highest reactivity toward the addition of the next amino acid. The nitrobenzyl (NB) caged and carboxyfluorescein (CF) labeled CMP of sequence CF-Gly_3-$(GlyProHyp)_4$-^{NB}**Gly**ProHyp-$(GlyProHyp)_4$ [designated as $CF^{NB}(GPO)_9$, Fig. 1*B*] was synthesized by incorporation of Fmoc(N-*o*-nitrobenzyl)Gly-OH (15) during conventional Fmoc-mediated solid-phase peptide synthesis (SPPS). Coupling of Hyp to the sterically hindered ^{NB}Gly termini of the growing peptide was sluggish under HBTU/HOBT coupling condition; however, with the more powerful activating agent, PyBroP (16), we were able to achieve almost quantitative coupling efficiency and continue coupling the remaining peptide by SPPS, including the triple Gly spacer and the CF fluorescent tag (*SI Appendix, Materials and Methods*, Fig. S2) (17).

As we had anticipated, $CF^{NB}(GPO)_9$ exhibited photo-triggered triple-helix folding behavior (Fig. 1 *C*–*E*). The NB cage group completely suppressed the CMP's ability to fold into a triple helix as evidenced by the linear CD intensity decrease during melting (Fig. 1*D*, and *SI Appendix*, Fig. S3). Exposure to UV light (365 nm, approximately 10 mW/cm^2) efficiently cleaved the NB (Fig. 1*C*, and *SI Appendix*, Table S1) which allowed the CMP to regain its full triple-helical folding capacity as exhibited by the sigmoidal CD melting curve (heating rate: 60 °C/h) with T_m at 75 °C and fast refolding kinetics after thermal quenching from 80 °C to 25 °C (Fig. 1 *D* and *E*).

Photo-Triggered CMP-Collagen Hybridization. Using the new caged CMP, we were able to study comparative CMP binding toward intact and thermally denatured (gelatin) type I collagen because collagen denaturation could be completely decoupled from CMP melting. Photo-triggered binding affinity of the caged CMP was studied by applying $CF^{NB}(GPO)_9$ to a 96-well assay microplate coated with collagen/gelatin films, followed by UV (365 nm) exposure and measuring the fluorescence intensity of the collagen films after washing. While caged CMP binding (UV−) remained negligible on both collagen and gelatin substrates, photo-activated caged CMPs (UV+) exhibited binding to both substrates with the level of binding an order of magnitude higher for gelatin (Fig. 2*A*). These results indicate that CMP's triple helical folding is required for the binding, and collagen denaturation produces unfolded collagen strands that avidly hybridize with photo-decaged CMPs. The binding affinity was further confirmed for both type I and type II gelatin in comparison to sequence-scrambled CMPs which exhibited no triple-helical folding capacity (*SI Appendix*, Fig. S4) and negligible affinity to gelatin (Fig. 2*B*).

Although these experiments demonstrated collagen binding mediated by CMP's ability to fold into a triple helix, questions remain as to the precise mechanism underlying the CMP-collagen interactions. We addressed this question by studying the collagen affinity of a specially synthesized CMP composed of D-proline (^{D}P) which folds into an oppositely twisted left-handed triple helix. Since D-hydroxyproline is not readily available, we synthesized two caged Hyp-free CMPs; $CF^{NB}(GPP)_9$, which folds into a natural right-handed twist, and $CF^{NB}(G^{D}P^{D}P)_9$, which was expected to fold into an unnatural left-handed twist after photo-decaging. The CD melting curves of the two peptides after photo-cleavage were exact mirror images with identical T_m at 51 °C (*SI Appendix*, Fig. S5). Despite almost identical CD melting behaviors, $CF^{NB}(G^{D}P^{D}P)_9$ exhibited an order of magnitude lower levels of gelatin binding to that of $CF^{NB}(GPP)_9$ after photo-cleavage (Fig. 2*C*). Natural collagen strands can only fold into right-handed triple helices and are unlikely to form a triple-helical hybrid with a CMP having propensity for a left-handed twist (18). The results clearly show that the binding is not due to CMP trimers merely trapping the gelatin strands during triple-helical assembly, but that it is primarily driven by stereo-selective CMP-collagen strand hybridization, most likely in the form of a triple helix.

To investigate the low but apparent CMP-binding affinity to intact collagen films (Fig. 2*A*), we further performed a series of binding experiments using a noncaged, triple-helical $CF(GPO)_9$ and UV-triggered $CF^{NB}(GPP)_9$/$CF^{NB}(G^{D}P^{D}P)_9$ pair as well as thermally melted single-stranded $CF(GPO)_9$ (*SI Appendix, Text*, Figs. S6 and S7). The results confirm that CMP's binding affinity to intact type I collagen is real and also stereo-selective. We speculate that the low-level binding is caused by CMPs hybridizing with thermally unstable domains of the native collagen (19) or collagens partially denatured during purification and fiber regeneration. The density of photo-induced CMP binding to intact collagen was determined to be as high as 0.56 ± 0.03 $nmol/cm^2$, which is well above the bioactive ligand density for a variety of cell scaffold interactions in cell culture and tissue development (20, 21). Using $CF^{NB}(GPO)_9$, we were also able to photo-pattern collagen and gelatin films demonstrating the potential for local immobilization of CMP conjugated bioactive components (10, 22, 23) to collagen-containing tissue engineering scaffolds (Fig. 2*D*) (24, 25).

Since many pathologic conditions are associated with collagen remodeling by MMP activity, degraded collagens in diseased tissue and circulation are potential diagnostic and therapeutic targets (26, 27). Anti-collagen antibodies and low molecular weight targeting agents have been used to image collagens in fibrotic tissues and tumors, but they suffer from poor pharmacokinetics, and/or low specificity and binding affinity (2, 5). We tested the

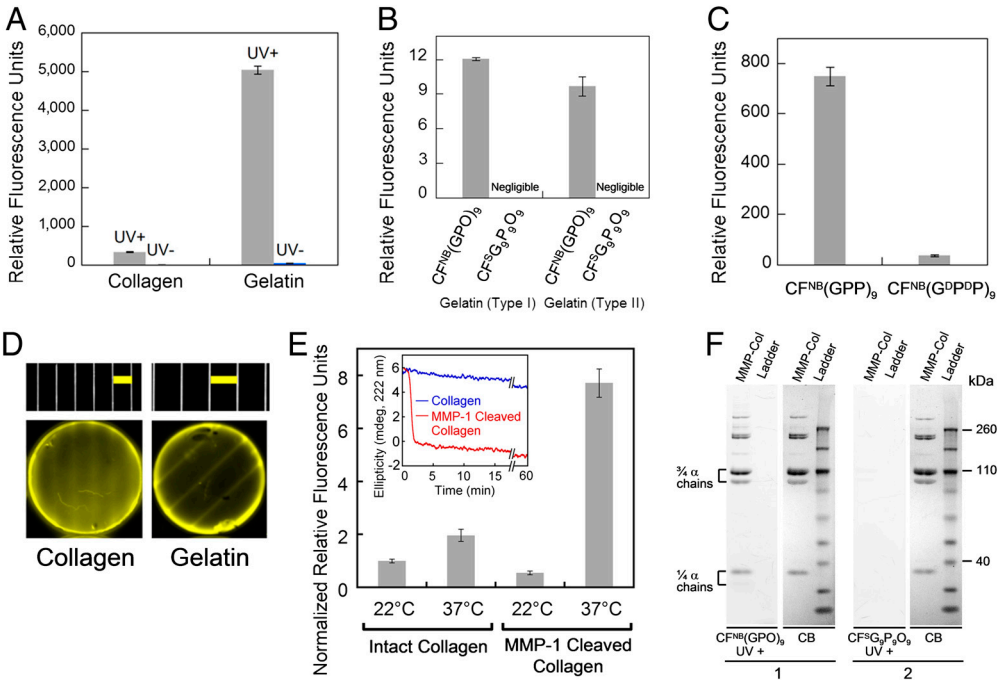

Fig. 2. Characterization of photo-triggered CMP-collagen hybridization. (*A*) Fluorescence levels of collagen films (fibrillar collagen) and thermally denatured collagen (gelatin) films treated by $CF^{NB}(GPO)_9$, with and without UV exposure. (*B*) Comparative fluorescence levels of type I and type II gelatin coatings treated with UV-exposed $CF^{NB}(GPO)_9$ and the sequence-scrambled control peptide, $CF^{S}G_9P_9O_9$ (CF-GGG-PGOGPGPOPOGOGOPPGOOPGGOOPPG). (*C*) Fluorescence levels of type I gelatin films treated with UV-exposed $CF^{NB}(GPP)_9$ and control peptide of opposite helicity, $CF^{NB}(G^DP^DP)_9$. (*D*) Fluorescence photographs of the photo-patterned collagen (*Left*) and gelatin (*Right*) films along with photographs of the transparency masks (*Top*, in scale with the photo-patterned films, *Below*) showing the line patterns [Scale bars: 2 mm (*Left*), 3 mm (*Right*)]. (*E*) Comparative fluorescence levels after photo-triggered $CF^{NB}(GPO)_9$ binding to nonfibrillar form of intact or MMP-1 cleaved type I collagens before and after 1 min of 37 °C incubation. *Inset*: CD signals after a temperature jump from 22 °C to 37 °C indicated fast denaturation (90% signal reduction in less than 3 min) of MMP-1 digested type I collagens at 37 °C while intact collagen maintained most of its triple-helical structure. (*F*) Fluorescence images of SDS-PAGE gels of MMP1-cleaved type I collagen (MMP-Col) and protein ladder stained with $CF^{NB}(GPO)_9$ (gel 1) or $CF^{S}G_9P_9O_9$ (gel 2) upon UV-activation, and white light photographs of the same gels stained with coomassie brilliant blue (CB). Bands labeled as 3/4α and 1/4α chains are MMP-1 digested collagen fragments. All CMP binding assays were performed in triplicate (±s.d.).

caged CMP [$CF^{NB}(GPO)_9$]'s photo-triggered binding affinity to type I collagen after MMP-1 digestion (*SI Appendix*, Fig. S8 for SDS-PAGE and CD characterization). MMP-1 cleaves the ¾ position of the collagen molecule, resulting in two collagen fragments with T_m around 34 °C that spontaneously denature at body temperature (Fig. 2*E*, *Inset*) (28). The photo-triggered CMP-binding assay was performed on intact and MMP-1 digested collagens before and after incubation at 37 °C. For intact collagens, the level of CMP binding was similarly low for the two temperature conditions. In contrast, MMP-1 digested collagens after the 37 °C incubation exhibited approximately four to tenfold higher levels of CMP binding compared to all other collagens tested (Fig. 2*E*). These results show that CMPs preferentially hybridize with MMP-1 digested collagens, which are spontaneously denatured at body temperature, over intact collagens. This hybridization was further verified by SDS-PAGE staining experiment. When used as a gel-staining agent, only the photo-cleaved CMP and not the scrambled control peptide was able to stain the MMP-1 digested collagen bands (Fig. 2*F*). No other bands from the protein ladder were stained by the CMP, which demonstrates its high binding specificity to collagen chains.

In Vivo Tumor Targeting by CMP Hybridization. To demonstrate CMP's ability to target pathologic tissues of high MMP activity, we performed an in vivo tumor-targeting experiment, using the same caged CMP conjugated to a near-infrared fluorophore (NIRF). Tumor progression involves proteolytic remodeling of the extracellular matrix (ECM) by various MMPs that results in the accumulation of stromal collagens with a unique structural and biochemical signatures (27, 29–31). We conjugated IRDye800CW (IR) to the N-termini of the caged CMP $^{NB}(GPO)_9$ and the scrambled peptide $^{S}G_9P_9O_9$ with flexible aminohexanoic acid (Ahx) spacers (*SI Appendix, Materials and Methods*, Fig. S9 for synthesis and CD melting curves). The NIRF-labeled CMPs were rapidly decaged under intense UV light (365 nm, >25 mW/cm^2) and immediately injected into the tail vein of mice bearing subcutaneous PC-3 prostate tumor xenografts. Considering the slow folding rate of the CMP triple helix (half time of CMP refolding is approximately 50 min) and the short time delay before the injection (<5 min), most of the CMPs were expected to enter the bloodstream in single-stranded form (32). Once in the blood, the CMP solution is diluted by a factor of 20, which results in dramatic reduction in the folding rate because of the third-order folding kinetics (33). Therefore, we expected that the single-stranded CMPs would be able to circulate the body and eventually bind to denatured collagen strands by triple-helical hybridization. Serial in vivo fluorescence imaging over four days indicated that the IR-Ahx-$(GPO)_9$ was able to permeate the tumor vasculature and accumulate at the tumor sites, whereas the scrambled sequence (IR-Ahx-$^{S}G_9P_9O_9$) lacking triple-helix folding capacity showed minimal accumulation at the tumor sites (Fig. 3*A* and *SI Appendix*, Fig. S10). Furthermore, coinjection of mice with MMPSense680™ (34), a fluorescent beacon for MMP activity, clearly showed the colocalization (in yellow) of MMP activity (in red) and CMP binding (in green) in the tumors 102 h after CMP injection (Fig. 3*B*). Ex vivo fluorescence microscopy of the tumor sections indicated that IR-Ahx-$(GPO)_9$ (in blue) was present near the CD31 positive perivascular tissue (in red) and colocalized in part with antibody for MMP-1 cleaved collagen fragments (in green) (Fig. 3*C*). This confirms that the tumor uptake was caused by CMP reaching the tumor via the blood vessels followed by binding to MMP digested collagens

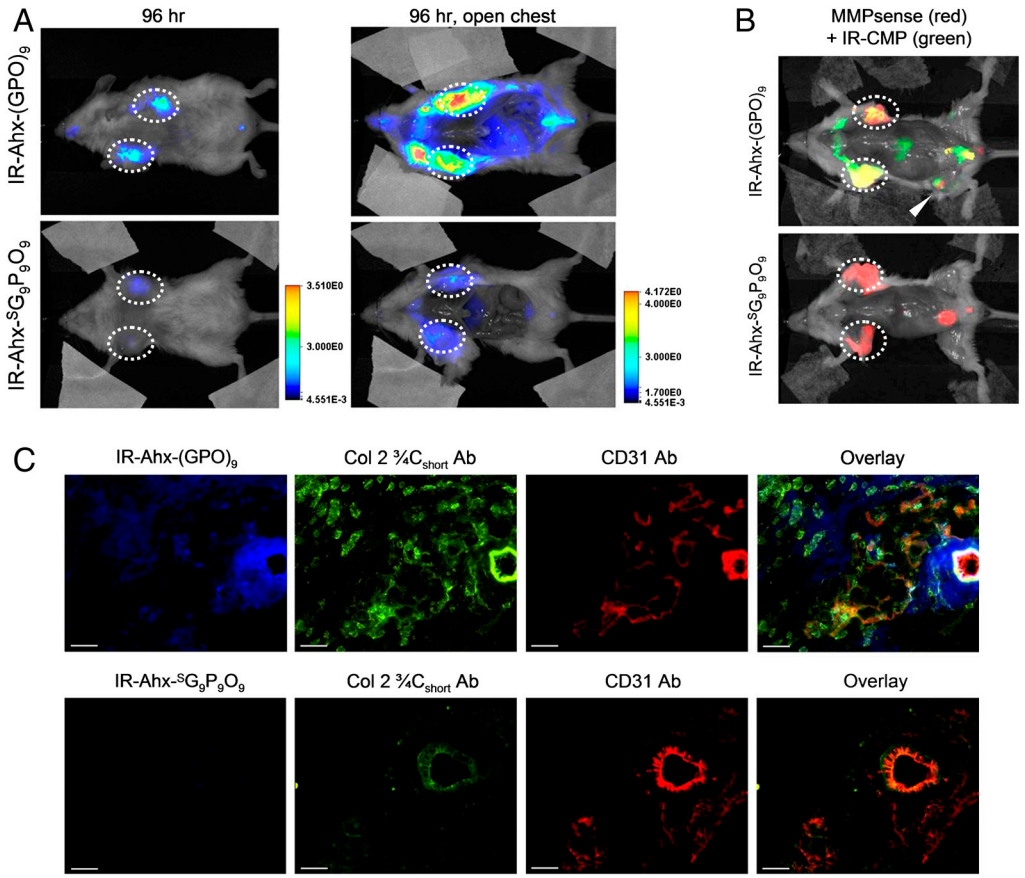

Fig. 3. In vivo targeting of tumors by CMP hybridization with MMP-digested collagens. (*A*) In vivo NIRF images of mice bearing PC-3 prostate tumors at forward right and left flanks (circled) administered with 3.7 nmol of UV-activated IR-Ahx-$^{NB}(GPO)_9$ or sequence-scrambled control peptide, IR-Ahx-$^{S}G_9P_9O_9$ via tail vein injection. Ventral views of both mice at 96 h post-injection (PI), and after midline surgical laparotomy (open chest) indicate tumor specific and stable accumulation of only the IR-Ahx-$(GPO)_9$ and not the control peptide. (*B*) NIRF images of another pair of mice bearing PC-3 tumors at the same location at 102 h after IR-CMP injection and 24 h after MMPSense680 injection, showing colocalization (in yellow) of MMP activity (red) and CMP binding (green) in the tumors (circled) and knee joint (arrowhead). (*C*) Epifluorescence micrographs of the unfixed PC-3 tumor sections from (*B*), additionally stained in vitro with anti-Col 2 ¾C_{short} csc antibody (green) and anti-CD31-PE antibody conjugate (red). IR-Ahx-$(GPO)_9$ (blue) colocalized partially with anti-Col 2 ¾C_{short} antibody (green) particularly within the peri-vasculatures. No such colocalization was detected for the control peptide (Scale bars: 100 μm).

within the tumor tissue. Similar results were obtained for mice bearing pancreatic tumor xenografts (*SI Appendix*, Fig. S11).

In Vivo Targeting of Collagen Remodeling in Bones and Cartilages. In both the prostate and pancreatic tumor targeting studies, we were surprised to see consistent and high level accumulation of CMPs at the knee joints, which also colocalized with MMP activity (Fig. 3*B*, and *SI Appendix*, Fig. S11*A*, arrowhead). Normal joints are known for continual tissue remolding by MMP; however, targeting this area by systemic delivery is difficult due to the avascular nature of the cartilage and fast synovial fluid clearance (35). To study the CMP accumulation at the joints and other tissues specifically, we conducted further in vivo CMP targeting experiments using BALB/c mice. This time, we used CMP conjugated to a slightly different NIRF dye, IRDye680RD (IR′) which has lower background fluorescence compared to 800CW. Fig. 4*A* shows the whole-body fluorescence image of the normal mouse four days after intravenous injection of the photo-decaged peptide. The images show clear accumulation of the CMPs within the skeleton, especially in the spine and ribs, as well as within the knees, ankles, wrists, and lower mandibles. Signals from other organs (harvested organs, *SI Appendix*, Fig. S12) were negligible except for the digestive system, which contained fluorescent chlorophylls from food (arrows). A mouse injected with sequence-scrambled peptide (IR′-Ahx-$^{S}G_9P_9O_9$) showed signal only from the digestive system. Furthermore, under similar experimental condition, neither the caged-CMP lacking the folding capacity nor the prefolded triple-helical CMP showed signs of skeletal uptake after four days (Fig. 4*B*). These results strongly suggest that the targeting of the skeletal tissue was mainly driven by the triple-helical propensity of the monomeric CMPs.

To identify the location of CMP binding more clearly, mice were coinjected with the calcium-chelating fluorescent probe (IRDye800CW BoneTag™) which targets calcifying tissues (36). Although the overall distributions of the two probes [IR′-Ahx-$(GPO)_9$: red; BonTag™: green] seemed similar (Fig. 4*C*, *Top*, and *SI Appendix*, Fig. S13*A*), close observation (Fig. 4*C*, *Bottom*, and *SI Appendix*, Fig. S13*B*) revealed that CMP targets both calcified and noncalcified bones (cartilages of the wrists, ribs, and knees) while the BoneTag™ targets only the calcified bones. The highest CMP intensity was detected at the articular cartilage of the knee joints (red arrow) sandwiched between two endochondral junctions (green arrows) targeted by both the BoneTag™ (green) and CMP (red). Ex vivo histologic analysis of the knee joint cartilage (unfixed frozen tissue section) showed CMP localizing at the superficial zone which was also costained by antibodies for MMP-1 cleaved, type II collagen fragments (Fig. 4*D*). The superficial zone is densely populated by type II collagen fibers, part of which are reported to be in denatured state due to steady remodeling activity (37). Because of continual bone remodeling, collagens within bone are metabolized throughout the lifespan, and products of collagen degradation (e.g., protein fragments, hydroxyproline) are markers for bone resorption activity (38). Considering the abundance of collagens in other organs, it is

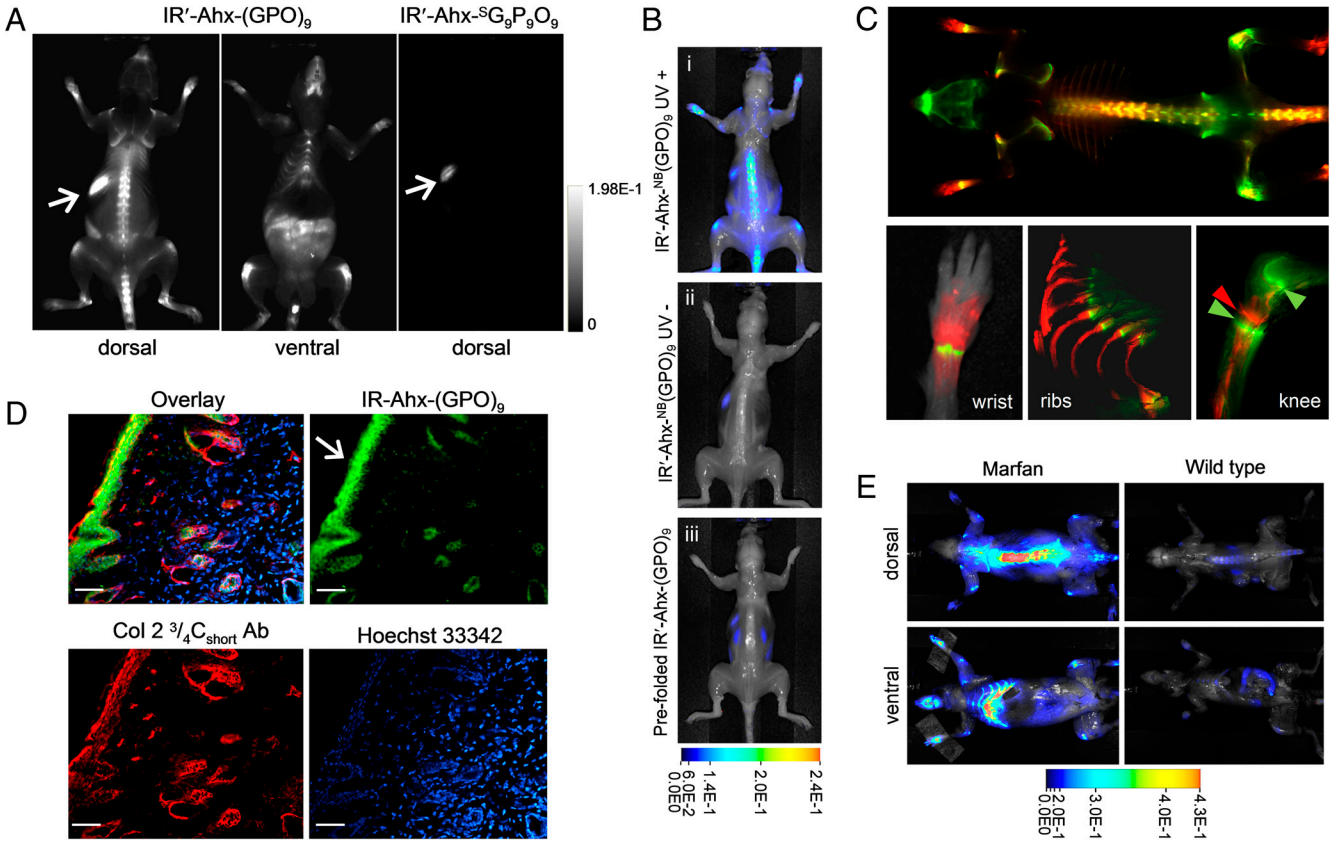

Fig. 4. In vivo targeting of collagen remodeling in bones and cartilages by CMP hybridization. (*A*) Whole-body NIRF images of BLAB/c mice injected intravenously with photo-decaged IR′-Ahx-$(GPO)_9$ or IR′-Ahx-$^{S}G_9P_9O_9$ showing skeletal uptake of only the IR′-Ahx-$(GPO)_9$ probes. Arrows show fluorescence from the chlorophyll in the digestive system. (*B*) Dorsal NIRF images of mice injected intravenously with photo-decaged IR′-Ahx-$(GPO)_9$ (*i*), caged IR′-Ahx-$^{NB}(GPO)_9$ (*ii*), or prefolded triple-helical IR′-Ahx-$(GPO)_9$ (*iii*). The absence of signal from mice *ii* and *iii* strongly suggests that the skeletal CMP uptake is due to its triple-helical folding propensity. (*C*) Dual-NIRF image of the whole skeleton showing the overall uptake of IR′-Ahx-$(GPO)_9$ (red) and BoneTag™ (stains calcifying tissues in green) and corresponding high-resolution images (colocalization shown in yellow). In the wrist, specific CMP uptake (red) is seen in carpal/metacarpal structures and BoneTag uptake is seen in epiphyseal line of radius and ulna; costochondral junctions within the ribs are visualized where mineralized bone ends (green-yellow) and cartilaginous ribs begin (red); CMPs colocalize with BoneTag™ at endochondral junctions (green arrowheads) in the knee while CMP-specific uptake can be seen within the articular cartilage and meniscus (red arrowhead) as well as focal regions within the tibia and the femur head. (*D*) Immunofluorescence micrographs of ex vivo knee cartilage sections subsequently stained with anti-Col 2 ¾C_{short} antibody and Hoechst 33342 showing high CMP accumulation at the superficial zone of the cartilage (Scale bars, arrow: 100 μm). (*E*) Whole-body NIRF images of mouse model with Marfan syndrome 96 h after IR′-Ahx-$(GPO)_9$ administration showing high CMP uptake in the skeleton of the diseased mouse. Whole body images were taken after skin removal.

remarkable to see such localized and apparently stable accumulation of CMPs in the bones and joints (little reduction in fluorescence intensity over 96 h). This suggests that the CMPs are preferentially hybridizing with denatured collagens within the tissue and not with collagen fragments in circulation which may be too small to fold into triple helix (10). These results suggest that the CMP could be used as cartilage-imaging agent, and appropriate derivatives may likewise become bone- and cartilage-seeking therapeutics. More work is under way to determine the effects of CMP hybridization on the process of collagen remodeling in the skeletal tissue and in tumor growth.

Finally, we tested CMP's potential to detect bone abnormality in a mouse model of Marfan syndrome, a genetic disorder of the ECM (39). Photo-triggered IR′-Ahx-$(GPO)_9$ was injected into mice with a heterozygous missense mutation in fibrillin-1, which was previously shown to exhibit marked skeletal pathology, including severe kyphosis (*SI Appendix*, Fig. S14) and rib overgrowth (39). Whole-body fluorescence images of the mutant and normal mice 96 h after the CMP injection showed a striking difference in CMP uptake: strong CMP signal was detected at the spine and ribs of the mutant mice with at least four times the intensity of the wild-type mice (Fig. 4*E*). The mechanism of bone overgrowth in Marfan syndrome is complex and still not fully understood; however, the strong correlation between collagen remodeling and bone growth in both physiological and pathological contexts (38), as well as high TGF-β signaling in multiple tissues of this mouse model support the conclusion that prominent CMP uptake in the Marfan mice, at least in part, derives from increased collagen remodeling in skeletal tissues that display pathological overgrowth.

More work is needed to fully understand the nature of CMP uptake in the skeletal tissues. The turnover rate of collagen in cartilages is reported to be significantly slower than that of the mineralized bones (40), and aortic aneurysm in Marfan disease is associated with an abnormally high concentration of mature collagens (41). Therefore, it is possible that the accumulation of degraded and damaged collagens, and not necessarily the fast rate of collagen degradation is responsible for the high CMP uptake seen in these tissues. It is also possible that calcification of collagens (i.e., mineralization) reduces CMP uptake. This could explain the high CMP uptake in the cartilage as well as the skeletal tissues of Marfan mouse which have reduced mineral content.

To our knowledge, this is the first time that the structural remodeling of ECM has been directly interrogated by peptide hybridization. CMP is a simple peptide that can be readily conjugated to imaging and therapeutic moieties. Therefore, CMP-mediated collagen strand targeting opens new avenues, beyond tumor, bone, and joint imaging, for applications in detection

and treatment of a wide range of pathologic conditions associated with high MMP activity, such as wound healing, ECM degeneration, and fibrous tissue formation.

Materials and Methods

Peptide Synthesis. Fmoc(N-*o*-nitrobenzyl)Gly-OH was synthesized as described in (15) (*SI Appendix*, Fig. S2*A*). Caged CMPs were coupled using standard solid-phase Fmoc and HBTU chemistry (10), with the exception of the amino acid following ^{NB}Gly, which was conjugated by 9 molar eq of the amino acid, 8.8 molar eq of PyBroP, and 20 molar eq of DIPEA for 24 h. The peptides were purified by reverse-phase HPLC and analyzed by MALDI-ToF (*SI Appendix*, Table S1) and circular dichroism spectroscopy.

Photo-Triggered Collagen Hybridization. Photo-triggered collagen binding studies were conducted by exposing CF-labeled, caged CMPs (50 μM or, as specified, 40 μL in 1 × PBS) to 365 nm UV light (10 mW/cm^2) directly on reconstituted type I collagen or gelatin films (0.742 mg of protein per film) at 4 °C, followed by 3 h of incubation, extensive washing, and fluorescence reading (ex: 489 nm; em: 533 nm). Type I collagen (416 μg/mL) was digested using MMP-1 (6.6 μg/mL) activated by p-aminophenylmercuric acetate. For comparative binding assays, wells of maxisorp microplates coated with intact and MMP-1 cleaved collagens (100 μg/mL) were blocked with 5% BSA and treated with CF^{NB}(GPO)$_9$ (20 μM; 50 μL in 1 × PBS), followed by UV exposure, incubation (2.5 h), extensive washing, and fluorescence reading.

In Vivo Tumor Targeting. All animal studies were undertaken in compliance with the regulations of the Johns Hopkins Animal Care and Use Committee. Prostate cancer cells (PC-3) were implanted (1 × 10^6 in 50 μL of HBS) subcutaneously behind the right and left forearms of non-obese diabetic (NOD)/severe-combined immunodeficient (SCID) mice. The tumors were grown until 5—7 mm in diameter, at which point, saline solution (100 μL) containing 3.7 nmol of IR-Ahx-^{NB}(GPO)$_9$ or IR-Ahx-^{S}G$_9$P$_9$O$_9$, and 1 nmol of cysteine (for quenching photo-cleaved aldehyde byproduct), activated by UV exposure (365 nm, >25 mW/cm^2, 5 min) was immediately injected via lateral tail vein. MMPSense 680™ (2 nmol in 150 μL 1 × PBS) was administered intravenously 80 h post CMP injection. Images were acquired at designated times using a LI-COR Pearl Impulse Imager at both 710 nm (MMPSense) and 800 nm (CMP). The unfixed tissue sections were probed with antibodies (anti-CD31, anti-Col 2 ¾C$_{short}$), followed by a secondary anti-rabbit-Alexa-Fluor488 and viewed using a Nikon 80i epifluorescence microscope.

In Vivo Skeleton Targeting. Male BALB/c mice (or Marfan mice developed as reported in ref. 39) were dosed with 4 nmol of UV-activated IR′-Ahx-^{NB}(GPO)$_9$ or IR′-Ahx-^{S}G$_9$P$_9$O$_9$ via tail vein as described. IRDye800CW BoneTag™ (10 nmol) was administered to each mouse 72 h post-CMP injection. After 24 h, the mice were imaged after their skins removed to allow imaging of deep tissues. Ex vivo hind limb and right hemisphere of ribs were scanned laterally using a LI-COR Odyssey imager in both 710 nm (CMP) and 800 nm (BoneTag) channels. For full detailed *Materials and Methods*, see *SI Appendix*.

ACKNOWLEDGMENTS. We thank Gilbert Green and Mrudula Pullambhatla for technical assistance, and Xuesong Jiang, Elena Makareeva, Robert Visse, and William Wilson for discussion. This work was supported by grants from NSF (DMR-0645411), NIAMS/NIH (R01-AR060484), and DOD awarded to S.M.Y., and from NIH (U24 CA92871 and U54 CA151838) awarded to M.G.P. Development and maintenance of Marfan mice was supported by NIH (AR-41135), the National Marfan Foundation, the William S. Smilow Center for Marfan Syndrome Research, and the Howard Hughes Medical Institute.

1. Pernasetti F, et al. (2006) Novel anti-denatured collagen humanized antibody D93 inhibits angiogenesis and tumor growth: An extracellular matrix-based therapeutic approach. *Int J Oncol* 29:1371–1379.
2. Xu J, Rodriguez D, Kim JJ, Brooks PC (2000) Generation of monoclonal antibodies to cryptic collagen sites by using subtractive immunization. *Hybridoma* 19:375–385.
3. Mueller J, Gaertner FC, Blechert B, Janssen K-P, Essler M (2009) Targeting of tumor blood vessels: A phage-displayed tumor-homing peptide specifically binds to matrix metalloproteinase-2-processed collagen IV and blocks angiogenesis in vivo. *Mol Cancer Res* 7:1078–1085.
4. Goldenberg DM (2002) Targeted therapy of cancer with radiolabeled antibodies. *J Nucl Med* 43:693–713.
5. Caravan P, et al. (2007) Collagen-targeted MRI contrast agent for molecular imaging of fibrosis. *Angew Chem Int Ed* 46:8171–8173.
6. Engel J, Bächinger HP (2005) *Collagen*, eds J Brinckmann, H Notbohm, and PK Müller (Verlag Berlin Heidelberg, Springer), pp 7–33.
7. Nielsen PE, Egholm M, Berg RH, Buchardt O (1991) Sequence-selective recognition of DNA by strand displacement with a thymine-substituted polyamide. *Science* 254:1497–1500.
8. Yu SM, Li Y, Kim D (2011) Collagen mimetic peptides: Progress toward functional applications. *Soft Matter* 7:7927–7938.
9. Wang AY, Mo X, Chen CS, Yu SM (2005) Facile modification of collagen directed by collagen mimetic peptides. *J Am Chem Soc* 127:4130–4131.
10. Wang AY, et al. (2008) Spatio-temporal modification of collagen scaffolds mediated by triple helical propensity. *Biomacromolecules* 9:1755–1763.
11. Li Y, Mo X, Kim D, Yu SM (2011) Template-tethered collagen mimetic peptides for studying heterotrimeric triple-helical interactions. *Biopolymers* 95:94–104.
12. Shoulders MD, Raines RT (2009) Collagen structure and stability. *Annu Rev Biochem* 78:929–958.
13. Fallas JA, O'Leary LER, Hartgerink JD (2010) Synthetic collagen mimics: Self-assembly of homotrimers, heterotrimers, and higher order structures. *Chem Soc Rev* 39:3510–3527.
14. Hyde TJ, Bryan MA, Brodsky B, Baum J (2006) Sequence dependence of renucleation after a Gly mutation in model collagen peptides. *J Biol Chem* 281:36937–36943.
15. Tatsu Y, Nishigaki T, Darszon A, Yumoto N (2002) A caged sperm-activating peptide that has a photocleavable protecting group on the backbone amide. *FEBS Lett* 525:20–24.
16. Nandy SK, Agnes RS, Lawrence DS (2007) Photochemically activated probes of protein-protein interactions. *Org Lett* 9:2249–2252.
17. Stahl PJ, Cruz JC, Li Y, Yu SM, Hristova K (2012) On-the-resin N-terminal modification of long synthetic peptides. *Anal Biochem* 424:137–139.
18. Punitha V, et al. (2009) Molecular dynamics investigations on the effect of D amino acid substitution in a triple-helix structure and the stability of collagen. *J Phys Chem B* 113:8983–8992.
19. Mo X, An YJ, Yun CS, Yu SM (2006) Nanoparticle-assisted visualization of binding interactions between collagen mimetic peptide and collagen fibers. *Angew Chem Int Ed* 45:2267–2270.
20. Anderson SM, Chen TT, Iruela-Arispe ML, Segura T (2009) The phosphorylation of vascular endothelial growth factor receptor-2 (VEGFR-2) by engineered surfaces with electrostatically or covalently immobilized VEGF. *Biomaterials* 30:4618–4628.
21. Rowley JA, Mooney DJ (2002) Alginate type and RGD density control myoblast phenotype. *J Biomed Mater Res* 60:217–223.
22. Chan TR, Stahl PJ, Yu SM (2011) Matrix-bound VEGF mimetic peptides: Design and endothelial cell activation in collagen scaffolds. *Adv Funct Mater* 21:4252–4262.
23. Wang AY, et al. (2008) Immobilization of growth factors on collagen scaffolds mediated by polyanionic collagen mimetic peptides and its effect on endothelial cell morphogenesis. *Biomacromolecules* 9:2929–2936.
24. Gillette BM, et al. (2008) In situ collagen assembly for integrating microfabricated 3D cell-seeded matrices. *Nat Mater* 7:636–640.
25. Nichol JW, et al. (2010) Cell-laden microengineered gelatin methacrylate hydrogels. *Biomaterials* 31:5536–5544.
26. Cretu A, Brooks PC (2007) Impact of the noncellular tumor microenvironment on metastasis: Potential therapeutic and imaging opportunities. *J Cell Physiol* 213:391–402.
27. Kessenbrock K, Plaks V, Werb Z (2010) Matrix metalloproteinases: Regulators of the tumor microenvironment. *Cell* 141:52–67.
28. Danielsen CC (1987) Thermal stability of human-fibroblast-collagenase-cleavage products of type-I and type-III collagens. *Biochem J* 247:725–729.
29. Liotta LA, et al. (1980) Metastatic potential correlates with enzymatic degradation of basement membrane collagen. *Nature* 284:67–68.
30. Conklin MW, et al. (2011) Aligned collagen is a prognostic signature for survival in human breast carcinoma. *Am J Pathol* 178:1221–1232.
31. Burns-Cox N, Avery NC, Gingell JC, Bailey AJ (2001) Changes in collagen metabolism in prostate cancer: A host response that may alter progression. *J Urol* 166:1698–1701.
32. Boudko S, et al. (2002) Nucleation and propagation of the collagen triple helix in single-chain and trimerized peptides: Transition from third to first order kinetics. *J Mol Biol* 317:459–470.
33. Ackerman MS, et al. (1999) Sequence dependence of the folding of collagen-like peptides. *J Biol Chem* 274:7668–7673.
34. Bremer C, Tung C, Weissleder R (2001) In vivo molecular target assessment of matrix metalloproteinase inhibition. *Nat Med* 7:743–748.
35. Rothenfluh DA, Bermudez H, O'Neil CP, Hubbell JA (2008) Biofunctional polymer nanoparticles for intra-articular targeting and retention in cartilage. *Nat Mater* 7:248–254.
36. Zaheer A, et al. (2001) In vivo near-infrared fluorescence imaging of osteoblastic activity. *Nat Biotechnol* 19:1148–1154.
37. Hollander AP, et al. (1995) Damage to type II collagen in aging and osteoarthritis starts at the articular surface, originates around chondrocytes, and extends into the cartilage with progressive degeneration. *J Clin Invest* 96:2859–2869.
38. Risteli J, Risteli L (2006) *Dynamics of Bone and Cartilage Metabolism*, eds MJ Seibel, SP Robins, and JP Bilezikian (Academic, New York) p 391.
39. Judge DP, et al. (2004) Evidence for a critical contribution of haploinsufficiency in the complex pathogenesis of Marfan syndrome. *J Clin Invest* 114:172–181.
40. Sivan S-S, et al. (2008) Collagen turnover in normal and degenerate human intervertebral discs as determined by the racemization of aspartic acid. *J Biol Chem* 283:8796–8801.
41. Lindeman JHN, et al. (2010) Distinct defects in collagen microarchitecture underlie vessel-wall failure in advanced abdominal aneurysms and aneurysms in Marfan syndrome. *Proc Natl Acad Sci USA* 107:862–865.

Soft Matter

Cite this: *Soft Matter*, 2012, **8**, 10409

www.rsc.org/softmatter

PAPER

Encoding cell-instructive cues to PEG-based hydrogels *via* triple helical peptide assembly†

Patrick J. Stahl[ab] and S. Michael Yu*[ab]

Received 19th April 2012, Accepted 3rd August 2012
DOI: 10.1039/c2sm25903f

Effective synthetic tissue engineering scaffolds mimic the structure and composition of the natural extracellular matrix (ECM) to promote optimal cellular adhesion, proliferation, and differentiation. Among many proteins of the ECM, collagen and fibronectin are known to play a key role in the structural integrity of the scaffold as well as its ability to support cell adhesion. Here, we present photocrosslinked poly(ethylene glycol) diacrylate (PEGDA) hydrogels displaying collagen mimetic peptides (CMPs) that can be further conjugated to bioactive molecules *via* a CMP–CMP triple helix association. Pre-formed PEGDA–CMP hydrogels can be encoded with varying concentrations of cell-signaling CMP–RGD peptides similar to cell adhesive fibronectin decorating the collagen fibrous network by non-covalent binding. Furthermore, the triple helix mediated encoding allows facile generation of spatial gradients and patterns of cell-instructive cues across the cell scaffold that simulate the distribution of insoluble factors in the natural ECM.

Introduction

Most mammalian cells grow within a scaffold composed of diverse structural and cell adhesive biomacromolecules that display tissue specific factors to control organization, proliferation and differentiation of cells.[1] This scaffold, broadly known as the extracellular matrix (ECM), gives both mechanical and biochemical signals to the cells during tissue development that are both dynamic and spatio-temporal in nature. Many biochemical signals are soluble factors that freely permeate the ECM, but some cell-instructive signals are bound to the matrix scaffold. These insoluble factors are known to play a critical role in the development of complex tissues (*e.g.* vasculatures).[2,3]

As tissue engineers attempt to mimic this highly complex natural ECM structure, they often employ synthetic hydrogels as the starting scaffold material. The synthetic scaffolds consist of crosslinked hydrophilic macromolecules with viscoelastic properties similar to the natural ECM, and these scaffolds can be tailor designed to present cell-instructive cues that mediate cell–scaffold interactions.[4] Poly(ethylene glycol) (PEG) has been FDA approved for a number of biomedical uses, and PEG-based synthetic hydrogels are frequently used in tissue engineering research due to a wealth of information on their synthesis and physico-chemical characteristics.[5] Because PEG is inert to cell interaction, it acts as a blank slate that accentuates cellular reaction to the bioactive cues conjugated to the scaffold.[6]

Previously, our lab showed that photocrosslinked PEG diacrylate (PEGDA) featuring collagen mimetic peptides (CMPs) can enhance the scaffold retention of collagens (and other ECM proteins) secreted by encapsulated chondrocytes.[7] Furthermore, this PEGDA–CMP scaffold promoted chondrogenic differentiation of encapsulated mesenchymal stem cells.[8] The improved bioactivity of the PEGDA–CMP scaffolds over PEGDA alone was attributed to CMP's ability to bind to cell-secreted collagens, which was first revealed by our research group.

Although CMPs were originally developed to model collagen's distinct triple helical structure, CMPs have since been shown to bind to natural collagen, presumably through CMP–collagen triple helical hybridization.[9] CMPs are short, synthetic peptides that feature collagen's prototypical (glycine-X-Y) repeating amino acid sequence in which X and Y positions are predominantly filled by proline and hydroxyproline, respectively.[10] The CMPs form thermally reversible triple helices in which three strands intertwine into a triple helix below the peptide's melting temperature (T_m) and melt into single strands above the T_m.[11] The CMP's ability to undergo such a specific folding process has motivated scientists to extend their studies beyond triple helix stability[12,13] to employing CMPs for diverse biomedical applications including natural scaffold functionalization,[14,15] macroscale peptide assembly,[16] and drug delivery.[17]

Taking advantage of their respective functionalities, researchers have begun using PEG-based hydrogels and CMPs together to generate synthetic tissue scaffolds. For example, physically crosslinked gels from CMP and starshape PEG

[a]*Department of Materials Science & Engineering, The Johns Hopkins University, Maryland Hall 3400 N. Charles St, Baltimore, MD 21218, USA. E-mail: yu@jhu.edu*
[b]*Institute for NanoBioTechnology, The Johns Hopkins University, Maryland Hall 3400 N. Charles St, Baltimore, MD 21218, USA*

† Electronic supplementary information (ESI) available: MALDI-ToF mass spectra and CD melting curves of peptides, SEM and phase contrast micrographs of seeded cells. See DOI: 10.1039/c2sm25903f

complexes were reported to be a viable 3D scaffold for human mesenchymal stem cells.[18] Researchers have also created CMP platforms featuring direct cell-adhesive cues found in natural collagen such as GFOGER and GFPGER.[19–21] Since these adhesion peptides are active only in the triple helical conformation, scientists have flanked this peptide with CMP sequences of high triple helical propensity.[22,23] These experiments demonstrated the compatibility of CMP-presenting scaffolds with cells that are either encapsulated or seeded onto them.

In our previous work, we demonstrated that PEG–CMP hydrogels featuring triple helix-mediated physical crosslinks can be further modified by strand-invasion and triple helix assembly of exogenously added CMPs.[24] These exogenous CMPs were able to compete with CMPs of the gel in triple helix assembly and bind to the hydrogel through heterotrimeric helix formation. Local CMP injection allowed modification of the gel in a spatially controlled manner, and particle tracking microrheology showed that exogenous CMPs can locally affect the mechanical properties of the gel by disrupting the triple helix crosslinks.

Here, we extend the exogenous CMP binding strategies to incorporate bioactive CMPs into a photocrosslinked PEGDA–CMP scaffold using the triple helical folding propensity of the peptides. The collagen triple helix is a unique multiplex protein structure rarely seen in other proteins. We present the use of CMP assembly as a non-covalent yet target-specific conjugation tool and demonstrate that CMP triple helix assembly can be a simple and robust tool for functionalization of scaffolds with cellular cues. While it is possible to use covalent grafting of cellular cues to promote cell–matrix interactions,[25] the CMP-mediated functionalization more closely mimics the physical binding interactions between structural and cell-signaling proteins in natural ECM.[26–28] We also demonstrate that the triple helix-mediated scaffold modification can create spatial patterns and gradients of cell-instructive cues, which can help us understand the role that insoluble factors play in cellular behaviors and complex tissue formation.

Experimental

Materials

Peptide synthesis reagents including Fmoc-amino acids, 2-(1*H*-benzo-triazole-1-yl)-1,1,3,3-tetra-methyluronium hexfluorophosphate (HBTU), *N*,*N*-diisopropylethylamine (DIPEA), *N*-methylpyrrolidone (NMP), and trifluoroacetic acid (TFA) were purchased from Advanced ChemTech (Louisville, KY). Rink-type Tentagel R RAM resin was purchased from Peptides International (Louisville, KY). Triisopropylsilane (TIS), piperidine, carboxyfluorescein (CF), rhodamine B, acrylic acid, and 2-hydroxy-4′-(2-hydroxyethoxy)-2-methylpropiophenone (Irgacure 2959) were obtained from Sigma-Aldrich (St Louis, MO). Activating agents PyBOP, PyAOP, and HATU were obtained from EMD Chemicals (Philadelphia, PA). *N*-Fmoc-amido-dPEG$_4$-acid (dPEG) and poly(ethylene glycol) diacrylate (PEGDA; M_w 3400 Da) were purchased from Advanced ChemTech and Glycosan BioSystems (Salt Lake City, UT), respectively. Round glass cover slips (15 mm diameter) were purchased from Electron Microscopy Sciences (Hatfield, PA). Fibroblasts (human dermal, neonatal) were obtained from American Type Culture Collection (Manassas, VA), and DMEM/F12 + GlutaMAX media was obtained from Invitrogen. HUVECs and EGM-2 endothelial cell media were obtained from Lonza (Walkersville, MD). WST-1 proliferation assay kit was purchased from Roche Applied Science (Indianapolis, IN). For fixing and staining, 10% neutral buffered formalin was obtained from Sigma-Aldrich, tris-buffered saline (TBS) was obtained from Bio-Rad Laboratories (Hercules, CA), and Alexa-Fluor 488 phalloidin and 4,6-diamidino-2-phenylindole (DAPI) were purchased from Invitrogen and Roche Applied Science, respectively.

Peptide synthesis

Peptides were synthesized manually on Tentagel resin with conventional Fmoc mediated coupling chemistry using 4.5-fold molar excess of amino acids activated by HBTU and deprotected by treatment with piperidine. Coupling and deprotection steps were monitored with ninhydrin or chloranil tests. For Acrl–PEG–CMP synthesis, after completion of the CMP synthesis and Fmoc deprotection of the last Gly, the resin was reacted with the Fmoc-dPEG spacer (4-fold molar excess) using PyBOP. The resin was treated with piperdine to remove the Fmoc from the dPEG spacer, and the N-terminus of the PEG–CMP conjugate was reacted with 5-fold molar excess of acrylic acid activated by PyBOP. Fluorescently labeled CMPs were prepared by reacting CMPs (on resin) with CF (6-fold excess) or rhodamine B (10-fold excess) using PyAOP and HATU, respectively. All peptide conjugates were cleaved from the resin by incubation with a cleavage cocktail (95% TFA, 2.5% TIS, 2.5% deionized water) for 3 h. The cleaved peptide solution was filtered from the resin and added dropwise to cold ethyl ether to precipitate the crude CMP product. The peptides were then pelleted by centrifugation and dried under vacuum.

Crude peptides were purified using reverse-phase high performance liquid chromatography (HPLC) on a Varian Polaris 210 series liquid chromatograph (Agilent Technologies, Santa Clara, CA) equipped with a semiprep Vydac reverse-phase C18 column. Mobile phase gradients of deionized water (DI H_2O) and acetonitrile containing 0.1% TFA were passed through the column at a flow rate of 4 mL min^{-1}. Peptides were detected by UV absorption at 220 nm for Acrl–PEG–CMP or at 275 nm for CMP–RGD peptides. The elutions containing target peptides were collected, combined, and lyophilized. The purity of peptides was determined by matrix-assisted laser desorption/ionization time-of-flight (MALDI-ToF) mass spectrometry (Voyager DE-STR, Applied Biosystems, Foster City, CA) (ESI, Fig. S1†).

PEGDA–CMP hydrogel synthesis

PEGDA–CMP hydrogel precursor solutions were created from a mixture of 1 wt% Acrl–PEG–CMP, 9 wt% PEGDA, and 0.05 wt% Irgacure 2959 photoinitator dissolved in PBS. The gel precursor solution was heated at 80 °C for 30 min to melt CMP triple helices into single strands. Each gel was prepared by first depositing 100 μL of the hot precursor solution onto a glass cover slip followed by placing another cover slip on top of the solution to form a glass–solution–glass sandwich. These samples were then placed under a 365 nm UV lamp (McMaster-Carr,

Atlanta, GA) for 10 min with an intensity of ~5 mW cm^{-2}. The resulting photocrosslinked gel was revealed by peeling off the top glass cover slip and the gel was transferred to a multiwell plate for further experiments as described below.

Circular dichroism study

To prepare samples for CD studies, the gel precursor solution consisting of PEGDA (6.75 wt%), Acrl–PEG–CMP (0.75 wt%), and Irgacure 2959 (0.05 wt%) was dissolved in PBS. The sample was heated for 30 min at 80 °C to melt CMPs into single strands, and 400 μL of this solution was pipetted into a CD cuvette. For CD measurements on the uncrosslinked precursor solution, the sample was incubated in the cuvette at 4 °C overnight to allow complete folding of the triple helix. For CD measurements on photopolymerized gels, the hot precursor solution was exposed to UV light for 20 min, which led to the formation of a self-supporting gel inside the cuvette. Longer exposure time ensured full photopolymerization of the gel which contained reduced amount of monomers to minimize background CD signal. This PEGDA–CMP gel was then incubated at 4 °C overnight. For CD measurements on PEGDA–CMP gels photopolymerized under cold conditions, the precursor solution was first incubated at 4 °C in the cuvette prior to UV light exposure for photocrosslinking. The CD spectra were recorded on a JASCO 710 spectrometer with a JASCO PTC-348 WI temperature controller (Easton, MD). The CD thermal melting curves were generated by monitoring the triple helix CD ellipticity at 231–232 nm while heating the sample from 5 °C to 90 °C at a rate of 0.5 °C min^{-1}. The T_m of CMPs was assigned to the minimum of the first derivative of the ellipticity *versus* temperature curve.[29]

CMP–RGD binding and release study

After the photopolymerization, PEGDA–CMP gels were transferred to 24-well plates, covered with 500 μL PBS, and incubated at 37 °C. CF–CMP–RGD solutions (761, 152, and 76 μM) in PBS were heated at 80 °C for 30 min. After removing the excess PBS coverage from the wells containing PEGDA–CMP gels, 500 μL of the 80 °C CF–CMP–RGD solution was added to each well. The gels were incubated overnight at 37 °C to allow CMP-scaffold triple helical hybridization. Gels were then washed with PBS (1 mL × 10) at room temperature to remove unbound CF–CMP–RGD. Subsequently, 500 μL of fresh PBS were added to the gels, and samples were returned to 37 °C incubation. In the following days, for the CF–CMP–RGD binding and release study, the PBS solution was removed from the well before each fluorescence measurement and replaced with fresh PBS solution. The amount of bound CF–CMP–RGD peptide was determined by measuring the CF absorbance at 493 nm with a Tecan Infinite 200 plate reader (Männedorf, Switzerland). The absorbance readings were converted into moles of peptide using a standard curve generated from absorbance values of a series of solutions with a known CF–CMP–RGD concentration.

Cell culture

Human dermal neonatal fibroblasts were cultured in 1 : 1 DMEM/F12 + GlutaMAX supplemented with 10% fetal bovine serum (FBS), amphotericin B, and gentamicin from Lonza (Walkersville, MD). HUVECs were cultured in a complete endothelial-cell growth medium (EGM-2). All cells were grown at 37 °C with a fully humidified atmosphere and 5% CO_2. The growth media were changed every two days. For scaffold seeding experiments, passage 3–7 cells were harvested by treating the culture plate with 0.05% trypsin/0.53 mM ethylenediaminetetraacetic acid (EDTA) in HBSS (Mediatech, Manassas, VA).

Cell seeding onto CMP–RGD modified PEGDA–CMP scaffolds

PEGDA–CMP precursor solutions were created under sterile conditions in the cell culture hood and photopolymerized using the previously described protocol. The synthesized gels were placed into a 24-well plate, covered with 500 μL PBS, and kept at 37 °C in an incubator. Next, CMP–RGD solutions in PBS were heated at 80 °C for 30 min. The PBS was removed from the wells containing the PEGDA–CMP gels and replaced with 500 μL of 80 °C CMP–RGD peptides. The modified gels were then placed at 37 °C in an incubator overnight. The next day, CMP–RGD solutions were removed from the wells, and gels were washed with PBS to remove unbound peptides. Subsequently, fibroblasts were seeded onto scaffolds by adding 750 μL of media (without FBS) containing 50 000 cells per mL into the wells. All phase-contrast images of seeded cells were taken using an EVOS phase-contrast microscope (Advanced Microscopy Group, Botwell,WA).

Cell proliferation assays

Twenty four hours after fibroblast seeding, 50 μL of the WST-1 reagent was added to each well and incubated for 2 h at 37 °C. Afterwards, the formazan dye absorbance generated from metabolically active cells was measured at 440 nm. Each modified scaffold condition was tested in triplicate, and two-tailed unpaired Student's *t* tests were conducted to determine the statistical significance of differences in cell proliferation.

Quantification of cell adhesion and morphology

Twenty four hours after seeding, fibroblasts were fixed with 200 μL of 10% neutral buffered formalin for 90 min. Fixed cells were then permeabilized and blocked with 200 μL TBS supplemented with 0.25% Triton X-100 and 5% donkey serum. The cells were then stained overnight with 200 μL of PBS solution containing DAPI (1 μg mL^{-1}) and phalloidin (0.165 μM). After washing the wells with TBS, fluorescent cell images were captured on a Nikon Eclipse TE2000-E (Nikon Instruments, Melville, NY). Each sample type was tested in triplicate, and fluorescent images from at least 5 regions were randomly taken from each scaffold. A customized pipeline from CellProfiler[30] software was used to analyze cell adhesion and morphology from each fluorescent image (1000 × 1000 pixels) corresponding to an area of 0.41 mm^2. The mean of values from triplicate gels was plotted in a cell population *vs.* area histogram for each condition.

Spatial modification of PEGDA–CMP with CF–CMP–RGD

For spatially controlled modification of PEGDA–CMP scaffolds with CF–CMP–RGD, 650 μL of 80 °C CF–CMP–RGD solution

(1 mM in PBS) was added to a dipping container. PEGDA–CMP gels were then partially submerged in the hot CF–CMP–RGD solution and incubated at 37 °C for 2 h to allow CF–CMP–RGD to bind to the exposed CMP in the gel. Gels were then removed from the dipping solutions and allowed to cool at room temperature for 30 min before transferring to a 24-well plate. Gels were covered with 500 μL of PBS and kept at room temperature overnight. The next day, gels were washed with PBS, a procedure that mimics the cell seeding conditions, and the CF–CMP–RGD absorbance at 493 nm was measured by scanning across the gel surface with a plate reader.

Studying the morphology of cells on the PEGDA–CMP hydrogel with the CMP–RGD gradient

PEGDA–CMP gels were synthesized under sterile conditions in the cell culture hood. These gels were then partially submerged into dipping containers filled with 80 °C CMP–RGD solutions (2.5 mM in PBS) and incubated at 37 °C for 2 h. The gels were then removed from the dipping solution, allowed to cool to room temperature in the cell culture hood for 30 min, and transferred into a 24-well plate. Gels were covered with 500 μL PBS and stored at room temperature overnight. To prepare for cell seeding, gels were washed with fresh PBS to remove unbound CMP–RGD. Fibroblasts (50 000 cells per mL in 750 μL media without FBS) were added to the wells containing the modified PEGDA–CMP scaffolds. After 24 h, the cells were fixed, permeabilized, blocked, and stained using the previously described protocol. Fluorescent images of the stained cells were taken, capturing 9 or more images each from the submerged, middle, and unsubmerged regions of the gels. These data were averaged to create histograms of cell frequency *vs.* area for the corresponding three regions of the scaffolds featuring the CMP–RGD gradient.

Creating multiple peptide gradients across PEGDA–CMP scaffolds

PEGDA–CMP scaffolds were photopolymerized from PEGDA, Acrl–PEG–CMP, and Irgacure 2959 precursor solutions in DI H_2O as described above. These gels were then partially submerged in 700 μL rhodamine–CMP–RGD (1 mM in DI H_2O) at 80 °C and incubated for 1 h at 37 °C. The rhodamine–CMP–RGD modified gels were removed and allowed to cool at room temperature for 30 min. A quenched CF–CMP–RGD solution was prepared by heating a stock CF–CMP–RGD solution (175 μL at 4 mM in DI H_2O) to 80 °C and diluting it into room temperature DI H_2O (525 μL) to generate 700 μL of quenched single-stranded CF–CMP–RGD at 1 mM concentration. This quenched CF–CMP–RGD solution was pipetted into the dipping container. To create PEGDA–CMP gels with opposing peptide gradients, the gels were inserted into the quenched CF–CMP–RGD in the dipping container in the opposite gel orientation compared to the rhodamine–CMP–RGD exposure. To create gels with quadrants of peptide modification, the gels were inserted into CF–CMP–RGD at 90° rotation from the rhodamine–CMP–RGD dipping orientation. After 37 °C incubation for 1 h, the multi-peptide treated gels were removed from the CF–CMP–RGD solution and cooled to room temperature for 30 min. The gels were transferred to a 24-well plate with 500 μL DI H_2O and incubated overnight at room temperature. The gels were rinsed with DI H_2O, and the local CF–CMP–RGD absorbance was measured at 493 nm using a plate reader. For absorbance measurements of rhodamine B, the gel coverage solution was replaced with 500 μL of 0.1% acetic acid in DI H_2O, and the absorbance was read at 564 nm. The resulting data were presented as average values with the standard error of the mean (SEM).

Results and discussion

Design and synthesis of photocrosslinkable collagen mimetic peptides and PEGDA–CMP hydrogels

Photopolymerization of PEG diacrylate (PEGDA) to generate a covalently crosslinked biocompatible hydrogel is a well-established technique.[31] The photopolymerization, which involves photoinitiation followed by radical polymerization, occurs in minutes even at high temperature (80 °C). In order to incorporate CMP covalently into the PEGDA network, we designed polymerizable CMP in the form of acrylamide–PEG–CMP that can be copolymerized with PEGDA. Since the photopolymerization process is quick and can be performed at a moderately high temperature, the precursor solution can be heated prior to the photopolymerization to ensure that the CMPs are incorporated into the PEGDA network in the form of melted single strands.

Despite previous success with $(POG)_7$, attempts to conjugate CMP of the sequence G_3-$(POG)_8$ onto commercially available acrylate–PEG–NHS resulted in a low yield. This could be explained by the lower reactivity of the long CMP [$(POG)_8$] compared to a shorter peptide sequence [$(POG)_7$], which was further exacerbated by the triple helical conformation that creates steric crowding at the N-terminus. Furthermore, dialysis or size exclusion column purification techniques were ineffective due to the size similarity between the acrylate–PEG–NHS and the CMP as well as triple helical associations of unreacted CMP with PEG–CMP complexes.

We chose to generate a new type of photocrosslinkable CMPs (Acrl–PEG–CMP) entirely by solid phase peptide synthesis (Scheme 1). The G_3-$(POG)_8$ peptide sequence was prepared on a solid support resin by manual peptide synthesis. Using Fmoc chemistry, we conjugated a short discrete PEG (dPEG) spacer at the N-terminus of the peptide to provide flexibility and hydrophilicity. The dPEG spacer gives flexibility to the CMP after it is

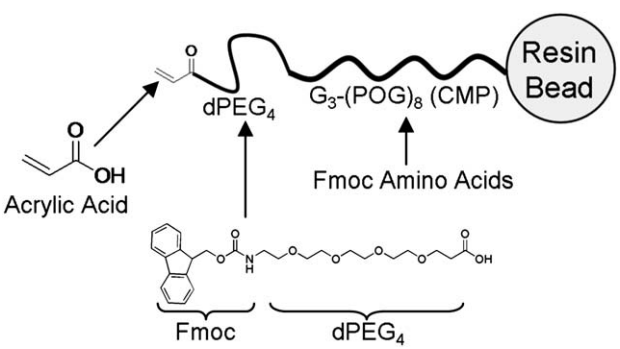

Scheme 1 Design of the photocrosslinkable Acrl–PEG–CMP peptide prepared by solid-phase peptide synthesis.

photopolymerized into the PEGDA hydrogel but is short enough to mitigate triple helical association of neighboring CMPs in the photocrosslinked gel. Finally, acrylic acid was coupled to the peptide's N-terminus to provide the photopolymerizable vinyl group. MALDI-ToF mass spectrometry indicated the pure product with no side products lacking in dPEG or acrylic acid groups (ESI, Fig. S1†).

The high reaction yield was mainly a result of the peptide's enhanced reactivity as it resides on the solid support in the single-stranded form without tertiary structure. In addition, unreacted reagents can be removed by washing the resin before Acrl–PEG–CMP cleavage, eliminating the need for yield-reducing dialysis purification.

PEGDA–CMP gels were created by first generating a precursor solution in PBS with 9 wt% PEGDA (3400 Da), 1 wt% Acrl–PEG–CMP, and 0.05% photoinitiator (Irgacure 2959). The precursor solution was heated to 80 °C in order to melt the CMPs into single strands, loaded between two glass cover slips, and exposed to UV-light (5 mW cm^{-2} for 10 min) to form a gel. The top cover slip was lifted to reveal the PEGDA–CMP gel for further experiments. This synthesis approach of co-photopolymerizing single-stranded Acrl–PEG–CMP with PEGDA allowed maximum preservation of CMP's single-stranded form in the hydrogel, which was critical for peptides to work as available binding partners for further modification of the hydrogel.

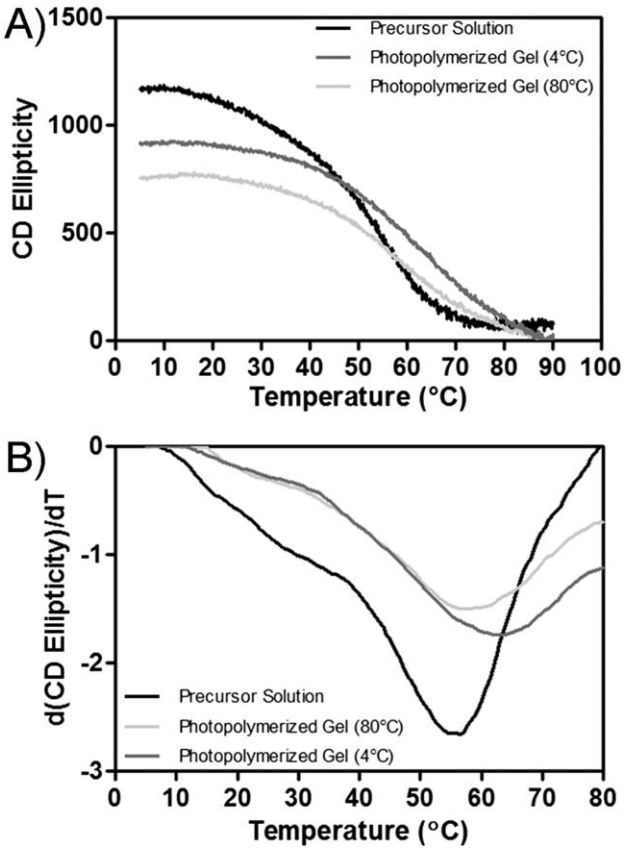

Fig. 1 (A) Circular dichroism melting curves of the PEGDA–CMP precursor solution and PEGDA–CMP gel photopolymerized at 4 °C and 80 °C. (B) First derivatives of corresponding CD melting curves.

Study of the triple helical structure in the PEGDA–CMP hydrogel

To investigate the tertiary structure of CMPs in the photocrosslinked hydrogel, we measured the triple helical content using circular dichroism (CD). The CD melting curve of the PEGDA–CMP gel precursor solution (before UV photocrosslinking) showed a clear sigmoidal melting transition with T_m at 57 °C (Fig. 1). In the case of PEGDA–CMP gel photocrosslinked from the 80 °C precursor solution, the CD melting curve showed an overall reduced intensity as well as a much broader melting transition. The CD melting curve of the PEGDA–CMP gel photocrosslinked from the 4 °C precursor solution showed a partial recovery of the CD signal towards the precursor solution.

The low CD signal for the gel photocrosslinked after 80 °C incubation of the precursor indicates that portions of the CMPs are conjugated to the PEGDA hydrogel network in a way that does not support a triple helix assembly with other CMPs in the hydrogel. The shallow slope of this temperature-dependent CD melting curve mirrors the case of a mixture of triple helical CMPs and single-stranded peptides having a non-triple helical polyproline-II structure (ESI, Fig. S2†). While the CD signal does show a gradual sigmoidal transition of triple helix melting, the intensity and slope of the signal are tempered by the contribution from single-stranded CMPs in polyproline-II conformations whose CD signal (ellipticity at 231 nm) decreases linearly with rising temperature.[24]

The notion of a mixture of triple helical and single-stranded peptides in the PEGDA–CMP gel was further supported by studying the PEGDA–CMP samples photocrosslinked from cold (4 °C) precursor solutions, which have the full triple helical content at the start of gelation. The increase in the CD signal and steeper sigmoidal curve suggest a higher triple helical content for these gels compared to those photopolymerized from 80 °C precursors. This signal intensity is still lower than that obtained from the precursor solution before the gelation. It seems that the heat generated during UV exposure may have melted some of the peptides during gelation. It is also possible that the polymerization/gelation processes force an imperfect triple helix registry that lowers the triple helix thermal stability.

Triple helical hybridization between the CMPs in the photocrosslinked hydrogel and exogenously added CMPs can only occur if the two peptides are initially in a single-stranded form. The results indicate that the CMPs are photocrosslinked into the PEGDA–CMP scaffold in a single-stranded form, acting as open binding partners for bioactive CMPs that can be added to a preformed gel. We note that even triple helical CMPs in PEGDA–CMP can participate in binding with other CMPs if a hot CMP solution is used since the high temperature can melt the homotrimeric CMPs of the gel and allow CMP exchange for heterotrimeric triple helix formation.

Bioactive CMP–RGD peptides and PEGDA–CMP functionalization

For the bioactive CMPs to be used for PEGDA–CMP gel functionalization, we synthesized bifunctional CMP–RGD with a sequence of $(POG)_8$-G_3-RGDSY that features a CMP

sequence, $(POG)_8$, for triple helix-mediated binding to photopolymerized PEGDA–CMP and an RGDS sequence for cell adhesion. Tyrosine was added to the C-terminus for peptide quantification by UV-vis spectroscopy. The peptide was designed with the CMP sequence at the N-terminus so that after the triple helical hybridization to the PEGDA–CMP scaffold, the RGDS ligand is positioned away from the PEG backbone toward potential binding receptors (*e.g.* integrins on the cell surface). These CMP–RGD peptides can be heated to melt into a single-stranded state and then added to pre-formed PEGDA–CMP gels for triple helix-mediated conjugation. In this construct, the PEGDA–CMP system mimics the structural framework of the ECM while the CMP–RGD peptide imitates the adhesive proteins of the ECM (*e.g.* fibronectin) by physically binding to the scaffold and mediating cellular adhesion.

The RGDS cell adhesion sequence is one of the many RGD-type sequences associated with integrin binding. Specific cell types produce the predominant cell adhesion integrins, such as αvβ3, α5β1, and αIIβ3, at different expression levels.[32] These different integrin types, in turn, exhibit varying affinities for different RGD sequences, *e.g.* RGDS, RGDVY, and RGDNP. For example, endothelial cells have shown enhanced attachment to αvβ3 integrin selective RGD sequences, whereas fibroblasts preferably attach to an α5β1 integrin selective surface.[33] We chose to use an RGDS adhesion sequence because it shows intermediate affinity to both αvβ3 and α5β1 integrins and therefore provides some flexibility in the cell types to be used for adhesion studies.[34]

To investigate the binding of CMP–RGD peptide to the PEGDA–CMP scaffold, the peptide's N-terminus was labeled with carboxyfluorescein (CF–CMP–RGD). CD studies showed that this peptide forms a stable triple helix with $T_m = 57$ °C and was expected to form stable triple helices with photocrosslinked PEGDA–CMP at cell culture conditions (37 °C). Hot CF–CMP–RGD solutions (80 °C) were applied to photocrosslinked PEGDA–CMP gels, incubated at 37 °C overnight, and the gel was washed with PBS to remove unbound CMPs before measuring the fluorescence of the gels. The initial binding level was determined, and the cumulative release of peptides from the gels at 37 °C was tracked for several days (Fig. 2).

The cumulative release profile indicated sustained release behavior that correlated with the loading level. Adding a more concentrated CF–CMP–RGD solution resulted in a higher initial binding level. However, the percentage of added CF–CMP–RGD peptides that bound to the scaffold was decreased when the concentration of the loading solution was increased. This may be due to the limited number of available Acrl–PEG–CMP binding partners in the gel. Additionally, concentrated CF–CMP–RGD peptide solutions have a greater tendency to form homotrimeric triple helices before hybridization with CMPs in the photocrosslinked gel. The initial binding assay from 761 μM CF–CMP–RGD solutions indicated 14.7 nmoles cm^{-2} of bound peptide, a density far exceeding the minimum RGD concentrations (picomole per cm^2) previously reported to promote cell adhesion *via* integrin–RGD interactions.[35,36] In contrast, peptide solutions added to PEGDA-only scaffolds did not exhibit significant binding because without the photocrosslinked CMPs in the scaffold, the bioactive peptides lack binding partners in the gel and are removed during washes.

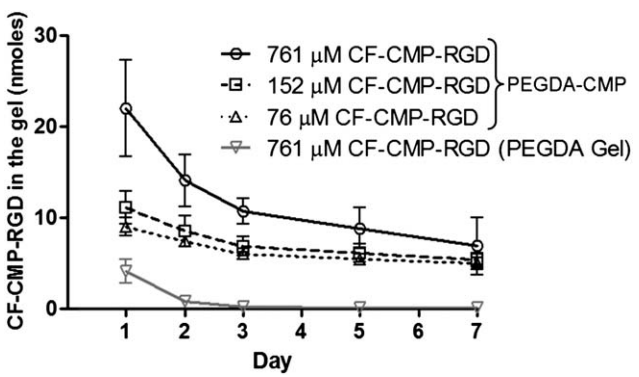

Fig. 2 Cumulative release profiles of CF–CMP–RGD from PEGDA–CMP gels and from PEGDA-only gels. Single-stranded CF–CMP–RGD were added to gels at varying concentrations and left at 37 °C overnight to allow triple helix-mediated binding. The gels were washed with PBS to remove unbound peptides and their CF absorbance was monitored over the following days at 37 °C. Data reported as mean ± SD.

Cell seeding experiments on CMP–RGD modified PEGDA–CMP scaffolds

To create bioactive PEGDA–CMP scaffolds, photopolymerized gels were covered with 80 °C CMP–RGD peptide solutions, allowed to cool, and incubated overnight at 37 °C. The modified gels were then washed with PBS to remove unbound CMP–RGD. Human dermal neonatal fibroblasts were seeded onto these scaffolds at 50 000 cells per mL in 750 μL of fetal bovine serum free media. Control samples included PEGDA–CMP gels modified with the CMP peptide lacking the RGD sequence and PEGDA-only gels treated similarly with a hot CMP–RGD solution.

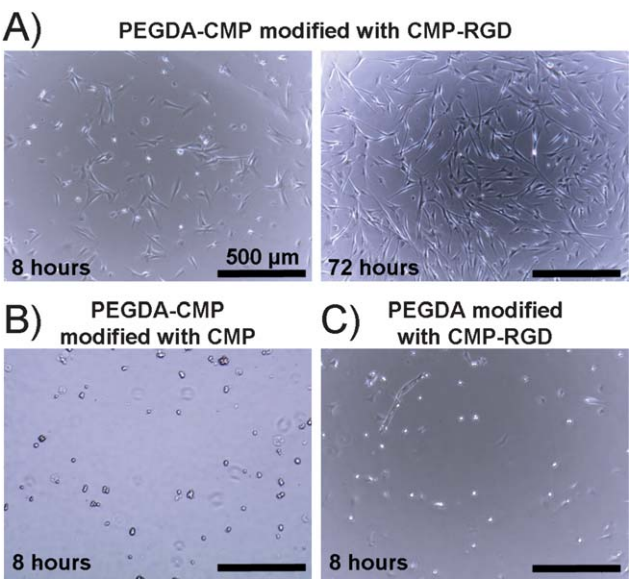

Fig. 3 Phase contrast micrographs of human dermal neonatal fibroblasts seeded onto PEGDA–CMP scaffolds modified with CMP–RGD (A), PEGDA–CMP modified with CMP (B), and PEGDA modified with CMP–RGD (C).

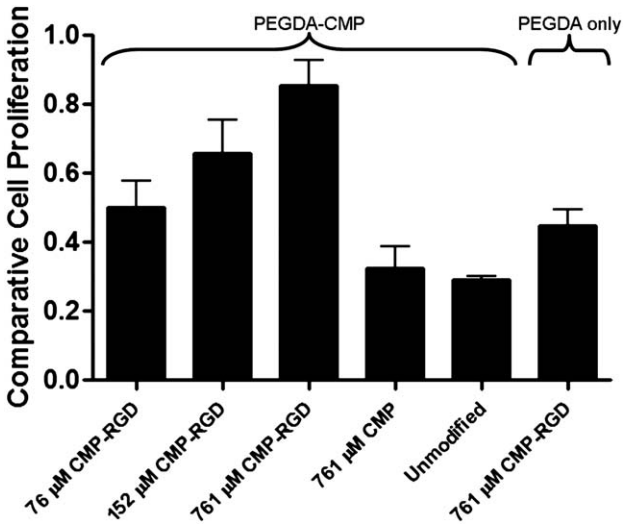

Fig. 4 WST-1 proliferation assay (absorbance at 440 nm) of fibroblasts seeded on PEGDA–CMP modified with CMP–RGD and control hydrogels: PEGDA–CMP modified with CMP and PEGDA hydrogel (without CMP) modified with CMP–RGD. CMP–RGD modified PEGDA–CMP scaffolds showed higher cell proliferation compared to control samples (Student's t test, $p < 0.005$). Data reported as mean ± SD.

Several hours after seeding, fibroblasts adhered and began to spread on CMP–RGD modified PEGDA–CMP scaffolds (Fig. 3A and ESI, Fig. S3†). In contrast, primarily rounded cell morphology was seen on control scaffolds (Fig. 3B and C). Cell culture experiments using human umbilical vein endothelial cells (HUVECs) showed similar results in which HUVECs only exhibited characteristic cobblestone morphology on CMP–RGD modified PEGDA–CMP scaffolds but not on control gels (ESI, Fig. S4†). The bioactive PEGDA–CMP gels spurred fibroblast attachment and proliferation over several days and up through cell confluency (ESI, Fig. S5†). However, cells on all control scaffolds remained rounded and began to clump together overtime as they underwent apoptosis.

The viability of cells on these scaffolds was quantified by a colorimetric WST-1 proliferation assay, 24 h after cell seeding (Fig. 4). Fibroblasts exhibited markedly increased proliferation on scaffolds with higher CMP–RGD concentrations. Control samples of unmodified PEGDA–CMP and PEGDA–CMP modified with CMPs without an RGD sequence retained the lowest cell viability. The PEGDA-only scaffold modified with CMP–RGD (761 μM) also showed significantly lower cell viability than the PEGDA–CMP modified with CMP–RGD (761 μM) ($p < 0.005$). These findings clearly indicate that cells

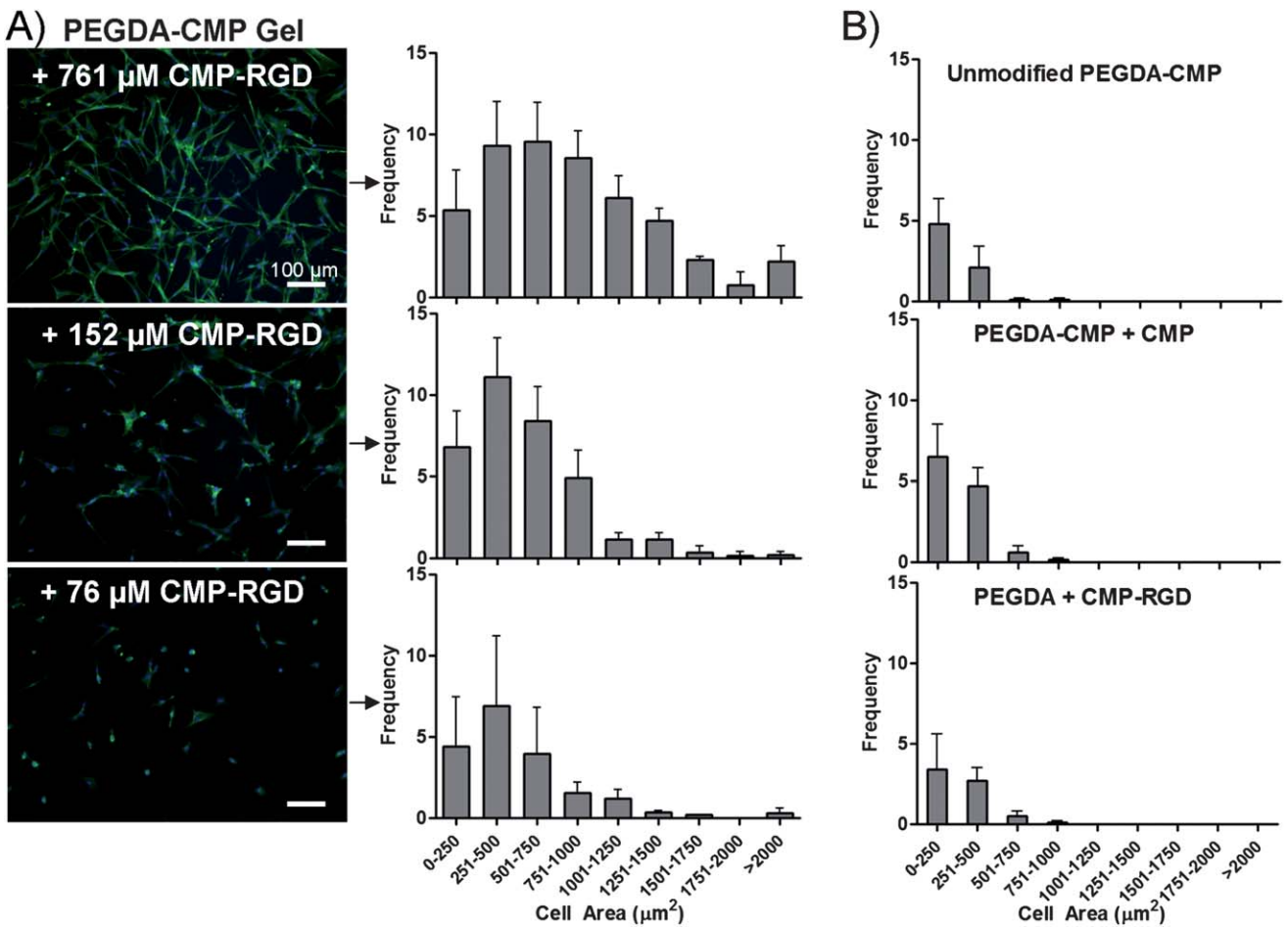

Fig. 5 (A) Fluorescence micrographs and corresponding cell area histograms of fibroblasts stained with DAPI (stains nucleus in blue) and phalloidin (stains actin in green). Cells exhibited enhanced adhesion and spread morphology on PEGDA–CMP scaffolds modified with increasing concentrations of CMP–RGD. (B) Cell area histograms for cells seeded on control scaffolds showing reduced cell adhesion. Data reported as mean ± SD.

require both the cell-adhesive capacity of the CMP–RGD ligand and the CMP–CMP hybridization partners that immobilize the RGD units to the PEGDA scaffold to mediate lasting cell adhesion and proliferation.

The cell morphology in response to the CMP–RGD concentration was further quantified by image analysis. Fibroblasts cultured on PEGDA–CMP hydrogels were fixed and treated with DAPI and phalloidin for nuclei and F-actin staining, respectively. We took fluorescent images of these cells on scaffold surfaces and conducted image analysis to quantify the cell coverage area using CellProfiler software. As shown in the cell area histograms of Fig. 5, use of higher concentrations of CMP–RGD resulted in higher cell adhesion and average cell coverage area on the PEGDA–CMP scaffolds. In contrast, the control scaffolds showed fewer adhered cells and very low cell coverage area. This study demonstrates that the base PEGDA–CMP scaffold can be encoded with varying concentrations of cell-instructive cues to induce a range of cell spreading morphology.

Spatially controlled modification of PEGDA–CMP scaffolds

Natural ECMs often exhibit spatial gradients of biochemical and mechanical signals that allow continuous transition of one tissue type to another. Such gradients can be very helpful for engineering complex tissues but are difficult to reproduce in conventional polymeric scaffolds that do not possess specific sites for scaffold modification. We created a spatial gradient of CF–CMP–RGD in PEGDA–CMP gels and quantified it by mapping CF absorbance across the gel (Fig. 6A). The gradient was achieved by partially dipping PEGDA–CMP gels into a hot CMP–RGD solution and allowing the peptide to diffuse into the gel and hybridize with CMPs of the PEGDA–CMP scaffold (ESI, Fig. S6†). Fibroblasts were seeded onto these gels, and the cellular morphology across the scaffold was quantified using the CellProfiler image analysis as described above. The spatial transition of the cell morphology clearly mirrored the spatial gradient of the bioactive peptides on the gel (ESI, Fig. S7†). Specifically, we saw the highest number of adhered cells with well-spread morphology at the area of the scaffold with the highest CF–CMP–RGD concentration. Moving from the submerged regions (high CF–CMP–RGD) towards the unsubmerged regions (low CF–CMP–RGD) of the scaffold, the fibroblast adhesion and spreading gradually decreased (Fig. 6B). These results demonstrate that the CMP-based modification system can be used to develop biomaterials with spatial gradients of cell-instructive cues that continuously influence cell–scaffold interactions.

The CMP mediated gradient formation in the PEGDA–CMP hydrogel can be further developed to produce spatial patterns and gradients of more than one component. We created PEGDA–CMP hydrogels modified with two opposing CMP gradients by dipping one side of the hydrogel in 80 °C rhodamine–CMP–RGD solution followed by dipping the opposing side in a quenched CF–CMP–RGD solution. The second solution was quickly quenched from 80 °C just prior to the hydrogel treatment to ensure that the CMPs that were already bound by prior treatment do not thermally melt and release from the hydrogel. Previously, we reported successful modification of the collagen scaffold with the quenched CMP solution by taking advantage of the slow folding rate of the triple helix.[37,38] This procedure is readily applicable to modifying 3D scaffolds that contain live cells and heat sensitive bioactive molecules. Fig. 7A shows the two opposing fluorescent CMP gradients in the

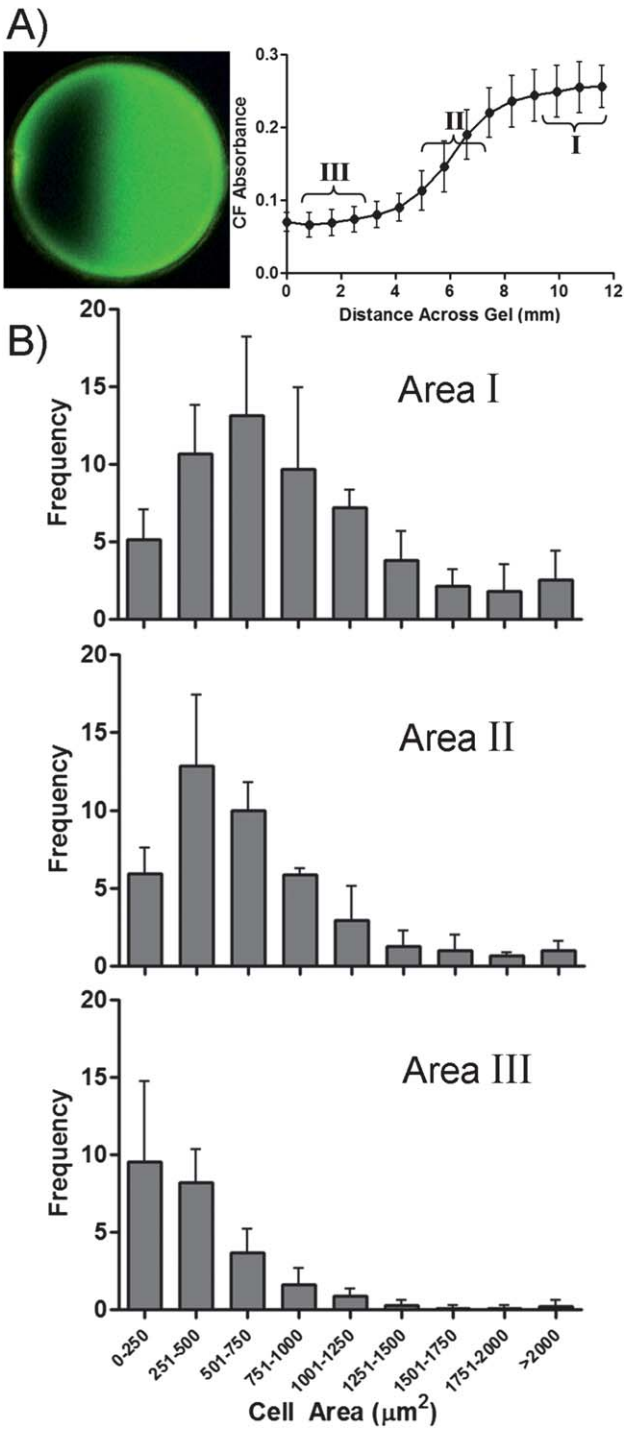

Fig. 6 (A) Image of PEGDA–CMP gel partially treated with CF–CMP–RGD and CF absorbance profile across the gel. (B) Cell area histograms (fibroblasts after 24 h culture) corresponding to the three areas defined in A demonstrating modulation of the cell morphology across PEGDA–CMP scaffolds with an RGD gradient formed by triple helical CMP association. Data reported as mean ± SD.

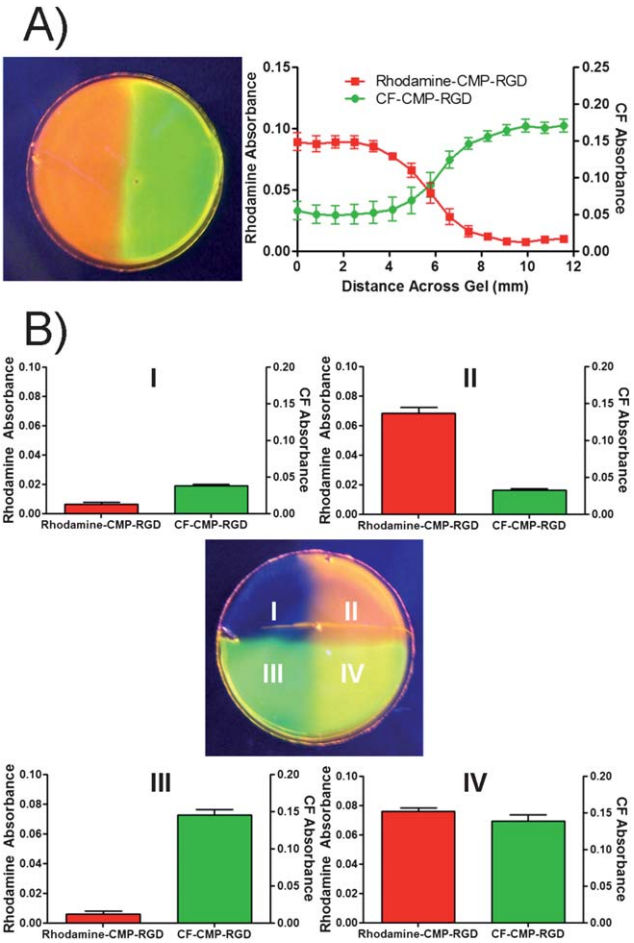

Fig. 7 (A) PEGDA–CMP gel modified with rhodamine (red) and CF (green) labeled CMP–RGD. Local absorbance measurements for rhodamine (564 nm) and CF (493 nm) labeled peptides show opposing gradients across the gel. (B) PEGDA–CMP scaffolds modified into quadrant patterns with rhodamine and CF labeled peptides. Data reported as mean ± SEM ($n \geq 3$).

PEGDA–CMP hydrogel across a 12 mm distance. Using a similar approach of selectively exposing the hydrogel to CMP solutions, we also produced PEGDA–CMP hydrogels modified with the rhodamine tagged and CF tagged CMPs in quadrant patterns (Fig. 7B).

The triple helical hybridization interactions between CMP and the PEGDA–CMP provide a convenient way to encode spatially defined bioactive signals to the biologically inert PEGDA hydrogel. Therefore, in addition to serving as scaffolds for complex tissue engineering, the PEGDA–CMP system could be used for testing a spatially defined library of matrix-bound cell signals to identify concentration/composition dependent activity of insoluble signals in the ECM which are critical for differentiation and tissue development of cells with therapeutic potential (*e.g.* stem cells).[39,40]

Conclusions

The collagen triple helix is a distinct protein structure that is rarely found in other non-collagenous proteins.[41] By taking advantage of the structural scarcity and the stability of the triple helix, we developed a highly specific, non-covalent conjugation tool based on triple helical hybridization. We synthesized PEGDA hydrogels displaying CMPs that serve as triple helix-mediated conjugation sites by copolymerization of PEGDA with Acrl–PEG–CMP. This PEGDA–CMP hydrogel can be readily encoded with CMP conjugates simply by the addition of a solution containing single-stranded CMP. With the use of CMP–RGD conjugates, we were able to create not only individual PEGDA–CMP hydrogels that vary in the RGD peptide concentration but also those with spatially defined gradients and patterns, which mimic the distribution of matrix-associated cell signaling molecules in natural ECM. The morphology of seeded fibroblasts directly indicated the level of concentration and concentration gradients of CMP–RGD bound to the PEGDA–CMP hydrogel. Others have created cell adhesive gradients by photo-patterning or by using a microfluidic device and gradient makers.[42–44] Although these methods may offer better control over the composition of the spatial gradients, they are either limited to 2D surfaces or require complicated fabrication processes. We believe that the CMP hybridization approach is a simple system that is conducive to producing multiple components of gradients. Since diffusion is used to create the gradient, it can be readily extended to fabricating 3D gradient systems. This is a new approach to encoding insoluble cellular signals to polymer scaffolds which could be useful for studying cell behaviors in response to spatially displayed signals and ultimately for complex tissue engineering.

Acknowledgements

We thank Stephen Fisher, Yang Li, Xingyu Liu, and Hai-Quan Mao for useful discussions, J. Michael McCaffery and Erin Price for help with electron microscopy, and Tania Chan for help with cell culture. This work was supported by grants from the NSF (DMR-0645411), NIAMS/NIH (R01AR060484), and DOD to S.M.Y., as well as fellowships to P.J.S. from HHMI Graduate Training Program (NBMed) and National Defense Science and Engineering Graduate Fellowship Program (32 CFR 168a).

References

1 M. P. Lutolf and J. A. Hubbell, *Nat. Biotechnol.*, 2005, **23**, 47–55.
2 J. Taipale and J. Keski-Oja, *FASEB J.*, 1997, **11**, 51–59.
3 J. E. Park, G. A. Keller and N. Ferrara, *Mol. Biol. Cell*, 1993, **4**, 1317.
4 K. Y. Lee and D. J. Mooney, *Chem. Rev.*, 2001, **101**, 1869–1880.
5 J. L. Drury and D. J. Mooney, *Biomaterials*, 2003, **24**, 4337–4351.
6 E. A. Phelps, N. Landázuri, P. M. Thulé, W. R. Taylor and A. J. García, *Proc. Natl. Acad. Sci. U. S. A.*, 2010, **107**, 3323.
7 H. J. Lee, J. S. Lee, T. Chansakul, C. Yu, J. H. Elisseeff and S. M. Yu, *Biomaterials*, 2006, **27**, 5268–5276.
8 H. J. Lee, C. Yu, T. Chansakul, N. S. Hwang, S. Varghese, S. M. Yu and J. H. Elisseeff, *Tissue Eng., Part A*, 2008, **14**, 1843–1851.
9 A. Y. Wang, X. Mo, C. S. Chen and S. M. Yu, *J. Am. Chem. Soc.*, 2005, **127**, 4130–4131.
10 M. D. Shoulders and R. T. Raines, *Annu. Rev. Biochem.*, 2009, **78**, 929.
11 X. Mo, Y. An, C. S. Yun and S. M. Yu, *Angew. Chem.*, 2006, **118**, 2325–2328.
12 Y. Li, X. Mo, D. Kim and S. M. Yu, *Biopolymers*, 2011, **95**, 94–104.
13 C. Kelliher, S. Chakravarti, N. Vij, S. Mazur, P. J. Stahl, C. Engler, M. Matthaei, S. M. Yu and A. S. Jun, *Exp. Eye Res.*, 2011, **93**, 880–888.
14 A. Y. Wang, C. A. Foss, S. Leong, X. Mo, M. G. Pomper and S. M. Yu, *Biomacromolecules*, 2008, **9**, 1755–1763.

15 A. Y. Wang, S. Leong, Y.-C. Liang, R. C. C. Huang, C. S. Chen and S. M. Yu, *Biomacromolecules*, 2008, **9**, 2929–2936.
16 C. M. Yamazaki, S. Asada, K. Kitagawa and T. Koide, *Pept. Sci.*, 2008, **90**, 816–823.
17 C. Kojima, S. Tsumura, A. Harada and K. Kono, *J. Am. Chem. Soc.*, 2009, **131**, 6052–6053.
18 C. M. Pérez, A. Panitch and J. Chmielewski, *Macromol. Biosci.*, 2011, **11**, 1426–1431.
19 J. Luo and Y. W. Tong, *ACS Nano*, 2011, **5**, 7739–7747.
20 M. B. Browning, D. Dempsey, V. Guiza, S. Becerra, J. Rivera, B. Russell, M. Höök, F. Clubb, M. Miller, T. Fossum, J. F. Dong, A. L. Bergeron, M. Hahn and E. Cosgriff-Hernandez, *Acta Biomater.*, 2012, **8**(3), 1010–1021.
21 S. Q. Liu, Q. Tian, J. L. Hedrick, J. H. Po Hui, P. L. Rachel Ee and Y. Y. Yang, *Biomaterials*, 2010, **31**, 7298–7307.
22 C. D. Reyes and A. J. García, *J. Biomed. Mater. Res., Part A*, 2003, **65**, 511–523.
23 O. D. Krishna, A. K. Jha, X. Jia and K. L. Kiick, *Biomaterials*, 2011, **32**, 6412–6424.
24 P. J. Stahl, N. H. Romano, D. Wirtz and S. M. Yu, *Biomacromolecules*, 2010, **11**, 2336–2344.
25 Z. Junmin, *Biomaterials*, 2010, **31**, 4639–4656.
26 M. Chen, M. P. Marinkovich, A. Veis, X. Cai, C. N. Rao, E. A. O'Toole and D. T. Woodley, *J. Biol. Chem.*, 1997, **272**, 14516–14522.
27 M. C. Erat, D. A. Slatter, E. D. Lowe, C. J. Millard, R. W. Farndale, I. D. Campbell and I. Vakonakis, *Proc. Natl. Acad. Sci. U. S. A.*, 2009, **106**, 4195–4200.
28 M. L. C. Erat, U. Schwarz-Linek, A. R. Pickford, R. W. Farndale, I. D. Campbell and I. Vakonakis, *J. Biol. Chem.*, 2010, **285**, 33764–33770.
29 V. Gauba and J. D. Hartgerink, *J. Am. Chem. Soc.*, 2007, **129**, 2683–2690.
30 A. Carpenter, T. Jones, M. Lamprecht, C. Clarke, I. Kang, O. Friman, D. Guertin, J. Chang, R. Lindquist, J. Moffat, P. Golland and D. Sabatini, *Genome Biol.*, 2006, **7**, R100.
31 K. T. Nguyen and J. L. West, *Biomaterials*, 2002, **23**, 4307–4314.
32 U. Hersel, C. Dahmen and H. Kessler, *Biomaterials*, 2003, **24**, 4385–4415.
33 S. P. Massia and J. Stark, *J. Biomed. Mater. Res., Part A*, 2001, **56**, 390–399.
34 M. Pfaff, K. Tangemann, B. Müller, M. Gurrath, G. Müller, H. Kessler, R. Timpl and J. Engel, *J. Biol. Chem.*, 1994, **269**, 20233–20238.
35 S. P. Massia and J. A. Hubbell, *J. Cell Biol.*, 1991, **114**, 1089–1100.
36 D. L. Elbert and J. A. Hubbell, *Biomacromolecules*, 2001, **2**, 430–441.
37 T. R. Chan, P. J. Stahl and S. M. Yu, *Adv. Funct. Mater.*, 2011, **21**, 4252–4262.
38 M. S. Ackerman, M. Bhate, N. Shenoy, K. Beck, J. A. M. Ramshaw and B. Brodsky, *J. Biol. Chem.*, 1999, **274**, 7668–7673.
39 D. S. W. Benoit, M. P. Schwartz, A. R. Durney and K. S. Anseth, *Nat. Mater.*, 2008, **7**, 816–823.
40 F. Yang, S.-W. Cho, S. M. Son, S. P. Hudson, S. Bogatyrev, L. Keung, D. S. Kohane, R. Langer and D. G. Anderson, *Biomacromolecules*, 2010, **11**, 1909–1914.
41 B. Brodsky and J. A. M. Ramshaw, *Matrix Biol.*, 1997, **15**, 545–554.
42 B. P. Harris, J. K. Kutty, E. W. Fritz, C. K. Webb, K. J. L. Burg and A. T. Metters, *Langmuir*, 2006, **22**, 4467–4471.
43 J. A. Burdick, A. Khademhosseini and R. Langer, *Langmuir*, 2004, **20**, 5153–5156.
44 D. Guarnieri, A. De Capua, M. Ventre, A. Borzacchiello, C. Pedone, D. Marasco, M. Ruvo and P. A. Netti, *Acta Biomater.*, 2010, **6**, 2532–2539.

Available online at www.sciencedirect.com

ScienceDirect

Current Opinion in Chemical Biology

Targeting and mimicking collagens via triple helical peptide assembly☆

Yang Li[1] and S Michael Yu[1,2]

Q1 I confirm that given names and surnames have been identified correctly.

As the major structural component of the extracellular matrix, collagen plays a crucial role in tissue development and regeneration. Since structural and metabolic abnormalities of collagen are associated with numerous debilitating diseases and pathologic conditions, the ability to target collagens of diseased tissues could lead to new diagnostics and therapeutics. Collagen is also a natural biomaterial widely used in drug delivery and tissue engineering, and construction of synthetic collagen-like materials is gaining interests in the biomaterials community. The unique triple helical structure of collagen has been explored for targeting collagen strands, and for engineering collagen-like functional assemblies and conjugates. This review focuses on the forefront of research activities in the use of the collagen mimetic peptide for both targeting and mimicking collagens via its triple helix mediated strand hybridization and higher order assembly.

Addresses
[1] Department of Bioengineering, University of Utah, Salt Lake City, UT 84112, USA
[2] Institute for NanoBiotechnology, Johns Hopkins University, Baltimore, MD 21218, USA

Corresponding author: Yu, S Michael (michael.yu@utah.edu, yu@jhu.edu)

Current Opinion in Chemical Biology 2013, **17**:xx–yy

This review comes from a themed issue on **Synthetic biomolecules**

Edited by **Shang-Cheng Hung** and **Dek Woolfson**

1367-5931/$ – see front matter,

http://dx.doi.org/10.1016/j.cbpa.2013.10.018

Introduction

Collagen, the most abundant protein in mammals, plays a critical role in tissue development and regeneration. It is a major structural component of the extracellular matrix (ECM), where cells proliferate and differentiate. While fibrous collagens (e.g., type I, II) provide mechanical strength to connective tissues, network-like collagens (e.g., type IV) form the basic scaffold of the basement membrane where cells attach and grow into organized tissues. Abnormal collagen remodeling activities are typically seen during wound healing response and in chronic pathological conditions such as cancer, osteoporosis, arthritis, and fibrosis. Therefore, the ability to target remodeling collagens could help understand the progression of such diseases, as well as provide new diagnostic and therapeutic opportunities. Collagen is one of the most widely used natural biomaterials for medical applications in biocompatible coatings, drug delivery and tissue engineering. However, in order to overcome the structural and compositional complexity of animal-derived collagen, researchers are constructing artificial collagen-like scaffolds with tunable physico-chemical properties and unique biological functions. Collagen mimetic peptide (CMP) is a family of small synthetic peptides that mimic natural collagens: they share the collagen's hallmark structural motif — the triple helix, as well as the Gly-Xaa-Yaa triplet repeat sequence, where Xaa and Yaa are largely populated by proline and 4(*R*)-hydroxylproline, respectively [1]. These peptides were traditionally used as synthetic models to study the structure and folding behaviors of collagens [1]. In this review, we will discuss recent progress in two distinct research areas in the biomedical application of CMPs: firstly targeting collagens in pathological tissues [2••,3,4,5•], and secondly creating self-assembled collagen-like biomaterials and molecular constructs [6,7,8••], both of which are based on the CMP's unique triple helical structure. With our eyes set on identifying applications in bioimaging, drug delivery, and tissue engineering, we will review recent progress in CMP-based collagen/gelatin targeting in the context of other collagen-targeting molecules, as well as highlight various CMP derivatives, and collagen mimetic assemblies and conjugates that are inspired by the structure and function of natural collagen.

Collagen-targeting molecules

Among many collagen binding molecules, only a few have been explored in the context of collagen targeting. One example is CNA35, a 35 kDa collagen-binding domain in the adhesin protein found on the surface of bacterium *Staphylococcus aureus*, which hugs the triple helical collagen molecule with its two subdomains through hydrophobic interactions [9]. Merkx group and others developed fluorescently labeled recombinant CNA35 and CNA35-functionalized micelles for visualization of collagens in various biological samples including cell culture (e.g., collagen-producing myofibroblasts), engineered tissue constructs, and animal tissues (e.g., blood

Please cite this article in press as: Li Y, Yu SM. Targeting and mimicking collagens via triple helical peptide assembly, Curr Opin Chem Biol (2013), http://dx.doi.org/10.1016/j.cbpa.2013.10.018

vessels and kidney) [10–12]. They found out that fluorescent CNA35 administered *in vivo* shows high uptake in atherosclerotic arteries, particularly in the areas of atherosclerotic plaque that are rich in collagen networks [13]. Using the phage display method, Caravan and coworkers developed a type I collagen-binding cyclic peptide which was used as MRI contrast agent for myocardial scar [14]. During the phage display efforts to find cartilage binding peptides, Hubbell's research group identified a type II collagen binding peptide of sequence WYRGRL. This peptide supported local delivery and immobilization of polymeric nanoparticles in knee cartilages after intra-articular injection [15]. A peptide mimetic of glycoprotein VI, the main platelet receptor of type I and III collagens, was used for *in vivo* radioactive imaging of lung fibrosis and scars in healed myocardial infarction [16]. A peptide derived from the collagen-binding proteoglycan, decorin, was also used to target collagens to modulate collagen fibrillogenesis [17], and to reduce collagen degradation and dermal scarring [18].

Since collagen is present ubiquitously in the body, collagen-binding molecules discussed above face the challenge of distinguishing collagens in the diseased tissue from those in the healthy tissue, if they are to be used for targeted drug delivery and molecular imaging [13]. Some strategies have been taken to design or select collagen targeting molecules that are more specific to collagens in diseased tissues. Recombinant CNA35 constructs whose collagen-binding is activated by matrix metalloproteinases (MMPs) showed improved selectivity for collagens undergoing MMP-mediated remodeling [19,20]. Library approaches have been used to identify monoclonal antibody [21,22] and peptides [23] that specifically bind to cryptic sites in collagen strands that become exposed after denaturation. For example, humanized monoclonal antibody (D93) that recognizes the GPO repeating sequence in denatured collagen strands was developed by Baeuerle and coworkers [22,24]. Studies showed that D93 specifically adheres to vascular basement membrane in tumors but not to blood vessels in normal tissues [22]. The peptide sequence, TLTYTWS, which was selected by phage display for binding to MMP2-modified type IV collagen was found to accumulate in tumors and inhibit angiogenesis *in vivo* [23].

CMP-collagen hybridization

The triple helix, which is the hallmark structure of collagen, provides a unique mechanism for targeting denatured collagen strands. The triple helical tertiary structure is nearly exclusively seen in collagens except as small sub-domains in a few non-collagen proteins [1]. During tissue remodeling, the collagen molecules within the collagen fibers and networks are degraded by proteases (e.g., MMPs or cathepsin) and become denatured at body temperature. We recently discovered that the collagen mimetic peptide [sequence: $(GPO)_n$, $n = 6–10$] with its strong triple helix folding propensity can specifically bind to such denatured collagen strands both *in vitro* and *in vivo* (Figure 1) [2••,3,25]. This binding is primarily driven by the triple helix hybridization between monomeric CMPs and the denatured collagen strands, which is

Figure 1

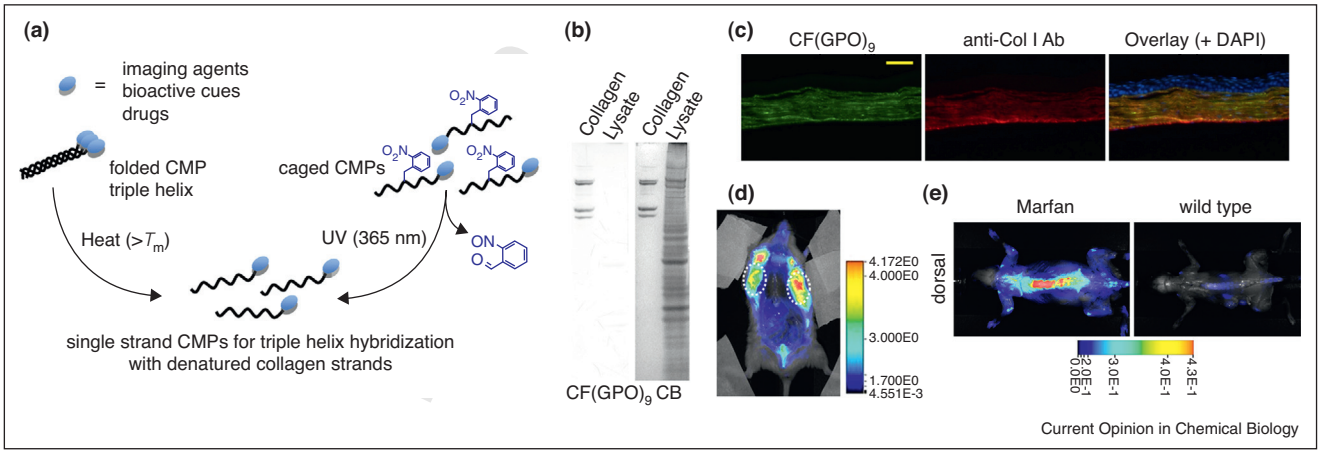

(a) Schematic illustration of two approaches (heat and UV activation) to generate single strand CMPs that hybridize with denatured collagen strands. **(b)** Fluorescent images of SDS-PAGE gel loaded with type I collagen and endothelial cell lysate stained by carboxyfluorescein-labeled CMP [$CF(GPO)_9$] (left) in comparison to the same gel stained by coomassie blue (CB) (right) showing high specificity of CMP-collagen hybridization (adapted from Ref. [3]). **(c)** Fluorescent micrographs of fixed mouse cornea sections stained by photo-triggered caged carboxyfluorescein-labeled CMP (green), and co-stained with anti-collagen I antibody (red) and DAPI (blue). The CMP staining clearly reveals the parallel organization of collagen fibrils in the corneal stroma (adapted from Ref. [3]). **(d)** Near infrared (NIR) fluorescence image of a mouse bearing PC-3 prostate tumors at forward flanks (circled) administered with UV-activated caged and NIR fluorophore labeled CMPs, indicating stable and tumor specific CMP uptake (adapted from Ref. [2••]). **(e)** Comparative NIR fluorescence images of mouse model with Marfan syndrome showing high CMP uptake in the skeleton of the diseased mouse (adapted from Ref. [2••]).

Please cite this article in press as: Li Y, Yu SM. Targeting and mimicking collagens via triple helical peptide assembly, Curr Opin Chem Biol (2013), http://dx.doi.org/10.1016/j.cbpa.2013.10.018

similar to DNA fragments binding to complimentary DNA strands. Because homotrimeric CMPs have little driving force for collagen hybridization, CMPs had to be thermally dissociated to the monomeric state before binding to collagen substrates (Figure 1a, left panel). Such thermally induced CMP hybridization allowed us to firstly directly detect collagenous proteins in SDS-PAGE gel [3] (Figure 1b), secondly image collagens in tissue sections [4,26], and thirdly immobilize angiogenic signals to collagen scaffolds [27,28].

Since addition of hot CMP solution can damage tissues, non-thermal means to control the triple helix folding and collagen binding have been developed. The Raines group synthesized a 4-fluoroproline containing CMP analog that is incapable of self-trimerizing due to inter-strand steric hindrance, but capable of hybridizing with natural collagen strands *in vitro* [5•]. Recently, our group developed a caged CMP with a photo-cleavable nitrobenzyl (NB) group attached to the central glycine [sequence: $(GPO)_4{}^{NB}GPO(GPO)_4$]. The NB cage group sterically prevented the CMP from folding into triple helix; yet removal of the cage group by UV irradiation immediately triggered the triple helical folding of the peptide and its hybridization with unfolded collagen strands [2••] (Figure 1a, right panel). Systemically delivered freshly de-caged CMPs were able to bind to denatured collagens in tissues undergoing normal (e.g., in bone and cartilage) and pathological remodeling (e.g., in tumors, Marfan syndrome) even up to 7 days (Figure 1d) [2••]. The CMP-collagen hybridization is a revolutionary new way to target collagens of abnormal tissues which complements the conventional library approaches, and could lead to new opportunities for management of numerous pathologic conditions associated with collagen remodeling (e.g., cancer, osteoporosis, arthritis, and fibrosis).

Functional collagen-like assemblies and conjugates

From surface coatings to tissue engineering, natural collagens are used extensively in biomedical applications, due to their biocompatibility and natural abundance. However, animal-derived collagens have complex physico-chemical properties that are difficult to control, and can pose potential problems of immunogenicity and pathogen transmission. Therefore, bioengineers have been developing a variety of assemblies and conjugates based on synthetic CMPs, aimed to recapitulate the structure and function of collagens as well as to generate new collagen-like scaffold materials that are tunable and conducive to functionalization.

Collagen mimetic peptide assemblies

Almost all CMP-based materials utilize the CMP's triple helical structure [29], largely because it is extremely stable under physiological condition. Conjugation of CMPs [$(POG)_{8\ or\ 9}$] to multiarm poly(ethylene glycol) (PEG) polymers led to a formation of hydrogels via triple helix mediated crosslinks (Figure 2a) [30,31], which was used to encapsulate human mesenchymal stem cells [30]. Kojima and coworkers prepared PAMAM dendrimers with CMP [$(GPP)_{5\ or\ 10}$] end groups [32,33], which were also shown to form hydrogels with potential application in controlled drug release [32]. Because the triple helix folding of CMPs is thermally reversible, these hydrogels [30–33] can be cycled through melting and gelation processes by heating and cooling, similar to gelatin (i.e., thermally denatured collagen).

Many types of natural collagens form supramolecular structures of fibers and networks. Therefore, researchers have been creating new CMP designs that could also self-assemble into higher order architecture beyond the triple helix. Brodsky group first reported that triple helical CMP of simple POG repeats, $(POG)_{10}$, can aggregate into branched filamentous structures by lateral hydrogen bonds mediated by hydroxyprolines [34]. Others have recently developed CMPs that can be triggered to form high order assemblies. Chmielewski group attached metal biding ligands (e.g., histidines, nitrilotriacetic acid) to the CMPs at residues within the sequence [35,36], and/or at the termini [7,37,38•] (Figure 2b). Similarly, CMP sequences containing multiple histidine residues [e.g., $HG(PPG)_4PHG(PPG)_4GH$] were developed by Horng and coworkers [39]. In the presence of divalent metal ions, these triple helical CMPs quickly formed microscale assemblies with distinct morphologies that correlated with the type of the metal ions and location of the metal binding ligands, while treatment with metal chelators (e.g., EDTA) resulted in instant dissolution of the assemblies [7,40]. It was determined that both the lateral CMP association and the metal-mediated crosslinking were critical to the assembly process. Surprisingly, these metal-supported hydrogels were able to encapsulate and support growth of human endothelial cells with no observable cytotoxicity [38•]. In addition, His-tagged proteins (e.g., GFP) were incorporated into the hydrogels by binding to unoccupied metal binding sites of the metal–ligand complexes [41]. These unique properties of the metal-CMP hydrogels could be utilized for cell delivery and controlled release of therapeutic agents.

Several approaches have been taken to generate artificial CMP assemblies that resemble the structure or thermal behaviors of native collagens. Collagen-like nanofibers were created by self-assembling amphiphiles composed of a hydrophilic CMP domain and a hydrophobic tail [6]. In contrast to gelatin and gelatin-like hydrogels [30–33] which melt when heated, native collagens (e.g., type I) assemble from individual molecules to fibrils when heated (e.g., from 25 to 37 °C). To mimic such thermal behavior, Kojima and coworkers synthesized a $(POG)_{10}$-conjugated PAMAM dendrimer that forms a gel upon heating [42]. The gelation is thought to be mediated by

Please cite this article in press as: Li Y, Yu SM. Targeting and mimicking collagens via triple helical peptide assembly, Curr Opin Chem Biol (2013), http://dx.doi.org/10.1016/j.cbpa.2013.10.018

Figure 2

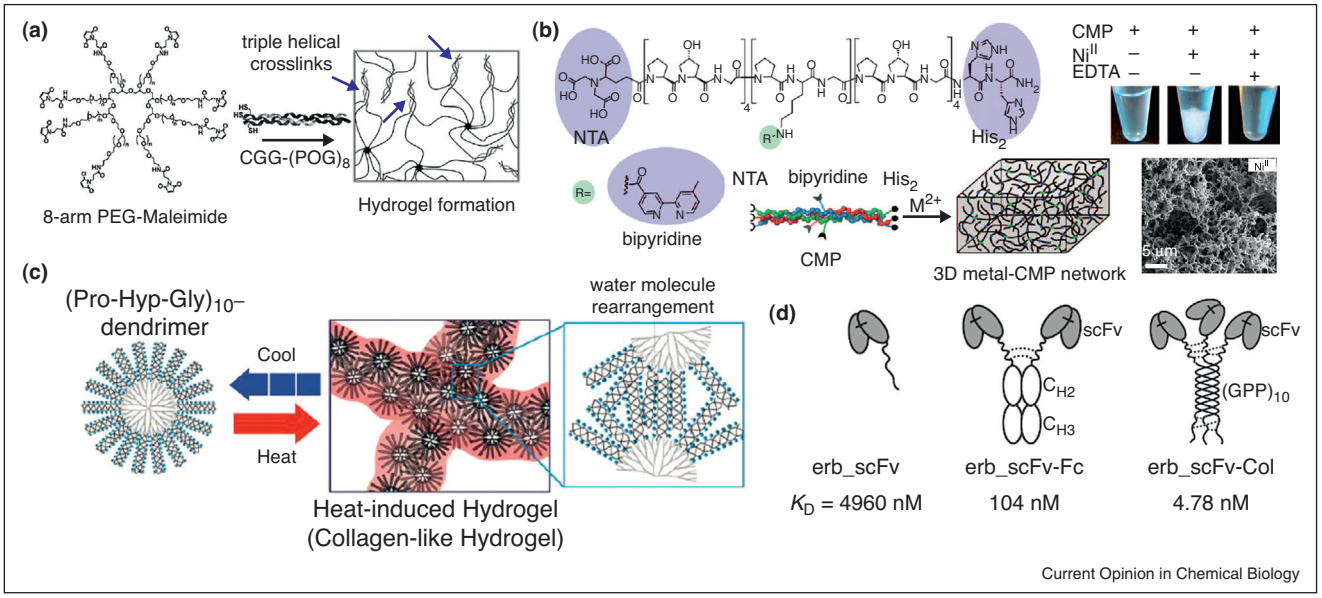

(a) Schematic illustration of hydrogel formation mediated by physical crosslinks of CMP triple helices (arrows) which are conjugated to an 8-arm PEG-maleimide star polymer (adapted from Ref. [30]). **(b)** Structure of a CMP conjugated to a nitrilotriacetic acid (NTA), two histidine residues (His_2), and a bipyridine group, and a schematic representation of this triple helical CMP assembling into 3D scaffold by metal ion supported crosslinks. Precipitation of the assembled CMPs can be seen in the presence of Ni^{II} ions while addition of EDTA dissolves the precipitates. The network-like microstructure of the Ni^{II} crosslinked CMP assembly can be observed in the scanning electron micrograph (adapted from Ref. [38•]). **(c)** $(POG)_{10}$-conjugated PAMAM dendrimers form heat-induced hydrogels which are crosslinked by triple helix-triple helix association mediated by rearrangement of water molecules on the surface of the dendrimers (adapted from Ref. [42]). **(d)** Three single-chain variable fragments (scFv) against extracellular domain of epidermal growth factor receptor are assembled into a trimer by triple helical folding of a CMP domain that is fused to the protein. The trimeric compound shows an antigen-binding affinity that is orders of magnitude higher than those of the mono-valent and bi-valent analogues (adapted from Ref. [8••]).

association of the triple helical $(POG)_{10}$ molecules on the surface of the dendrimers (Figure 2c), which is a entropy-driven process facilitated by heat [34,42]. More interestingly, Kiick group discovered that a conjugate of CMPs and thermoresponsive polymers can change its assembly structure from microspheres to fibrils upon thermal unfolding of the CMP triple helices [43]. These new CMP-based designs are revealing interesting possibilities for fabricating synthetic collagen-like materials.

Protein constructs assembled via collagen-like domains

The triple helix structural motif is found in a few non-collagenous proteins (e.g., complement factor C1q), typically as a spacer or oligomerization domain. This has inspired scientists to design multivalent protein constructs assembled via collagen-like sequences. By fusing human single-chain variable fragment (scFv) with a prolyl-hydroxylated $(GPP)_{10}$ CMP domain, Chou and coworkers produced a so-called 'collabody' in mammalian cells, where CMP's triple helical folding resulted in formation of trivalent antigen-binding fragments (Fab) (Figure 2d) [8••]. The collabody showed remarkable serum stability, and an antigen-binding affinity approximately 20-fold and 1000-fold higher than those of the bivalent and monovalent counterparts, respectively. The Álverz-Vallina group showed that the CMP sequence could be replaced with a trimerizing non-collagenous (NC1) subdomain of type XVIII collagen, which led to another type of recombinant trivalent antibodies for cancer imaging and therapeutic targeting [44,45]. These novel collagen-like domains are becoming a popular multimerizing units that can be conjugated to a variety of biomolecules (e.g., antibodies, growth factors, enzymes, monosaccharides [46]) to improve the binding affinity and ultimately their therapeutic effects.

Functionalized collagen mimetic peptides

One major advantage of the synthetic CMP is that its sequence or side chain chemical groups can be readily modified for new functions and bioactivities. Insertion of cell adhesion motifs (e.g., GFOGER, GEKGER) into the triple helical CMPs promoted attachment and growth of cells on surfaces modified with these CMPs [6,47,48]. The Koide group recently reported a novel arginine-rich heterotrimeric CMP with cell penetrating capacity (Figure 3a) [49•]. The peptide also exhibited high serum stability due to the triple helical structure that is resistant to proteases [49•]. Instead of the typical N-terminal modification [50], modified prolines were also used to

Please cite this article in press as: Li Y, Yu SM. Targeting and mimicking collagens via triple helical peptide assembly, Curr Opin Chem Biol (2013), http://dx.doi.org/10.1016/j.cbpa.2013.10.018

Figure 3

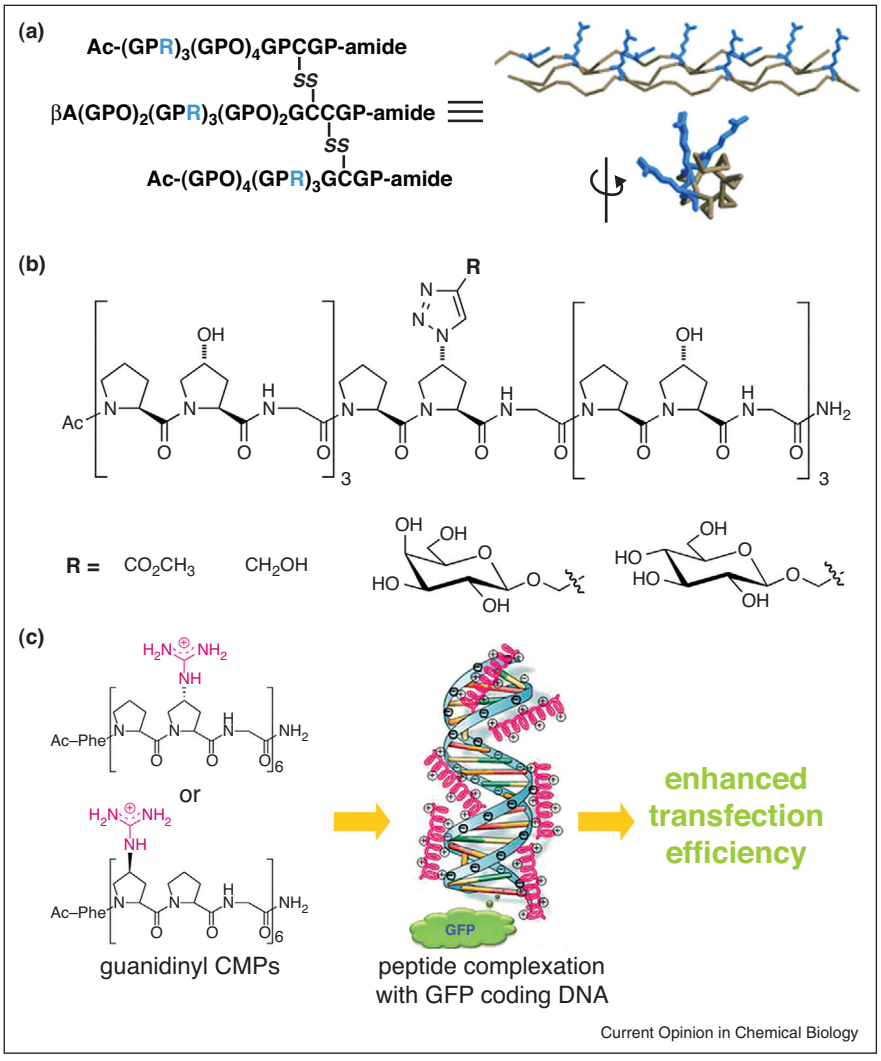

(a) Sequence of tethered Arg-rich heterotrimeric CMPs, and the spatial orientation of the Arg residues (in blue) on the triple helix which is critical for the peptide's cell penetrating capacity (adapted from Ref. [49•]). **(b)** Functionalization of CMPs through click reaction on the azido-prolines residue (adapted from Ref. [51]). **(c)** CMPs containing cationic guanidinyl-proline residues can complex with GFP encoding plasmid DNA through electrostatic interactions and enhance gene transfection (adapted from Ref. [52]).

develop CMPs with exotic functionalities [51,52]. Wennemer and Erdmann introduced azido groups into the prolines of conventional CMPs, which was further linked to various moieties (e.g., sugar molecules) via click chemistry (Figure 3b) [51]. Using this CMP system, they were able to gain insights into the conformational factors of the proline ring that are responsible for triple helix stabilization [53–55]. Nanda and Ganesh reported on-resin synthesis of CMPs containing cationic 4(*R*/*S*)-amino-proline or guanidinyl-proline residues. These CMPs formed complexes with negatively-charged plasmid DNA, which exhibited enhanced transfection efficiency (Figure 3c) [52]. The new chemical modification strategies have dramatically expanded the field of functional CMP family, and are expected to lead to unconventional but potentially high impact applications in biomedicine.

Perspective

As exemplified in this review, the CMP peptides in triple helical or single strand state exhibit distinct properties that can be exploited for different biomedical applications: as a folded triple helix, the CMP is a thermally and enzymatically stable structural motif that can assemble into synthetic ECMs, whereas single strand CMP has a strong triple helix folding propensity suited for hybridization with unfolded collagens in tissues with high ECM turnover rate (Figure 4). By drawing inspiration from both approaches, we envision many new designs and

Please cite this article in press as: Li Y, Yu SM. Targeting and mimicking collagens via triple helical peptide assembly, Curr Opin Chem Biol (2013), http://dx.doi.org/10.1016/j.cbpa.2013.10.018

Figure 4

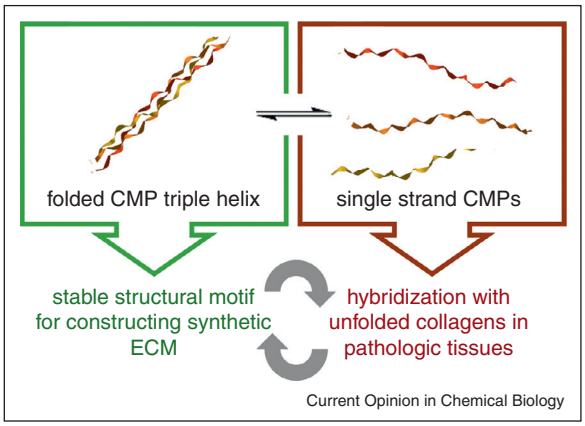

The triple helical (left box) structure and single strand (right box) conformation of CMP exhibit distinctively different physical properties that have been separately explored for various biomedical applications. Combining the two approaches in a synergistic fashion will inspire even more interesting CMP designs for targeting and mimicking collagens which could ultimately lead to a widespread use of CMP derivatives in the biomedical community.

applications of CMPs. For instance, CMP assemblies and conjugates discussed above can be turned into biologically active structures by having them hybridize with CMPs containing bioactive groups [31,56•]. One could also generate a family of novel molecules and polymers (e.g., fusion proteins, hydrogels [57], nanoparticles [58,59], dendrimers) displaying monomeric CMPs that can target collagens in remodeling tissues. Moreover, the interactions between folded CMP and collagen molecules need to be further explored. It was recently reported that 4-arm-PEG conjugated with triple helical CMPs $[(POG)_{10}]$ self-assembles into nanoparticles which can be used to create physical crosslinks between collagen fibrils, presumably by formation of hydrogen bonds between the hydroxyprolines of the triple helical CMPs and the collagen fibrils [60••]. This interesting discovery suggests that CMPs may be able to interact with collagens in a mechanism that is drastically different from the strand hybridization. Further investigation of this interaction could not only reveal new collagen assembly mechanisms, but also open new directions toward the tissue engineering applications of triple helical CMPs, particularly for tissues that are rich in collagen fibers (e.g., skin, cornea). With so many new possibilities, we believe that the CMP is a promising peptide family that could one day lead to new breakthroughs in many biomedical fields, particularly in molecular imaging, drug delivery, and tissue engineering.

Acknowledgements

Part of the work presented in this article was supported by National Institute of Health (R01-AR060484) and US Department of Defense (W81XWH-12-1-0555).

References and recommended reading

Papers of particular interest, published within the period of review, have been highlighted as:

- • of special interest
- •• of outstanding interest

1. Engel J, Bächinger HP: **Structure, stability and folding of the collagen triple helix**. In *Collagen*, vol 247. Edited by Brinckmann J, Notbohm H, Müller PK. Springer; 2005:7-33.

2. •• Li Y, Foss CA, Summerfield DD, Doyle JJ, Torok CM, Dietz HC, Pomper MG, Yu SM: **Targeting collagen strands by photo-triggered triple-helix hybridization**. *Proc Natl Acad Sci U S A* 2012, **109**:14767-14772.
This paper first demonstrated that single strand CMPs can hybridize with unfolded collagen strands in remodeling tissues *in vivo*.

3. Li Y, Ho D, Meng H, Chan TR, An B, Yu H, Brodsky B, Jun AS, Michael Yu S: **Direct detection of collagenous proteins by fluorescently labeled collagen mimetic peptides**. *Bioconj Chem* 2013, **24**:9-16.

4. Wang AY, Foss CA, Leong S, Mo X, Pomper MG, Yu SM: **Spatio-temporal modification of collagen scaffolds mediated by triple helical propensity**. *Biomacromolecules* 2008, **9**:1755-1763.

5. • Chattopadhyay S, Murphy CJ, McAnulty JF, Raines RT: **Peptides that anneal to natural collagen in vitro and ex vivo**. *Org Biomol Chem* 2012, **10**:5892-5897.
This paper introduced the fluoroproline containing CMP which does not self-assemble into homotrimers but can hybridize with unfolded natural collagen strands.

6. Luo JN, Tong YW: **Self-assembly of collagen-mimetic peptide amphiphiles into biofunctional nanofiber**. *Acs Nano* 2011, **5**:7739-7747.

7. Pires MM, Przybyla DE, Rubert Pérez CM, Chmielewski J: **Metal-mediated tandem coassembly of collagen peptides into banded microstructures**. *J Am Chem Soc* 2011, **133**:14469-14471.

8. •• Fan CY, Huang CC, Chiu WC, Lai CC, Liou GG, Li HC, Chou MY: **Production of multivalent protein binders using a self-trimerizing collagen-like peptide scaffold**. *FASEB J* 2008, **22**:3795-3804.
This paper showcased a novel strategy to bundle protein domains through triple helical folding of the fused CMPs.

9. Zong Y, Xu Y, Liang X, Keene DR, Hook A, Gurusiddappa S, Hook M, Narayana SVL: **A 'collagen hug' model for staphylococcus aureus CNA binding to collagen**. *EMBO J* 2005, **24**:4224-4236.

10. Reulen SWA, Dankers PYW, Bomans PHH, Meijer EW, Merkx M: **Collagen targeting using protein-functionalized micelles: the strength of multiple weak interactions**. *J Am Chem Soc* 2009, **131**:7304-7312.

11. Boerboom RA, Krahn KN, Megens RTA, van Zandvoort MAMJ, Merkx M, Bouten CVC: **High resolution imaging of collagen organisation and synthesis using a versatile collagen specific probe**. *J Struct Biol* 2007, **159**:392-399.

12. Chen J, Lee SK, Abd-Elgaliel WR, Liang L, Galende E-Y, Hajjar RJ, Tung C-H: **Assessment of cardiovascular fibrosis using novel fluorescent probes**. *PLoS ONE* 2011, **6**:e19097.

13. Megens RTA, oude Egbrink MGA, Cleutjens JPM, Kuijpers MJE, Schiffers PHM, Merkx M, Slaaf DW, van Zandvoort MAMJ: **Imaging collagen in intact viable healthy and atherosclerotic arteries using fluorescently labeled CNA35 and two-photon laser scanning microscopy**. *Mol Imaging* 2007, **6**:247-260.

14. Caravan P, Das B, Dumas S, Epstein FH, Helm PA, Jacques V, Koerner S, Kolodziej A, Shen L, Sun W-C *et al.*: **Collagen-targeted MRI contrast agent for molecular imaging of fibrosis**. *Angew Chem Int Ed* 2007, **46**:8171-8173.

15. Rothenfluh DA, Bermudez H, O'Neil CP, Hubbell JA: **Biofunctional polymer nanoparticles for intra-articular targeting and retention in cartilage**. *Nat Mater* 2008, **7**:248-254.

16. Muzard J, Sarda-Mantel L, Loyau S, Meulemans A, Louedec L, Bantsimba-Malanda C, Hervatin F, Marchal-Somme J, Michel JB, Le Guludec D *et al.*: **Non-invasive molecular imaging of fibrosis using a collagen-targeted peptidomimetic of the platelet collagen receptor glycoprotein VI**. *PLoS ONE* 2009, **4**:e5585.

17. Paderi JE, Panitch A: **Design of a synthetic collagen-binding peptidoglycan that modulates collagen fibrillogenesis**. *Biomacromolecules* 2008, **9**:2562-2566.

18. Stuart K, Paderi J, Snyder PW, Freeman L, Panitch A: **Collagen-binding peptidoglycans inhibit MMP mediated collagen degradation and reduce dermal scarring**. *PLoS ONE* 2011, **6**:e22139.

19. Breurken M, Lempens EHM, Merkx M: **Protease-activatable collagen targeting based on protein cyclization**. *ChemBioChem* 2010, **11**:1665-1668.

20. Breurken M, Lempens EHM, Meijer EW, Merkx M: **Semi-synthesis of a protease-activatable collagen targeting probe**. *Chem Commun* 2011, **47**:7998-8000.

21. Xu J, Rodriguez D, Kim JJ, Brooks PC: **Generation of monoclonal antibodies to cryptic collagen sites by using subtractive immunization**. *Hybridoma* 2000, **19**:375-385.

22. Pernasetti F, Nickel J, Clark D, Baeuerle PA, Van Epps D, Freimark B: **Novel anti-denatured collagen humanized antibody D93 inhibits angiogenesis and tumor growth: an extracellular matrix-based therapeutic approach**. *Int J Oncol* 2006, **29**:1371-1379.

23. Mueller J, Gaertner FC, Blechert B, Janssen K-P, Essler M: **Targeting of tumor blood vessels: a phage-displayed tumor-homing peptide specifically binds to matrix metalloproteinase-2-processed collagen IV and blocks angiogenesis in vivo**. *Mol Cancer Res* 2009, **7**:1078-1085.

24. Freimark B, Clark D, Pernasetti F, Nickel J, Myszka D, Baeuerle PA, Van Epps D: **Targeting of humanized antibody D93 to sites of angiogenesis and tumor growth by binding to multiple epitopes on denatured collagens**. *Mol Immunol* 2007, **44**:3741-3750.

25. Wang AY, Mo X, Chen CS, Yu SM: **Facile modification of collagen directed by collagen mimetic peptides**. *J Am Chem Soc* 2005, **127**:4130-4131.

26. Yu SM, Li Y, Kim D: **Collagen mimetic peptides: progress towards functional applications**. *Soft Matter* 2011, **7**:7927-7938.

27. Wang AY, Leong S, Liang YC, Huang RCC, Chen CS, Yu SM: **Immobilization of growth factors on collagen scaffolds mediated by polyanionic collagen mimetic peptides and its effect on endothelial cell morphogenesis**. *Biomacromolecules* 2008, **9**:2929-2936.

28. Chan TR, Stahl PJ, Yu SM: **Matrix-bound VEGF mimetic peptides: design and endothelial cell activation in collagen scaffolds**. *Adv Funct Mater* 2011, **21**:4252-4262.

29. Akers WJ, Xu B, Lee H, Sudlow GP, Fields GB, Achilefu S, Edwards WB: **Detection of MMP-2 and MMP-9 activity in vivo with a triple-helical peptide optical probe**. *Bioconj Chem* 2012, **23**:656-663.

30. Rubert Pérez CM, Panitch A, Chmielewski J: **A collagen peptide-based physical hydrogel for cell encapsulation**. *Macromol Biosci* 2011, **11**:1426-1431.

31. Stahl PJ, Romano NH, Wirtz D, Yu SM: **PEG-based hydrogels with collagen mimetic peptide-mediated and tunable physical cross-links**. *Biomacromolecules* 2010, **11**:2336-2344.

32. Kojima C, Tsumura S, Harada A, Kono K: **A collagen-mimic dendrimer capable of controlled release**. *J Am Chem Soc* 2009, **131**:6052-6053.

33. Suehiro T, Tada T, Waku T, Tanaka N, Hongo C, Yamamoto S, Nakahira A, Kojima C: **Temperature-dependent higher order structures of the (Pro-Pro-Gly)$_{10}$-modified dendrimer**. *Biopolymers* 2011, **95**:270-277.

34. Kar K, Amin P, Bryan MA, Persikov AV, Mohs A, Wang Y-H, Brodsky B: **Self-association of collagen triple helic peptides into higher order structures**. *J Biol Chem* 2006, **281**:33283-33290.

35. Przybyla DE, Chmielewski J: **Metal-triggered collagen peptide disk formation**. *J Am Chem Soc* 2010, **132**:7866-7867.

36. Przybyla DE, Rubert Pérez CM, Gleaton J, Nandwana V, Chmielewski J: **Hierarchical assembly of collagen peptide triple helices into curved disks and metal ion-promoted hollow spheres**. *J Am Chem Soc* 2013, **135**:3418-3422.

37. Pires MM, Lee J, Ernenwein D, Chmielewski J: **Controlling the morphology of metal-promoted higher ordered assemblies of collagen peptides with varied core lengths**. *Langmuir* 2012, **28**:1993-1997.

38. • Pires MM, Przybyla DE, Chmielewski J: **A metal-collagen peptide framework for three-dimensional cell culture**. *Angew Chem Int Ed* 2009, **48**:7813-7817.
This paper demonstrated that metal triggered assemblies of triple helical CMPs can encapsulate and support growth of endothelial cells with no observable cytotoxicity.

39. Hsu W, Chen YL, Horng JC: **Promoting self-assembly of collagen-related peptides into various higher-order structures by metal-histidine coordination**. *Langmuir* 2012, **28**:3194-3199.

40. Pires MM, Chmielewski J: **Self-assembly of collagen peptides into microflorettes via metal coordination**. *J Am Chem Soc* 2009, **131**:2706-2712.

41. Pires MM, Ernenwein D, Chmielewski J: **Selective decoration and release of his-tagged proteins from metal-assembled collagen peptide microflorettes**. *Biomacromolecules* 2011, **12**:2429-2433.

42. Kojima C, Suehiro T, Tada T, Sakamoto Y, Waku T, Tanaka N: **Preparation of heat-induced artificial collagen gels based on collagen-mimetic dendrimers**. *Soft Matter* 2011, **7**:8991-8997.

43. Krishna OD, Wiss KT, Luo T, Pochan DJ, Theato P, Kiick KL: **Morphological transformations in a dually thermoresponsive coil-rod-coil bioconjugate**. *Soft Matter* 2012, **8**:3832-3840.

44. Cuesta AM, Sanchez-Martin D, Sanz L, Bonet J, Compte M, Kremer L, Blanco FJ, Oliva B, Alvarez-Vallina L: **In vivo tumor targeting and imaging with engineered trivalent antibody fragments containing collagen-derived sequences**. *PLoS One* 2009, **4**:e5381.

45. Lobo V, Cuesta AM, Sanz L, Compte M, Garcia P, Prieto J, Blanco FJ, Alvarez-Vallina L: **Enhanced antiangiogenic therapy with antibody-collagen XVIII NCI domain fusion proteins engineered to exploit matrix remodeling events**. *Int J Cancer* 2006, **119**:455-462.

46. Okada T, Isobe C, Wada T, Ezaki S, Minoura N: **Switchable binding affinity of mannose tethered to collagen peptide by temperature-dependent triple-helix formation**. *Bioconj Chem* 2013, **24**:841-845.

47. Wojtowicz AM, Shekaran A, Oest ME, Dupont KM, Templeman KL, Hutmacher DW, Guldberg RE, Garcia AJ: **Coating of biomaterial scaffolds with the collagen-mimetic peptide GFOGER for bone defect repair**. *Biomaterials* 2010, **31**:2574-2582.

48. Krishna OD, Jha AK, Jia X, Kiick KL: **Integrin-mediated adhesion and proliferation of human MSCs elicited by a hydroxyproline-lacking, collagen-like peptide**. *Biomaterials* 2011, **32**:6412-6424.

49. • Yamazaki CM, Nakase I, Endo H, Kishimoto S, Mashiyama Y, Masuda R, Futaki S, Koide T: **Collagen-like cell-penetrating peptides**. *Angew Chem Int Ed* 2013, **52**:5497-5500.
This paper introduced an Arg-rich triple helical CMP with cell penetrating capacity and enhanced serum stability.

50. Stahl PJ, Cruz JC, Li Y, Yu SM, Hristova K: **On-the-resin N-terminal modification of long synthetic peptides**. *Anal Biochem* 2012, **424**:137-139.

51. Erdmann RS, Wennemers H: **Functionalizable collagen model peptides**. *J Am Chem Soc* 2010, **132**:13957-13959.

52. Nanda M, Ganesh KN: **4(R/S)-guanidinylprolyl collagen peptides: on-resin synthesis, complexation with plasmid DNA, and the role of peptides in enhancement of transfection**. *J Org Chem* 2012, **77**:4131-4135.

53. Erdmann RS, Wennemers H: **Importance of ring puckering versus interstrand hydrogen bonds for the conformational stability of collagen**. *Angew Chem Int Ed* 2011, **50**:6835-6838.

Please cite this article in press as: Li Y, Yu SM. Targeting and mimicking collagens via triple helical peptide assembly, Curr Opin Chem Biol (2013), http://dx.doi.org/10.1016/j.cbpa.2013.10.018

54. Erdmann RS, Wennemers H: **Conformational stability of collagen triple helices functionalized in the Yaa position by click chemistry**. *Org Biomol Chem* 2012, **10**:1982-1986.

55. Erdmann RS, Wennemers H: **Effect of sterically demanding substituents on the conformational stability of the collagen triple helix**. *J Am Chem Soc* 2012, **134**:17117-17124.

56. • Stahl PJ, Yu SM: **Encoding cell-instructive cues to PEG-based hydrogels via triple helical peptide assembly**. *Soft Matter* 2012, **8**:10409-10418.
This report showcased a new strategy to add bioactivities to synthetic hydrogels via triple helical strand hybridization of CMPs

57. Lee HJ, Yu C, Chansakul T, Hwang NS, Varghese S, Yu SM, Elisseeff JH: **Enhanced chondrogenesis of mesenchymal stem cells in collagen mimetic peptide-mediated microenvironment**. *Tissue Eng Part A* 2008, **14**:1843-1851.

58. Mo X, An YJ, Yun CS, Yu SM: **Nanoparticle-assisted visualization of binding interactions between collagen mimetic peptide and collagen fibers**. *Angew Chem Int Ed* 2006, **45**:2267-2270.

59. Ravikumar M, Modery CL, Wong TL, Dzuricky M, Sen Gupta A: **Mimicking adhesive functionalities of blood platelets using ligand-decorated liposomes**. *Bioconj Chem* 2012, **23**:1266-1275.

60. •• Matsusaki M, Amekawa R, Matsumoto M, Tanaka Y, Kubota A, Nishida K, Akashi M: **Physical and specific crosslinking of collagen fibers by supramolecular nanogelators**. *Adv Mater* 2011, **23**:2957-2961.
This paper demonstrated that nanoparticles featuring folded triple helical CMPs can form adhesive physical crosslinks with collagen fibers.

Please cite this article in press as: Li Y, Yu SM. Targeting and mimicking collagens via triple helical peptide assembly, Curr Opin Chem Biol (2013), http://dx.doi.org/10.1016/j.cbpa.2013.10.018